University of Pisa
Department of Physics
Graduate Course in Physics


Galileo Galilei School of Basic Sciences

Ph.D. Dissertation

# Critical behavior of lattice gases in a trapping potential

*Candidate*
Giacomo Ceccarelli

*Supervisor*
Prof. Ettore Vicari

**XXV Entrance, 2010-2012**

# Contents


**1 Introduction** **5**

**2 Ultracold atoms in optical lattices** **7**
2.1 Bose-Einstein condensation . . . 7
2.1.1 Theory of condensation for an ideal Bose gas . . . 7
2.1.2 Experimental realization of Bose condensates . . . 11
2.2 Optical lattices . . . 12
2.2.1 Neutral atoms in optical lattices . . . 14
2.2.2 Lattice structure . . . 16
2.3 Bose-Einstein condensates in optical lattices . . . 17

**3 Quantum phase transitions** **19**
3.1 Thermal and quantum fluctuations . . . 19
3.1.1 Classical scaling . . . 19
3.1.2 Continuous quantum phase transitions . . . 21
3.1.3 Classical-quantum mapping . . . 22
3.2 The Bose-Hubbard model . . . 23
3.2.1 The hard-core limit . . . 25
3.2.2 Quantum field theory of the Bose-Hubbard model . . . 27
3.3 Trap-size scaling of quantum phase transitions . . . 28

**4 Scaling of the Mott-insulator to superfluid transition** **31**
4.1 One-dimensional model . . . 32
4.1.1 Analytic results . . . 32
4.1.2 Low-density transition . . . 35
4.1.3 Local density approximation . . . 36
4.1.4 Mott insulator to superfluid transition at $n = 1$ . . . 37
4.1.5 Superfluid phase . . . 38
4.2 Two-dimensional model . . . 40
4.2.1 Low-density transition . . . 41
4.2.2 Local density approximation . . . 42
4.2.3 Mott-insulator to superfluid transition with $n = 1$ . . . 43
4.2.4 Superfluid phase . . . 45
4.3 Relationship with experiments . . . 46

**5 Scaling of the normal to superfluid transition** **49**
5.1 $U(1)$-symmetry breaking transitions . . . 49
5.2 Scaling relations for three-dimensional systems . . . 52
5.3 Finite-size scaling of the homogeneous model . . . 53
5.3.1 Invariant quantities . . . 53
5.3.2 Compressibility, particle density and its correlator . . . 55
5.4 Critical parameters from trap-size scaling . . . 57

5.4.1 Finite-size effects with the trap . . . . . 57
5.4.2 Trap-size scaling analyses of the Monte Carlo data . . . . . 59
5.4.3 Trap-size dependence of the particle density . . . . . 61
5.5 Relationship with experiments . . . . . 65

**A Quantum Monte Carlo simulations** **67**
A.1 Stochastic series expansion . . . . . 67
A.2 Observables . . . . . 70
A.3 Sampling and statistics . . . . . 71

**List of figures** **76**

**List of tables** **77**

**Bibliography** **79**

# Chapter 1

# Introduction

In recent years much progress has been made in the experimental manipulation of many-body systems. In particular, it has become possible to study the behavior of a statistically relevant number of atoms under well controlled external conditions and in the low-temperature regime. These results have been achieved thanks to the experimental improvements made along three different directions: cooling techniques, magnetic trapping and optical lattices.

First laser cooling [112, 113, 114] and then evaporative cooling [9, 10] made it possible to reach the very low temperatures needed for the establishment of quantum degeneracy in dilute gases. Furthermore, the particular field configurations constituting magnetic and optical traps [17] prevented neutral atoms and ions to escape a finite region of space, thus attaining a very good confinement of particles, while optical lattices [25, 28, 47], which are arrays of microscopic potentials induced by the alternate current Stark effect of interfering laser beams, realized an extremely precise localization of the single atoms. All of these progresses made it possible to study equilibrium and dynamical properties of a statistical number of atoms in a thermodynamic regime where quantum effects are relevant for the collective behavior of the system, thus entering a new field of research where the laws of quantum mechanics drive not only the physics of the single microscopic constituents, but also that of collective excitations. Moreover, modern experimental setups are very clean and tunable so that the basic feature of the underlying interactions can be studied with great precision and in a wide range of the external parameters.

The most important realization in this field has been the achievement of Bose-Einstein condensation in diluted atomic vapors [116, 117]. This basic phenomenon constitutes an example of a phase transition, that is one in which physical observables exhibit an anomalous (typically divergent) behavior. It is only the first of a series of experimental results where other similar situations were observed: as a benchmark example, a Mott-insulator to superfluid transition has been observed [37] and extensively studied in experiments with ultracold atomic gases loaded in optical lattices.

In the field of modern low-temperature physics we can distinguish two types of phase transitions: those driven by thermal (classical) fluctuations, where the disordering mechanism resides in thermal excitations, and those driven by quantum fluctuations, where the Heisenberg uncertainty principle is responsible for the loosing of order. The most interesting aspects for us is that we can now study in a controllable and essential manner the interplay of both of these mechanisms. For examples phase transitions related to the formation of the Bose-Einstein condensation in an interacting Bose gas at nonzero temperature are essentially driven by thermal fluctuations, giving rise to a classical critical behavior [124], while quantum fluctuations play a dominant role at zero-temperature transitions, as for the Mott-insulator to superfluid transition and related phenomena [15], where the low-energy properties show a quantum critical behavior.

As already mentioned, a common feature of these experiments is the presence of a confining mechanism which traps the atoms in a finite region of space. The inhomogeneity due to the trapping potential strongly affects the phenomenology of (classical and quantum) transitions in homogeneous systems: correlation functions are not expected to develop a divergent length scale in the presence of

the trap so that a theoretical description of how critical correlations develop in this kind of systems is of great importance for experimental investigation. The main purpose of this work will be to set the stage for a general interpretation of the emerging critical behaviors through a theory accounting for the effects of traps of finite size.

The work is organized as follows.

- In Chapter 2 we briefly describe the physics of cold atoms loaded in optical lattices. In particular we review the implications on the thermodynamics of the typical experimental conditions.
- In Chapter 3 we discuss the theory of quantum phase transitions. In particular we consider scaling relations and describe the phases of the Bose-Hubbard model. Finally, we expose the trap-size scaling theory.
- In Chapter 4 we use the trap-size scaling theory to study the effects of temperature on the phenomenology of quantum phase transitions in the presence of a trapping potential. In particular we consider the Mott-insulator to superfluid transitions of the Bose-Hubbard model in one and two dimensions.
- In Chapter 5 we study the effects of confinement on the finite-temperature phase transition from a superfluid to a normal fluid in the three-dimensional Bose-Hubbard model.
- In the Appendix we give the details of our quantum Monte Carlo simulations.

This thesis is based on the following publications.

- *Interplay between temperature and trap effects in one-dimensional lattice systems of bosonic particles*,
  G. Ceccarelli, C. Torrero, E. Vicari,
  *Phys. Rev. A*, **85** (2012) 023616 .
- *Scaling behavior of trapped bosonic particles in two dimensions at finite temperature*,
  G. Ceccarelli, C. Torrero,
  *Phys. Rev. A*, **85** (2012) 053637 .
- *Critical parameters from trap-size scaling in systems of trapped particles*,
  G. Ceccarelli, C. Torrero, E. Vicari,
  *Phys. Rev. B*, **87** (2013) 024513 .

# Chapter 2

# Ultracold atoms in optical lattices

A macroscopic system of identical particles in thermal equilibrium is described by the laws of statistical physics and usually the principles of classical mechanics can be applied in the external conditions met in daily life situations. Quantum effects become relevant at very low temperatures or very high densities and it is therefore of great interest to understand under which conditions quantum effects play a dominant role in the behavior of macroscopic systems.

For this purpose in this chapter we will describe the phenomenon of Bose-Einstein condensation and the realization of the Bose-Hubbard model. The physical relevance of these examples resides in the fact that they manifest collective quantum effects which involve the coherent behavior of a lot of particles, so that particle statistics and their interactions are at center stage rather than single atoms. Moreover, the trapped Bose-Hubbard model will provide our staring point for the study of criticality in phase transitions of the subsequent chapters.

## 2.1 Bose-Einstein condensation

Within the framework of a theoretical description of the quantum properties of light, in 1924 the Indian physicist S.N. Bose developed a new interpretation in which black-body radiation was treated as a gas of identical particles [22], called photons. These ideas were then extended by Einstein to the case of a set of noninteracting massive particles [23], eventually originating what is today called Bose-Einstein statistic. One of the first observation was that an ideal gas of massive particles would undergo a phase transition [24], called Bose-Einstein condensation. The peculiarity of this transition is that it is not driven by the interactions among constituents but by the quantum statistic. This subject is one of the most important in the field of condensed matter physics and has been extensively discussed in the literature: see for example Refs. [7, 14, 16, 18, 19].

### 2.1.1 Theory of condensation for an ideal Bose gas

Since this work will be mainly devoted to the study of inhomogeneous systems, we now describe the phenomenon of Bose-Einstein condensation for an ideal (noninteracting) gas in the presence of an external potential. Let us consider $N$ noninteracting identical particles of mass $m$ in thermal equilibrium at temperature $T$ in the presence of an external potential $V_{ext}(\mathbf{r})$. The hamiltonian for the whole system is given by

$$H = \sum_{i=1}^{N} H^{(1)}(i) \ , \tag{2.1}$$

where $H^{(1)}$ is the single particle hamiltonian which in our context reads

$$H^{(1)}(i) = \frac{\mathbf{p}_i^2}{2m} + V_{ext}(\mathbf{r}_i) \ , \tag{2.2}$$

where $\mathbf{r}$ is the particle position and $\mathbf{p}$ is the particle momentum. This factorization is made possible by the lack of interparticle interactions. Of course this does not mean that particles are not correlated, since we know from the axioms of elementary quantum mechanics that the global wave function of a system of identical particles must satisfy the constraint of symmetry (for bosons) or antisymmetry (for fermions). Eventually this leads to a correlation among particles which has no classical counterpart and emerges as a pure quantum effect. The eigenvalues $\epsilon_\alpha$ and the eigenfunctions $\varphi_\alpha(\mathbf{r})$ of (2.2) can be determined using the standard Schrödinger equation for one-particle systems and then, through the laws of statistical physics [3], we can compute all the thermodynamical quantities we need. The index $\alpha$ collects all the quantum numbers and takes on discrete values in a real (finite) system.

At thermal equilibrium the laws of quantum statistical mechanics describe the system giving the state occupation numbers, when the particles are bosons, as

$$n_\alpha = \frac{1}{\exp\left[\beta(\epsilon_\alpha - \mu)\right] - 1} \,, \tag{2.3}$$

where $n_\alpha$ is the mean number of particles which occupy the state $\alpha$ and $\beta = (k_B T)^{-1}$, with $k_B$ the fundamental Boltzmann constant. The parameter $\mu$ is the chemical potential and is related with the total number of particles. Since all the occupation numbers must be positive definite, we get the fundamental constrain $\mu < \epsilon_0$, where $\epsilon_0$ is the minimum of the energy levels.[1] The total number of particles must of course obey the normalization condition

$$N \equiv \sum_\alpha n_\alpha = \sum_\alpha \frac{1}{\exp\left[\beta(\epsilon_\alpha - \mu)\right] - 1} \,. \tag{2.4}$$

Since the fundamental level can diverge in the physical conditions for which $\mu \to \epsilon_0$, it is now useful to divide the total number of particles into two terms:

$$N(\mu, T) = N_0(\mu, T) + N_T(\mu, T) \tag{2.5}$$

where $N_0 \equiv n_0$ is the number of particles in the ground state while $N_T$ is the number of particles in the thermally exited states and we have emphasized the independent variables. It is common to call $N_0$ the condensed component and $N_T$ the thermal component. From equation (2.3) we see that all $n_\alpha$ turn out to be increasing functions of $\mu$ for any finite temperature: $N_0$ is always of order unity (we say it is macroscopically empty) except when $\mu \to \epsilon_0$ and in this case it diverges; $N_T$ is proportional to the number of states so that is always (except for $T = 0$) of order $N$ (we say it is macroscopically populated) and reaches its maximum value (possibly infinite) for $\mu = \epsilon_0$. The maximum of $N_T$ is called critical particle number $N_c$ and is given by $N_c(T) = N_T(T, \epsilon_0)$.[2] We now rewrite equation (2.4) in a continuous form replacing the summation with an integration:

$$N = N_0 + \int \frac{1}{\exp\left[\beta(\epsilon_\alpha - \mu)\right] - 1} \, d\alpha \,, \tag{2.6}$$

where we extracted the ground state contribution as before. This is permitted only if the excitation energy $k_B T$ is much bigger than the energy spacing between single particles levels and it is equivalent to assuming a semiclassical description of the excited states.

Let us consider a fixed number of particles and let the temperature vary. The ground state of the system is obtained by putting all the particles in the fundamental state $\varphi_0(\mathbf{r})$, so that the total wave function turns out to be $\Phi = \prod_i \varphi_0(\mathbf{r}_i)$, which is correctly symmetric. This corresponds to the $T = 0$ state where $N_0 = N$ and $N_T = 0$. We thus see that $\mu(N, 0) = \epsilon_0$. Turning on temperature, all energy levels will be populated according to the prescription (2.3) and the constrain (2.4): as the temperature is raised the condensate component will decrease while the thermal component will be populated more

[1] For fermions there is no restriction on the values of $\mu$ since $n_\alpha = (\exp\left[\beta(\epsilon_\alpha - \mu)\right] + 1)^{-1}$ is always well defined and positive definite.

[2] For fermions there is no maximum for $N_T$ since $\mu$ is unbounded.

and more. In the thermodynamic limit, from the occupation number of the fundamental level, we obtain $\epsilon_0 - \mu = k_B T \ln(1 - 1/N_0) \simeq k_B T/N_0$ which implies $\mu(N,T) = \epsilon_0$ as long as the fundamental state is macroscopically occupied. We call critical temperature $T_c$ the temperature such that the ground state is macroscopically empty and the gas is substantially thermal. If the temperature is high enough to have $N < N_c(T)$ then a value of $\mu < \epsilon_0$ exists which satisfies equations (2.3, 2.4) with a macroscopically empty ground state. When instead the temperature is so low that $N > N_c(T)$, the only way for the system to get thermal equilibrium is to fill without restriction the fundamental state. We thus see that for $T < T_c$ all the particles that cannot occupy the excited levels are stored in the fundamental one. Thus a macroscopic number of particles populate this state and we say that a condensate is formed. In the thermodynamic limit the critical temperature $T_c$ is thus defined as $N = N_c(T_c)$ which is equivalent to

$$N = N_T(T_c, \epsilon_0)\,. \tag{2.7}$$

At this point, to proceed further, we must somehow specify the form of the external potential. Two are the typical choices: the hard-wall potential and the harmonic potential. In the former case, of theoretical interest, particles are supposed free to move within a limited region of space, typically of cubic shape of length $L$. In the latter case, typical of experimental realizations with trapped atoms, we have

$$V(\mathbf{r}) = \frac{1}{2}\, m\,(\omega_x^2 x^2 + \omega_y^2 y^2 + \omega_z^2 z^2)\,. \tag{2.8}$$

We now expose the standard results concerning the Bose-Einstein condensation in homogeneous and harmonically trapped three-dimensional systems [115].

- *Hard-wall limit*
  In this case the eigenvalues are

$$\epsilon(n_x, n_y, n_z) = \frac{\mathbf{p}^2}{2m} = \frac{2\pi\hbar\mathbf{n}}{L}\,, \tag{2.9}$$

  where $\mathbf{n}$ is a vector of integer components and we have chosen periodic boundary conditions, while the eigenvectors are the usual plane waves $\varphi_{\mathbf{p}}(\mathbf{r}) = \exp(i\mathbf{p}\mathbf{x})/\sqrt{V}$ normalized to the volume $V = L^3$ of the system. The condition for the critical temperature and the ground state population read

$$k_B T_c = \frac{h^2}{2\pi m \zeta(3/2)^{2/3}} \left(\frac{N}{V}\right)^{2/3}\,, \tag{2.10}$$

$$\frac{N_0}{N} = 1 - \left(\frac{T}{T_c}\right)^{3/2} \quad \text{for} \quad T < T_c\,, \tag{2.11}$$

  where $\zeta$ is the Riemann zeta function.
  These results have been obtained setting $\mu = 0$, since $\epsilon_0 = 0$ for free particles, and using (2.6), which is justified if $k_B T \gg h^2/(2mV^{2/3})$. In order to have a well defined critical temperature, the thermodynamic limit must be defined, as usual, as $N, V \to \infty$ while keeping $n \equiv N/V$ fixed, which is consistent with the semiclassical approximation.
  At $T_c$ the specific heat turns out to have a discontinuity in its first derivative of $\Delta(\partial C_V/\partial T) = -3.66 k_B N/T_c$ and this justifies the interpretation of the Bose-Einstein condensation as a phase transition. Moreover this transition has the peculiarity of taking place in the space of momenta, since a fraction of particles accommodates in the state of zero speed while, from a spatial viewpoint, the system remains homogeneous: this is the reason for the name of condensation.
  We mention that the condition $N_0 \simeq N$, which corresponds to an almost perfect condensate, is fulfilled if $T \ll T_c$ and this can be realized even for macroscopic values of $T$. The analysis carried out so far is thus valid in the range $h^2/(2mV^{2/3}) \ll k_B T \ll k_B T_c$.

- *Harmonic confinement*
  In this case the eigenvalues are

$$\epsilon(n_x, n_y, n_z) = \left(n_x + \frac{1}{2}\right)\hbar\omega_x + \left(n_y + \frac{1}{2}\right)\hbar\omega_y + \left(n_z + \frac{1}{2}\right)\hbar\omega_z \,, \tag{2.12}$$

  where $n_x, n_y, n_z$ are the usual harmonic oscillator quantum numbers, while the corresponding eigenvectors are the Hermite special functions. The ground state density is $n(\mathbf{r}) = N|\varphi_0(\mathbf{r})|^2$, where the single particle ground state wavefunction is

$$\varphi_0(\mathbf{r}) = \left(\frac{m\omega_{\rm ho}}{\pi\hbar}\right)^{3/4} \exp\left[-\frac{m}{2\hbar}(\omega_x x^2 + \omega_y y^2 + \omega_z z^2)\right] \,. \tag{2.13}$$

  We get the important length scale

$$a_{\rm ho} = \left(\frac{\hbar}{m\omega_{\rm ho}}\right)^{1/2} \,, \tag{2.14}$$

  where $\omega_{\rm ho} \equiv (\omega_x\omega_y\omega_z)^{1/3}$ is the geometric average of the trapping frequencies. Thus the quantity $a_{\rm ho}$ fixes the order of magnitude for the spatial extension of the condensed cloud. The critical temperature and the ground state occupation number turn out to be

$$k_B T_c = \hbar\omega_{\rm ho}\left(\frac{N}{\zeta(3)}\right)^{1/3} \,, \tag{2.15}$$

$$\frac{N_0}{N} = 1 - \left(\frac{T}{T_c}\right)^3 \quad \text{for} \quad T < T_c \,. \tag{2.16}$$

  These results have been obtained setting $\mu = (3/2)\hbar\bar{\omega}$, where $\bar{\omega} \equiv (\omega_x + \omega_y + \omega_z)/3$ is the arithmetic average of the trapping frequencies, and the semiclassical assumption $\hbar\omega_{\rm ho} \ll k_B T$. In order to have a well defined critical temperature, the thermodynamic limit must be defined as $N \to \infty$ and $\omega \to 0$ while keeping $N\omega^3$ fixed, which is still consistent with the semiclassical approximation.
  For $0 < T < T_c$ a finite fraction of particles is thermally exited and, in the semiclassical limit, we can estimate the density $n_T(\mathbf{r})$ with the Boltzmann factor $n_T(\mathbf{r}) = \exp\left[-V(\mathbf{r})/k_B T\right]$, which leads to a gaussian profile whose extension is

$$R_T = a_{\rm ho}\left(\frac{k_B T}{\hbar\omega_{\rm ho}}\right)^{1/2} \,. \tag{2.17}$$

  We thus see that, in the semiclassical limit, the thermal component is always more broad then the condensed one and the above discussion reveals that Bose-Einstein condensation in harmonic traps shows up with the appearance of a sharp peak in the central region of the density distribution.

Simply rewriting equation (2.10) as $\lambda_{\rm dB} \sim n^{-1/3}$, where $\lambda_{\rm dB} = h/(2\pi m k_B T)^{1/2}$ is the thermal de Broglie wavelength and $n$ is the particle density, we can identify the onset of Bose-Einstein condensation with the condition that the thermal wavelength is comparable with the mean interparticle spacing. An analogous deduction can be made for trapped systems using equations (2.15, 2.17) and recalling that in this case for the density we must use $N/R_T^3$.

Until now we have considered only ideal gases in three dimensions. We now briefly discuss, still in the noninteracting case, the role of dimensionality. The condition identifying the occurrence of Bose-Einstein condensation is that the number $N_T$ of thermally exited particles has an upper bound for any value of the temperature $T$ when evaluated for $\mu = \epsilon_0$. Using equation (2.6) we see that in the homogeneous case the integral related to $N_T$ diverges at small momenta as $\ln p$ in two dimensions

and as $1/p$ in one dimension. This rules out the possibility of Bose-Einstein condensation for the ideal gas in low dimensionality. Passing to the harmonic confinement, a similar analysis shows that in two dimensions the integral in (2.6) is now convergent and this leads to a critical temperature given by

$$k_B T_c = \hbar\omega_{\rm ho}\left(\frac{N}{\zeta(2)}\right)^{1/2}, \tag{2.18}$$

where now $\omega_{\rm ho} = (\omega_x\omega_y)^{1/2}$. Finally for one-dimensional trapped systems the integral is divergent and no condensate can be formed. The above discussion clearly shows the close relationship between Bose-Einstein condensation and the density of states of the system.

### 2.1.2 Experimental realization of Bose condensates

The first experimental realizations of the Bose-Einstein condensation were realized in 1995 in a remarkable series of experiments with diluted atomic vapors [88, 89, 121]. In this section we enter in some details in order to give the values of the relevant experimental parameters and to introduce some aspects of the interactions among atoms which will be relevant for the subsequent discussion.

One of the first problem in obtaining a Bose-Einstein condensate was that of confinement: since real particles always interact with the walls of a container and can be captured by them, a lot of trapping techniques, both for charged and neutral particles, have been developed, mainly taking advantage of the magnetic and optical properties of atoms, in order to realize a stable and manageable ensemble. For a detailed discussion on this problem, see for example Ref. [26] and references therein.

Moreover real atoms have usually mutual interactions which eventually drive a system into the liquid and solid phases. The theory developed in Section 2.1.1 was carried on in the ideal limit, so that it is now important to understand under which conditions interactions can be neglected and what are their consequences, at least to a first approximation. In order to do this we need to study the scattering process involving a pair of identical atoms. We make the assumptions that the interparticle potential (*i*) diverges for very short distances and goes to zero at large separation and (*ii*) has a spherical symmetry. As a consequence, a natural basis onto which expand the diffusion process is that of the orbital angular momentum, whose quantum number is $l$. Being interested in the low-temperature physics, we consider the scattering in the low-energy limit, so that, since for the diffusion of two bosonic particles only even values of the angular momentum are allowed, the collision is dominated by the $s$-wave channel, while, since for the fermionic case only odd values are allowed, the $p$-wave channel dominates. In the limit where only $s$-wave ($p$-wave) scattering takes place for bosons (fermions), we say that we are in the *ultracold atoms regime*. For bosonic particles this condition is realized when the energy associated with the centrifugal barrier in the states of angular momentum $l \geq 1$ is much bigger than the thermal kinetic energy, so that only the $s$-wave survives. For the typical interatomic potentials and masses of the alkali atoms used in experiments this corresponds to temperatures in the millikelvin range.

Thus, from the quantum theory of scattering [2], we know that in a first approximation, for a low enough kinetic energy of the relative motion, the two-body scattering amplitude is completely specified by one parameter, the scattering length $a$, and is given by

$$f(k) = -\frac{a}{(1+ika)}, \tag{2.19}$$

where $\hbar k$ is the relative momentum. All the details of the interatomic potential are effectively taken into account by $a$: positive and negative values for $a$ correspond respectively to repulsive and attractive forces. For the typical atoms employed in Bose-Einstein condensation we have scattering lengths in the nanometer range: $a = 2.75$ nm for sodium; $a = 5.11$ nm for rubidium; $a = -1.45$ nm for lithium. Finally we note that the scattering amplitude (2.19) is the one that corresponds to the interaction potential

$$V_{int}(\mathbf{r}) = \frac{4\pi\hbar^2 a}{m}\,\delta(\mathbf{r}) \tag{2.20}$$

for any value of $k$. Within the framework of the ultracold atoms regime, we can quantify the interaction strength with the parameter

$$g \equiv \frac{4\pi\hbar^2 a}{m} \tag{2.21}$$

which has dimensions of an energy · volume.

In homogeneous systems, when $n|a|^3 \ll 1$, only a few particles are present in the scattering volume $|a|^3$: this is the condition which defines the *dilute gas regime*, where the interparticle spacing is much bigger than the scattering length. This definition can be used also for trapped gases with the minor change to use as $n$ the density at the center of the cloud, where the value is maximum. Typical values of density range from $10^{13}$ cm$^{-3}$ to $10^{15}$ cm$^{-3}$ so that $n|a|^3$ is always less than $10^{-3}$. It is clear that in homogeneous conditions the dilute gas regime also coincides with the *weakly interacting regime*, but in the presence of the harmonic trap we must also take care of the kinetic energy emerging from the confinement. For example, the interatomic energy in the ground state of the harmonic oscillator is given by $gnN$, where the average density is of order $N/a_{\rm ho}^3$, so that $E_{int} \propto N^2|a|a_{\rm ho}^{-3}/m$. For the kinetic energy we have $E_{kin} \propto N\hbar\omega_{\rm ho} \propto Na_{\rm ho}^{-2}/m$ and finally we find that the dimensionless parameter expressing the relevance of atom-atom interaction for a nearly perfect trapped Bose-Einstein condensate is

$$\frac{E_{int}}{E_{kin}} \propto \frac{N|a|}{a_{\rm ho}} \,. \tag{2.22}$$

In experiments this value can range from fractions of unity to thousands.

The basic procedure which leads to the formation of a Bose-Einstein condensate is the following: (*i*) alkali atoms are extracted from an oven and immediately trapped and cooled through magneto-optical methods; (*ii*) using the technique of laser cooling they are cooled to the lowest temperature compatible with the recoil limit; (*iii*) the cooling laser is turn off and the trapping potential is reduced causing evaporative cooling.

In typical experiments the number of trapped atoms at the end of the cooling procedure ranges from a few thousands to several millions while the final temperatures attained range from tens to hundreds of nanokelvins. The corresponding frequencies of magnetic traps are usually expressed as $\omega = 2\pi \times \alpha\,\mathrm{Hz}$, where $\alpha$ measures the strength of the confinement. Typical values of $\alpha$ for symmetric traps are of the order of tens.[3]

Moreover, for strongly asymmetric traps, an effective change of dimensionality is possible. Let us consider for example the situation $\hbar\omega_x = \hbar\omega_y \ll k_BT \ll \hbar\omega_z$. In this case, along the $z$-direction, only the fundamental state is accessible to the system and, since the gaussian extension $a_{\rm ho} \propto \omega_z$, atoms are very tightly confined while in the $xy$ plane exited states are available, so that the system becomes effectively two-dimensional. To get an effectively one-dimensional system, the condition $\hbar\omega_x \ll k_BT \ll \hbar\omega_y = \hbar\omega_z$ must instead be fulfilled. In order to get a strong confinement along some spatial direction typical used values for $\alpha$ are of the order of thousands.

## 2.2 Optical lattices

Optical lattices are arrays of microscopic potentials induced by the alternate current Stark effect of interfering laser beams and are realized by using counter-propagating laser fields. In this section we recall the basic physical aspects of the atom-light interaction relevant for our future discussion [15] and we will analyzed the similarities with solid state physics.

The simplest way to form a one-dimensional lattice is by superimposing two oppositely directed lasers, each with the same angular frequency $\omega$. For simplicity, we assume that both beams are linearly polarized with the electric field vector along the $z$ axis. The total field is thus

$$E_z = E_0\cos(kx - \omega t) + E_0\cos(-kx - \omega t) = 2E_0\cos(kx)\cos(\omega t) \,, \tag{2.23}$$

[3]This translates into a value for the harmonic confinement $a_{\rm ho}$ of the order of microns. Thus the particles cloud extends over a length of roughly $4a_{\rm ho}$.

where $k$ is the wavevector related to the wavelength $\lambda$ by $k = 2\pi/\lambda$.

The physical mechanism at the origin of trapping is the interaction of the atomic electron cloud with the electromagnetic radiation. When an atom is placed into laser light, the electric field induces an atomic dipole moment $\mathbf{d}$ that oscillates at the driving frequency and can be expressed in terms of the atomic polarizability $\alpha(\omega)$. In the usual complex notation $\mathbf{E}(\mathbf{r},t) = \bar{E}(\mathbf{r})\exp(-i\omega t) + c.c.$ and $\mathbf{d}(\mathbf{r},t) = \bar{d}(\mathbf{r})\exp(-i\omega t) + c.c.$ the amplitude $\bar{d}$ of the dipole moment is simply related to the field amplitude $\bar{E}$ by $\bar{d} = \alpha(\omega)\bar{E}$, where $\alpha$ is the polarizability which can be separated in a real and an imaginary part.

The resulting dipole potential is determined by time averaging over $\mathbf{d}\cdot\mathbf{E}$ and is

$$V_{dip}(\mathbf{r}) = \frac{1}{2}\langle \mathbf{d}\cdot\mathbf{E}\rangle = -\frac{1}{2\epsilon_0 c}\mathrm{Re}[\alpha(\omega)]I(\mathbf{r}) \ , \tag{2.24}$$

where the angular brackets denote the time average over the rapid oscillating terms, the field intensity is $I = 2\epsilon_0 c|\bar{E}|$ and the factor $1/2$ takes into account that the dipole moment is an induced and not a permanent one.

The interaction potential of the induced dipole moment is thus proportional to the light intensity times the real part of the polarizability, which describes the dispersive properties of the interaction. The laser intensity is space dependent and we get a dipole force that results from the gradient of the interaction potential:

$$F_{dip}(\mathbf{r}) = -\nabla V_{dip}(\mathbf{r}) = \frac{1}{2\epsilon_0 c}\mathrm{Re}[\alpha(\omega)]\nabla I(\mathbf{r}) \ . \tag{2.25}$$

The power absorbed by the oscillator from the driving field is reemitted as dipole radiation and is proportional to the laser intensity times the imaginary part of the atomic polarizability, which describes the dissipative properties of the interaction. The power absorbed by the oscillator from the driving field (and reemitted as dipole radiation) is given by

$$P_{abs} = \langle \dot{\mathbf{d}}\mathbf{E}\rangle = 2\omega\mathrm{Im}[\bar{p}\bar{E}^*] = \frac{\omega}{\epsilon_0 c}\mathrm{Im}[\alpha]I \ . \tag{2.26}$$

Considering the light as a stream of photons $\hbar\omega$, the absorption can be interpreted in terms of photon scattering in cycles of absorption and subsequent spontaneous reemisson processes. This results in a corresponding scattering rate of

$$\Gamma_{sc} = \frac{P_{abs}}{\hbar\omega} = \frac{1}{\hbar\epsilon_0 c}\mathrm{Im}[\alpha]I \ . \tag{2.27}$$

When the laser frequency is not resonant with the atomic frequencies, the scattering rate is small and the dipole force has a quasi conservative character: the minima or the maxima of its potential can be used for trapping the atoms while the scattering of light sets limits to the performances of dipole traps. When the difference $\Delta = \omega_{\mathrm{at}} - \omega$ is $\Delta > 0$ the laser is working at red-detuning and particles are trapped in the minima while for $\Delta < 0$ the blue-detuned laser traps particles in the maxima.

These considerations can be immediately generalized to two and three dimensions so that we write the lattice dipole potential as

$$V_{per}(\mathbf{r}) = V_0(\sin^2 kx + \sin^2 ky + \sin^2 kz) \ . \tag{2.28}$$

We observe that the periodicity of this potential is $d = \lambda/2$ and this will correspond to the optical lattice spacing. Typical values for $d$ are of order $10^{-7}$ m while the height of the potential barriers are of order $10^{-5}$ K.[4] For comparison the lattice spacing in crystals is of order $10^{-10}$ m and the barrier strength is of order $10^5$ K. Finally, we mention that optical lattices are very clean systems where the properties of interactions can be studied at a very fundamental level, contrary to situations met in common crystals, and moreover the lattice parameters $d$ and $V_0$ can be varied with great accuracy in a wide range of values.

[4]Comparing the values of $a_{\mathrm{ho}}$ and $d$ in typical situations, we get for the ratio $a_{\mathrm{ho}}/d$ the order of tens. This gives a rough estimate of the number of lattice sites that are occupied in the conditions described in Section 2.2.1. As a reference, the experiment reported in Ref. [37] involves $1.5\cdot 10^5$ sites in a three-dimensional lattice, corresponding to a linear size of 65.

### 2.2.1 Neutral atoms in optical lattices

Putting together all the considerations made so far, we consider the physical situation where neutral atoms subjected to a two-particle interaction $V_{int}$ are loaded in an optical lattice potential $V_{per}$ in the presence of a trapping external confinement $V_{ext}$. The total hamiltonian for this system is then

$$H = \sum_i \frac{\mathbf{p}^2}{2m} + \sum_i V_{per}(\mathbf{r}_i) + \sum_i V_{ext}(\mathbf{r}_i) + \sum_{i<j} V_{int}(\mathbf{r}_i - \mathbf{r}_j) \ , \tag{2.29}$$

where the last sum runs over all pairs of atoms and the other sums run over all atoms. We are now going to describe the dynamics of this system [27, 92] and to demonstrate that it reduces, under appropriate conditions, to a well known model of condensed matter physics: the Bose-Hubbard model.

It is well known from solid state physics [13] that the eigenstates of a periodic hamiltonian can be described by wave functions of the form $\psi_{n\mathbf{q}}(\mathbf{r}) = u_{n\mathbf{q}}(\mathbf{r})e^{i\mathbf{qr}}$, where $u_{n\mathbf{q}}(\mathbf{r})$ are functions with the same periodicity of the lattice, $n$ is the band index and $\mathbf{q}$ is the quasi-momentum. These functions are called Bloch functions and form a basis, called Bloch basis, for the one particle motion. The Bloch basis can be changed and we can define a new set of basis functions through the following relation:

$$\psi_{n\mathbf{q}}(\mathbf{r}) = \sum_{\mathbf{z}} w_{n\mathbf{z}}(\mathbf{r})e^{i\mathbf{qz}} \ , \tag{2.30}$$

where the sum is extended over all lattice sites. The functions $w_{n\mathbf{z}}(\mathbf{r})$ are known as Wannier functions and they are the lattice Fourier transform of the Bloch functions. Since the Wannier functions depend only on the distance $\mathbf{r} - \mathbf{z}$, by choosing a convenient normalization they obey the orthonormality relation

$$\int w_m^*(\mathbf{r} - \mathbf{x})w_n(\mathbf{r} - \mathbf{y})\, d^3r = \delta_{mn}\delta_{\mathbf{xy}} \ . \tag{2.31}$$

In the case of one dimensional systems, we know that Wannier functions are exponentially damped functions centered in the lattice sites, at least for the lowest band, and, in more than one dimension, this result can be trivially extended when the periodic potential is factored [49]. The characteristic distance over which the functions decay is of the order of the lattice constant $d$.

Let us now consider a statistically relevant number of atoms at very low temperatures. Working in the low-temperature regime means that we restrict our study to low-energy properties only. Our aim is to describe this system in the formalism of quantized fields, or equivalently of second quantization. Within this view, we promote the classical hamiltonian (2.29) to an operator and, following standard results, we write it in the form:

$$\begin{aligned} H \ = \ & \int \Psi^\dagger(\mathbf{r}) \left( -\frac{\hbar^2}{2m}\nabla^2 + V_{per}(\mathbf{r}) + V_{ext}(\mathbf{r}) \right) \Psi(\mathbf{r})\, d^3r + \\ & \frac{1}{2}\int \Psi^\dagger(\mathbf{r})V_{int}(\mathbf{r} - \mathbf{r}')\Psi(\mathbf{r}')\, d^3r\, d^3r' \ , \end{aligned} \tag{2.32}$$

where $\Psi$ and $\Psi^\dagger$ are bosonic field operators satisfying the well known commutation relation

$$[\Psi(\mathbf{x}), \Psi^\dagger(\mathbf{y})] = \delta^{(3)}(\mathbf{x} - \mathbf{y}) \ . \tag{2.33}$$

In the same spirit of second quantization, they correspond to the atomic wave function. Trivial extensions to one-dimensional and two-dimensional systems can be obtained for the previous formulas.

We thus expand the boson operators $\Psi$ and $\Psi^\dagger$ with respect of the Wannier basis

$$\Psi(\mathbf{r}) = \sum_{n\mathbf{z}} w_n(\mathbf{r} - \mathbf{z})b_{n\mathbf{z}} \tag{2.34}$$

so that the operators $b_{n\mathbf{z}}$ are implicitly defined by the previous relation. The physical interpretation of these operators emerges naturally: they destroy particles in the valence band $n$ which are localized in

the domain of the corresponding Wannier function, that is, for the lowest band, approximately around the lattice site $\mathbf{z}$. When the external field is sufficiently weak and in the absence of band crossings, the band index $n$ can be taken to be a constant of the motion and, keeping only the lowest band, our expansion (2.34) can be simplified in

$$\Psi(\mathbf{r}) = \sum_{\mathbf{z}} w(\mathbf{r}-\mathbf{z}) b_{\mathbf{z}} \ . \tag{2.35}$$

This assumption needs an explanation: what we are really assuming is that the thermal (kinetic) and the trapping (magnetic) energies of a single particle be much smaller than the separation of the first exited band.

Inserting equation (2.35) into equation (2.32) we arrive at the expression for the hamiltonian in terms of $b$-operators:

$$H = \sum_{ij} J_{ij} b_i^\dagger b_j + \sum_{ij} \epsilon_{ij} b_i^\dagger b_i + \frac{1}{2} \sum_{ij} U_{ij} b_i^\dagger b_j^\dagger b_i b_j \ , \tag{2.36}$$

where the spatial variables $\mathbf{x}, \mathbf{y}, \mathbf{z}, \mathbf{r}, \mathbf{r}'$ have been replaced by lattice variables $i$ and $j$ and all the sums run over all (ordered) pairs of lattice sites. The coupling parameters are given by

$$J_{ij} = \int w^*(\mathbf{r}-\mathbf{r}_i) \left( -\frac{\hbar^2}{2m} \nabla^2 + V_{per}(\mathbf{r}) \right) w(\mathbf{r}-\mathbf{r}_j) \, d^3 r \ , \tag{2.37}$$

$$U_{ij} = \int |w(\mathbf{r}-\mathbf{r}_i)|^2 V_{int}(\mathbf{r}-\mathbf{r}') |w(\mathbf{r}'-\mathbf{r}_j)|^2 \, d^3 r \, d^3 r' \ , \tag{2.38}$$

$$\epsilon_{ij} = \int w^*(\mathbf{r}-\mathbf{r}_i) V_{ext}(\mathbf{r}) w(\mathbf{r}-\mathbf{r}_j) \, d^3 r \ . \tag{2.39}$$

There are two reasons to make an explicit distinction between $V_{per}$ and $V_{ext}$ in writing down the interaction couplings. The first is that we have done an operator expansion using the Wannier functions as a basis; this is equivalent to take the hamiltonian $\sum(\mathbf{p}^2/2m + V_{per})$ as the imperturbated hamiltonian and the hamiltonian $\sum(V_{ext} + V_{int})$ as the interaction hamiltonian, even if we are not trying to use perturbation theory, and Wannier functions are the eigenstates of the imperturbated hamiltonian. The second reason is that the two potentials have a different spatial behavior: the external one is slowly varying over the lattice constant. Finally, using relations (2.31, 2.33, 2.34), we obtain the commutation relations for the bosonic operators:

$$[b_i, b_j] = [b_i^\dagger, b_j^\dagger] = 0 \ , \tag{2.40}$$

$$[b_i, b_j^\dagger] = \delta_{ij} \ . \tag{2.41}$$

We now make some simplifying considerations. In equation (2.37) the parameters $J_{ij}$ are site dependent, since the integrand functions are. Recalling that Wannier functions go to zero essentially in a lattice spacing, we can restrict the effectiveness of this sum only to on-site terms and to nearest-neighbor ones. For the on-site terms we see that all of them are site-independent, due to the translational invariance of Wannier functions, thus we can set $J_{ii} \equiv \mu$. For the nearest-neighbor terms, by the same reason, we can set $J_{ij} \equiv -J/2$ with $i \neq j$.[5] The parameter $J$ is positive definite because the ground state must have zero quasi-momentum and this means that the Wannier function $w_0(\mathbf{r})$ is symmetric around $\mathbf{r} = 0$. Taking advantage of these results, the first term of (2.36) can be rewritten as

$$H_1 = -\frac{J}{2} \sum_{\langle ij \rangle} (b_i^\dagger b_j + b_j^\dagger b_i) + \mu \sum_i n_i \ , \tag{2.42}$$

where the first sum is over the set of lattice bonds, the second over all lattice sites and we have defined the local operator number $n_i = b_i^\dagger b_i$ in the usual way.

[5] The convention for the signs and the 1/2 factor in the definitions of the parameters $\mu$ and $J$ is chosen to make equation (2.46) consistent with the normalizations of Refs. [60, 61].

In equation (2.38) we take the interaction potential to be that described in Section 2.1.2 by equations (2.20, 2.21). Since it is short-ranged, all parameters $U_{ij}$ with $i \neq j$ can be set to zero, due to the very low overlap of the modulus squared of two nearest-neighbor Wannier functions, while the parameters $U_{ii}$ can be set equal to

$$U = g \int |w(\mathbf{r})|^4 \, d^3r \, , \tag{2.43}$$

taking advantage of translational invariance. Thus the last term of equation (2.36) can be rewritten as

$$H_3 = \frac{U}{2} \sum_i n_i(n_i - 1) \, , \tag{2.44}$$

where the sum is over the lattice sites and we have used the relation $b_i^\dagger b_i = b_i b_i^\dagger - 1$ to get rid of the noncommutativity of bosonic operators.

In equation (2.39) the external trapping potential, as already mentioned, is supposed to be weak; as usual Wannier functions are well localized and only $\epsilon_{ii}$ terms survive, leading to the definition

$$\epsilon_i = \int V_{ext}(\mathbf{r}) |w(\mathbf{r} - \mathbf{r}_i)|^2 \, d^3r \, \approx \, V_{ext}(\mathbf{r}_i) \, . \tag{2.45}$$

As a consequence of the properties of $V_{ext}$, also the quantities $\epsilon_i$ are slowly varying over the lattice spacing.

What we have done is essentially to neglect next-nearest-neighbor terms in the hopping term and to consider only on-site interaction terms. Both of these assumptions are legitimate if Wannier functions decay essentially over a lattice spacing and if the interaction among particles is short-ranged and negligible with respect to the first band gap.

Collecting all the previous simplifications, we see that our effective hamiltonian can be further reduced, taking the following form:

$$H = -\frac{J}{2} \sum_{\langle ij \rangle} (b_i^\dagger b_j + b_j^\dagger b_i) + \mu \sum_i n_i + \frac{U}{2} \sum_i n_i(n_i - 1) + \sum_i \epsilon_i n_i \, . \tag{2.46}$$

Equation (2.46) is the well known hamiltonian of the Bose-Hubbard model, which was originally introduced in 1989 by Fisher *et al.* [70] in order to investigate the onset of superfluidity in bosonic systems. A theoretical study of this model will be considered in Section 3.2.

### 2.2.2 Lattice structure

In an optical lattice the experimental parameters are those related to the characteristics of the lasers and can be summarized, for $d$-dimensional hypercubic geometries, in the intensity $V_0$ and the wavelength $\lambda$. It is common to introduce an energy scale of reference, called the *recoil energy*, through the definition

$$E_r = \frac{\hbar^2 k^2}{2m} \, , \tag{2.47}$$

which is equivalent to the energy gained by an atom which emits a photon of frequency $\nu = c/\lambda$. For rubidium atoms typical values of $E_r$ are in the range of several kilohertz.

The band structure of an optical lattice can be obtained from the solution of the one-dimensional Schrödinger equation which, for a sinusoidal potential, is known as the Mathieu equation.[6] In the weak potential limit $V_0 \ll E_r$ the eigenvalues depend critically on the quasi-momentum $q$ and the energy gap between the $n$th and $(n+1)$th bands scales as $V_0^{n+1}$. Thus a particle is very well approximated as a free particle and the influence of the periodic potential is negligible.

[6] Two-dimensional and three-dimensional sinusoidal simple cubic lattices are in our case fully separable. Therefore the wave functions can be calculated separately for each axis and the total energy is given by the sum of the eigenenergies of all axes.

In the deep potential limit $V_0 \gg E_r$ the eigenvalues of the lowest bands are only weakly dependent on the quasi-momentum. The matrix element $J$, which describes the tunnel coupling between neighboring lattice sites, is directly related to the width of the lowest energy band through the well known relation of solid state physics

$$J = \frac{\max[E(q)] - \min[E(q)]}{4} \tag{2.48}$$

and can also be given analytically as

$$J = \frac{8}{\sqrt{\pi}} E_r \left(\frac{V_0}{E_r}\right)^{4/3} \exp\left[-2\left(\frac{V_0}{E_r}\right)^{1/2}\right] . \tag{2.49}$$

The dynamics in this regime involve typically the lowest band and, as we saw in Section 2.2.1, the use of localized Wannier functions is appropriate. The confinement in a single site is approximately harmonic and atoms are then tightly confined at a single lattice site with trapping frequencies $\omega_0$ of up to 100 kHz. Expanding the periodic potential around one minimum we obtain $\hbar\omega_0 = 2E_r(V_0/E_r)^{1/2}$ and this value gives the the energy gap to the first exited band for deep lattices. Considering the repulsion constant $U$, if we approximate the exact Wannier function $w(\mathbf{r})$ of equation (2.38) with the gaussian ground state in the local oscillation potential around of the sites, we get

$$U = \sqrt{\frac{8}{\pi}} k a E_r \left(\frac{V_0}{E_r}\right)^{4/3} , \tag{2.50}$$

where $a$ is the scattering length in the $s$-wave. This approximation is supposed to improve as the lattice depth is increased since, being the atoms strongly confined, the local harmonic approximation becomes exact.

For generic values of the lattice parameters we can however use numerical method to solve the Mathieu equation to get the exact Wannier function and then use the definitions (2.37, 2.38) to obtain $J$ and $U$.

## 2.3 Bose-Einstein condensates in optical lattices

In the previous sections we discussed two of the most important achievements of modern low-temperature physics: Bose-Einstein condensation and optical lattices. In this section we will describe the new and fascinating aspects that can be observed by loading a condensate into a lattice potential. The main relevance for the present work is that a Bose-Einstein condensate in the presence of a periodic lattice potential makes it possible to realize the quantum phase transition from a superfluid to a Mott-insulating state [37] that will be the subject of subsequent chapters. A detailed discussion of the physical aspects of cold atoms and Bose-Einstein condensates in optical lattices is given in Refs. [15, 30, 109, 118, 119].

Standard ultracold atoms, as obtained simply from laser cooling, have temperatures of the order of the microkelvin and densities of $10^{10}\,\mathrm{cm}^{-3}$ whereas Bose-Einstein condensates have temperatures of the order of tens or hundreds of nanokelvin and densities of $10^{14}\,\mathrm{cm}^{-3}$. The most important consequence of this order-of-magnitude difference is that, when the condensate is loaded in the optical lattice, we end up with a system which typically is in the fundamental state and each lattice site is populated by a mean of one atom or even more; instead, with simple ultracold atoms, we will have lots of vacancies and a non-negligible population of high energy levels. Moreover the optical array of wells introduces a new length scale, namely the lattice spacing $d$, which is much smaller than the condensed cloud of atoms; in this way it is possible to get an array of weakly interacting (or isolate) microcondensates or to observe phenomena typical of solid state physics.

The interplay between optical lattices and Bose-Einstein condensates is of extreme importance also because it makes it possible to enter a really new regime of quantum physics where gases interact in a

strongly way. The defining properties of a gas are diluteness and absence of long-distance correlations. Of course these conditions are well satisfied for weakly interacting systems where the kinetic energy per particle is much bigger than the mean interaction energy. Starting from the pseudopotential description of Section 2.1.2, which replaces the complicated interatomic potential by an effective contact interaction of the form (2.20, 2.21), at a given density $n$ the importance of direct interaction effects can be estimated from the ratio

$$\gamma = \frac{E_{int}}{E_{kin}} = \frac{g\, n}{\hbar^2 n^{2/3}/m} \sim n^{1/3} a \; . \tag{2.51}$$

In typical gaseous conditions we have $\gamma = 0.02$ so that we safely are in the weak-coupling regime. If one tries to enter the strong-coupling regime varying the $\gamma$ parameter then correlations lead to the formation of clusters of interacting particles or molecules and eventually drive the system into the liquid or solid state, so that the properties of the original interactions among constituents are hidden in the new configuration. An obvious way to enter the strong-coupling regime is to increase the interaction energy using Feshbach resonances to make $a$ bigger. The main drawback of this method is the strong decrease of the life-time of the condensate which occurs at a rate

$$\frac{\dot{n}}{n} \propto -\frac{\hbar}{m}(na^2)^2 \tag{2.52}$$

due to three-body losses. A completely alternative route to the strong-coupling regime relies, instead of increasing the $E_{int}$ term, on decreasing the $E_{kin}$ term. From Section 2.2.2 we know that, when atoms move through an optical lattice, the quantity which is the analog of the kinetic energy is the hopping parameter $J$. Thus, using equations (2.49, 2.50), we obtain for the control parameter

$$\gamma = \frac{U}{J} \propto ka \exp\left[2\left(\frac{V_0}{E_r}\right)^{1/2}\right] \; . \tag{2.53}$$

We see that, as the potential depth $V_0$ is increased, the kinetic hopping energy of the atoms across the lattice is exponentially suppressed so that $\gamma$ can reach very high values, even in a dilute gas where $ka$ is very small.[7] Our conclusion is that the interplay of Bose-Einstein condensates and optical lattices creates the dynamical conditions where gaseous systems can exist in a strong coupling regime.

A typical experiment starts creating a Bose-Einstein condensate practically without any thermal component. Then an optical lattice in rumped up in the region of the condensate. Now, if the lattice is ramped up slowly enough, the wave function of the condensate remains in the many-body ground state of the system. Two timescales for adiabaticity are relevant [50, 91]: (*i*) adiabaticity with respect to the band population and (*ii*) adiabaticity with respect to the extension of the cloud. The final situation is that of an optical lattice loaded with neutral atoms in the fundamental state which are splitted all over the sites, where the atom number on each lattice site is of order unity. The typical observables which are used in experiments as signatures of the properties of the atoms loaded in the lattice are: (*i*) density distribution functions; (*ii*) momentum distribution functions; (*iii*) atom number statistics; (*iv*) energy gaps.

In Section 2.2.1 we discussed the limits in which this system realizes the Bose-Hubbard model. In Chapter 3 we will discuss in detail the phase diagram of the Bose-Hubbard model and we will show that a phase transition appears. Then, in subsequent chapters, we will analyze the influence of the trapping potential on the phenomenology of this transition, both at zero and finite temperature.

[7] For the typical conditions of ultracold atoms loaded in optical lattices, the interparticle spacing is of the order of the lattice constant, that is $k \sim n^{1/3}$, so that the dilute gas parameter is now $ka$.

# Chapter 3

# Quantum phase transitions

In this chapter we recall the general features of the theory of phase transitions, both at the classical and quantum level, with a special emphasis on scaling relations. Then we recall the main results about the Bose-Hubbard model, whose physical relevance has been demonstrated in Chapter 2, showing that a quantum phase transition is present in its ground state as the relative strength of the parameters $J$ and $U$ is varied. Finally we expose the theory of trap-size scaling, which will constitute the framework for the analysis of Chapters 4 and 5.

## 3.1 Thermal and quantum fluctuations

### 3.1.1 Classical scaling

We know that in classical statistical mechanics phase transitions occur when the partition function exhibits some non analyticity. Since a finite sum of analytic functions is always analytic, we can infer, from the form of the classical partition function, that phase transitions can occur only in the thermodynamic limit, when the number of degrees of freedom tends to infinity. In classical mechanics the ground state of the system, for a given set of the values of the parameters of the system hamiltonian, is the one corresponding to the zero-temperature state.[1] Choosing a suitable redefinition constant for the energy, we can set the energy of the ground state to zero. All the other states of the system then have a definite positive energy $E$ and, when the system is in thermal equilibrium at temperature $T$, the Boltzmann weight factor, proportional to the probability for the system to be in that particular dynamical state, is $\exp(-E/k_{\mathrm{B}}T)$. In the classical regime we consider typically hamiltonians with a microscopic ordering interaction, which naturally leads to the introduction of a physical observable, called *order parameter*, that quantifies the degree of order and marks the onset of the transition. In turn this offers the opportunities to define the correlation length, that is a measure of the distance over which the fluctuations of the order parameter are correlated. Phase transitions can then be divided in two fundamental classes: discontinuous and continuous phase transitions, depending on the behavior of the correlation length. Phase transitions at which the correlation length remains finite are called discontinuous while transitions where it diverges are called continuous.[2] In this case, which is the one we are going to treat, the order parameter vanishes continuously through a phase transition and its correlation length is divergent. Points at which a second order phase transition occurs are called *critical points*.

We see that there are two competitive mechanisms: the microscopic interaction, which tries to minimize the energy, and the thermal excitation, which tries to bring the system in states different from the lowest one. A natural picture for this situation is that in the low-temperature regime the interaction dominates, so that the system is in an ordered state, while at high temperatures thermal

[1] We assume that the fundamental state is unique and, in case of a spontaneous symmetry breaking, the degeneration is resolved in the thermodynamic limit by a very tiny external field coupled to the microscopic degrees of freedom.

[2] Another common nomenclature refers to discontinuous and continuous transitions respectively as first order and second order phase transitions.

effects lead to a statistical superposition, corresponding to disordered configurations. So we can infer that there is a value of the temperature at which the two mechanisms exactly balance, forcing the system into a unique critical phase where correlations diverge and the order vanishes, that is a continuous phase transition. The main lesson of the classical theory of phase transitions is that the origin of the phenomenon rests in the competition of an ordering interaction and a randomizing fluctuation.[3]

We now describe the phenomenology of a typical continuous phase transition [12]. Let us consider a thermodynamic system controlled by a single external field $H$ (for concreteness we can think to an uniaxial ferromagnet). The critical point is at $T = T_c$ and $H = 0$. Defining $t = T/T_c - 1$, a continuous phase transition, at $H = 0$ and for $|t| \ll 1$, is characterized by the divergence of the correlation length

$$\xi \sim |t|^{-\nu} \tag{3.1}$$

and the equilibration time

$$\tau \sim |t|^{-z\nu} \tag{3.2}$$

from which we derive the relation

$$\tau \sim \xi^z \ . \tag{3.3}$$

These equations define the experimental exponents $\nu$ and $z$, which are examples of critical exponents (see below). Thus, exactly at the phase transition point, the correlation length and the correlation time are infinite: this implies that fluctuations occur on all length and time scales. Near a continuous phase transition the behavior of a physical observable $O$ is typically expressed by a power function of the form $O \propto |\delta|^{-x}$, where $\delta$ is a generic dimensionless quantity which measures the distance from the critical point. The exponent $x$ is called *critical exponent*.[4] Finally the correlation function of the fundamental degrees of freedom takes the form

$$G(r) \propto \frac{e^{-r/\xi}}{r^{(d-1)/2}} \quad \text{for } \ T \neq T_c \ , \tag{3.4}$$

$$G(r) \propto \frac{1}{r^{d-2+\eta}} \quad \text{at } \ T = T_c \ . \tag{3.5}$$

Equations (3.4, 3.5) are supposed to be valid asymptotically, that is for $r \gg \xi$ and $r \gg a$ respectively, where $a$ is the lattice spacing. At $T_c$ the correlation function has a pure power-law decay behavior, which is consistent with the absence of any length scale, characterized by the new critical exponent $\eta$.

Systems whose correlations are infinite are termed to be scale-invariant since, if we look at them on a certain fixed scale and then we enlarge the system, we cannot see any difference: the system is self-similar. This implies that observable quantities must be homogeneous functions of the corresponding variables (homogeneous functions have no intrinsic scale). These considerations can be summarized in the homogeneity relation for the singular part of the free energy density:

$$F(t, H) = b^{-d} F(t b^{y_t}, H b^{y_H}) \ , \tag{3.6}$$

where $y_t$ and $y_H$ are two new critical exponents and $b$ is an arbitrary positive number. Equation (3.6) is valid as long as the system can be considered scale-invariant, that is as long as the observation scale $b$ is shorter than the correlation length. The scaling theory of critical phenomena asserts that the divergences responsible for the singular behavior of the system are determined only by the divergence of the correlation length: this fact is known as *scaling hypothesis*. It means that, close to the critical point, $\xi$ is the only relevant scale of the problem so that the only relevant configurations are those with long distance fluctuations. Therefore the physical properties must be unchanged if we rescale all

[3] This competition is quantified in the free energy $F = U - TS$, where $U$ is the internal energy and $S$ is the entropy: when the entropy of thermal fluctuations is sufficient to overcome their energy cost, $F$ can lower its value in correspondence to a disordered situation.

[4] With such a definition, the critical exponents of non singular quantities, quantities with a logarithmic divergence and with a peak-like singularity are zero.

lengths in the system by a common factor and at the same time adjust the external parameters in such a way that the correlation length retains its old value. This is equivalent to assume $|t\xi^{y_t}| \sim 1$, from which we deduce $\nu = 1/y_t$.[5] Finally, fixing the observation scale at the correlation length, that is fixing $b = \xi$, and substituting into equation (3.6), we get the well known Widom scaling law

$$F = |t|^{d\nu} \mathcal{F}(H|t|^{-\nu y_H}) \; . \tag{3.7}$$

The scaling hypothesis asserts that only the fluctuations at the longest possible scales are important for the critical behavior; in this way the physics at small lengths can be completely ignored in the study of criticality. This picture suggests that systems defined by different hamiltonians can lead to a common critical behavior, if long-scale fluctuations have the same structure. In practice this is demonstrated through a *course graining* transformation and in turn this gives a natural explanation of the concept of *universality*. On this basis a theory, called *renormalization group theory* [6, 8, 11], can be constructed and the values of the fundamental critical exponents ($y_t$, $y_H$) can be determined *ab initio* from the knowledge of the microscopic hamiltonian. Within the renormalization group framework, it is possible to associate a field theory to a given hamiltonian, that is the local degrees of freedom now become the continuous field of a new functional-action, which has the same long distance behavior. From the perspective of the scaling hypothesis, the critical aspects of a set of different hamiltonians are mapped onto a well defined field theory, which is thus the starting point for the renormalization group analysis.

### 3.1.2 Continuous quantum phase transitions

Let us now study phase transitions in the quantum regime [20]. The hamiltonian of our system will in general be expressed in terms of its dynamical variables, which define the Hilbert space, and one control parameter $\mu$, which sets the relative strength of two interaction terms (for concreteness we can think to a quantum uniaxial ferromagnet in a transverse field): the first term would lead to an ordered ground state with a non vanishing order parameter while the second would favor a disordered ground state, the two limiting cases corresponding to $\mu = 0$ and $\mu = \infty$. In these circumstances we expect that at some intermediate value $\mu_c$ of the control parameter a qualitative change in the fundamental state properties, for instance the long-distance correlations, must occur, that is we expect a phase transition at zero temperature. Since the existence of two competitive interactions has its origin in the fact that a quantum state which favor a type of interaction can be considered a superposition of states which favor the other, we say that the transition is driven by quantum fluctuations. This justifies the name of quantum phase transition for transitions occurring at zero-temperature. A quantum phase transition arises when a non analyticity of some sort appears: in this case the non analyticity regards the ground state energy (as a function of the control parameter).[6]

We now give a general description of the phenomenology of a continuous quantum phase transition [107, 108, 111]. When varying the control parameter $\mu$, we get the relative spectrum and ground state. For each of the ground states we can compute the correlation length and the value of a properly defined order parameter. Moreover the spectrum will be characterized by a typical energy scale $\Delta$, which can be the energy gap of the first exited level or the scale at which there is a qualitative change in the nature of the low and high frequency parts of the spectrum. A continuous quantum phase transition shows up as the vanishing of the order parameter and the divergence of the correlation length, the non analytic behavior corresponding to the vanishing of $\Delta$. Defining $\bar{\mu} = \mu - \mu_c$ , our considerations

[5] Many other relations among the critical exponents appearing in phenomenological laws and the two ($y_t$, $y_H$) which are defined by equation (3.6) can also be derived.

[6] This is completely similar to what happens in the classical theory, except the fact that now thermal fluctuations are substituted by quantum fluctuations and both of these effects are now encoded in the hamiltonian (before the classical hamiltonian encoded only the interaction while the classical partition function took care of thermal fluctuations).

can be summarized in the following equations:

$$\xi \sim |\bar{\mu}|^{-\nu} , \tag{3.8}$$

$$\Delta \sim |\bar{\mu}|^{z\nu} , \tag{3.9}$$

$$\Delta \sim \xi^{-z} . \tag{3.10}$$

In the two limits $\mu = 0$ and $\mu = \infty$ the exited states of the spectrum can be described as pseudoparticles and a perturbative treatment in the corresponding small expansion parameter is usually very useful; however the physical interpretations of these modes can differ considerably. Of course, near the critical point $\mu_c$, this picture breaks down and a new treatment for the strong coupling regime of the microscopic degrees of freedom is needed.

Let us examine the case of finite temperatures. First of all the new energy scale $k_B T$ given by the thermal excitation must be compared with the ground state scale $\Delta$: for $\Delta > k_B T$ only a few levels will be thermally populated while for $\Delta < k_B T$ a classical description of thermodynamics will in general be correct. These two energy scales naturally define a crossover line through

$$T \approx |\mu - \mu_c|^{z\nu} . \tag{3.11}$$

Turning to the important question of whether or not the $T = 0$ phase transition present at $\mu_c$ survives also at finite temperatures, we note that both situations can occur depending on the details of the system.

Let us discuss the nature of the fluctuations in the various region of the phase space. When the transition occurs only at zero-temperature, for $\mu < \mu_c$ and relative small values of $T$ (the so-called thermally disordered region), the order present in the ground state is destroyed by thermal fluctuations. In the symmetric regime for $\mu > \mu_c$ and relative small values of $T$ (the so-called quantum disordered region), the states involved resemble a ground state which already has no long-distance correlations and the absence of order is substantially due to quantum fluctuations. At $\mu = \mu_c$ the system is critical with respect to quantum fluctuations and turning on temperature will drive the system away from criticality. In the region of relative high temperature for values of the control parameter near to the critical one (the so-called quantum critical region), we get an involved situation where thermal activation of (quasi) critical quantum states are relevant: this mean that both quantum and thermal fluctuation are present and equally important.

When a transition line exists also at finite temperature, the preceding picture is still valid with the only change that the thermally disordered region is separated by the $T = 0$ ordered line by a thermally ordered region where the order parameter decreases as temperature is turned on, until it vanishes at the finite-temperature transition. We thus see that the $T > 0$ transitions must lie under the crossover line of the quantum critical region, since in the last no order is possible. Across these transitions we can assume, as usual, that a diverging correlation in space and time is present, described by $\xi$ and $\tau_c$, where $\tau_c$ is the typical time in which local microscopic changes are propagated across the system. This introduces a frequency $\omega_c = 1/\tau_c$ which can be turned into an energy scale, namely $\hbar\omega_c$, which is the typical energy of long-distance order parameter fluctuations. Now, for any transition occurring along the finite temperature line $T_c(\mu)$, quantum mechanics will become unimportant if $\hbar\omega_c \ll k_B T$. Since $\tau_c \to \infty$ at a phase transition, $\hbar\omega_c \to 0$ and the critical behavior, asymptotically close to the transition, will be described by the theory of classical fluctuations. Recalling the scaling behavior of $\tau$, we have $\hbar\omega_c \propto |t|^{z\nu}$ so that the asymptotic region of classical fluctuations is given by the condition $|t| < T_c^{1/z\nu}$. This justifies calling all finite-temperature phase transitions classical. Quantum mechanics can still be important on microscopic scales, but classical thermal fluctuations dominate on the macroscopic scales that control the critical behavior.

### 3.1.3 Classical-quantum mapping

A peculiar aspect of quantum phase transitions is that statics and dynamics are inextricably connected. In classical mechanics if we know the phase space and the form of the hamiltonian then we also know

the spectrum, that is the values that the energy can take. The classical partition function can thus be computed without solving the equations of motion for the dynamical variables. In quantum mechanics instead we have to solve the Schrödinger equation in order to get the eigenvalues and the eigenstates needed to compute the quantum partition function. Another way of stating this fact is that in classical mechanics the kinetic and potential energy terms commute so that the partition function factorizes while in the quantum case they are always coupled. The main consequence is that any energy scale $\Delta$ translates into a time $\hbar/\Delta$, which will appear as the characteristic time scale for the dynamics.

The quantum partition function can be written as

$$Z = \sum_n \langle n|e^{-\beta H}|n\rangle \ , \tag{3.12}$$

where $|n\rangle$ is a basis for the Hilbert space of the system. The operator density matrix $e^{-\beta H}$ is formally equivalent to the time evolution operator $e^{-i\mathcal{T}H/\hbar}$ if we assign to the real time the value $\mathcal{T} = -i\hbar\beta$. In this way it is possible, for example through the Feynman path-integral formalism, to map a $d$-dimensional quantum mechanical system at temperature $T$ to an appropriate $(d+1)$-dimensional classical model in which the extra dimension has length $\hbar\beta$. It is thus obvious that the quantum system at $T = 0$ is mapped onto the infinite classical system. A crucial point is that the temperature of the classical system corresponds to the control parameter of the quantum system while the temperature of the quantum system corresponds to the classical extent in the $(d+1)$th direction.

Taking advantage of these considerations, we can guess the scaling relations for a quantum phase transition both at zero-temperature and finite-temperature. At $T = 0$ the classical temperature maps to the control parameter $\mu$ while the system gets an extra dimension scaling with the dynamical exponent $z$ so that

$$F(\bar{\mu}, H) = b^{-(d+z)} F(\bar{\mu} b^{1/\nu}, H b^{y_H}) \ . \tag{3.13}$$

When the temperature is finite, it acts like a new relevant field with renormalization exponent $z$ so that our generalization reads

$$F(\bar{\mu}, H, T) = b^{-(d+z)} F(\bar{\mu} b^{1/\nu}, H b^{y_H}, T b^z) \ . \tag{3.14}$$

## 3.2 The Bose-Hubbard model

The hamiltonian of the Bose-Hubbard model is given in equation (2.46). In this section we consider the homogeneous (without trap) system, thus we neglect the $\epsilon_i$ term. The relevant physical aspects of this model, at $T = 0$, have been extensively investigated in the seminal paper by Fisher *et al.* [70]. We here recall the basic results, giving a brief summary of theoretical studies [20].

Let us discuss in more detail the qualitative meaning of the single terms of the hamiltonian, which are related to the three parameters $J, \mu, U$. The first term (the hopping term $J$) is the equivalent of a kinetic term and describes the tendency of particles to be delocalized over the lattice. In fact the diagonal matrix elements of this term in the basis of occupation numbers are clearly vanishing and, to get a nonzero (negative) contribution, we must consider a superposition of such states. The second term (the chemical term $\mu$) is connected with the mean occupation number of the lattice sites; working in this representation is equivalent to working in the grand canonical ensemble and the mean total particle number can be obtained by a Legendre transformation. The last term (the on site repulsive term $U$) is the simplest repulsion term and describes the tendency of particles to be pinned at a lattice site. We see that this term is diagonal in the basis of occupation numbers and it has a positive contribution proportional to the number of particles pairs present at the lattice site.

A useful starting point for the study of the quantum phase transition is to consider the opposite limits $J = 0$ and $U = 0$ and explicitly write down the quantum ground state of the model. Let us suppose we have $N$ atoms distributed in a lattice with $V$ sites and that $\bar{n} = N/V = 1$.[7] We number

[7] The following line of reasoning can be trivially extended to the cases of integer occupancy $\bar{n} = 2, 3, \ldots$.

atoms with a label $n$ and similarly we number lattice sites with a label $j$. Since we are working in the canonical ensemble, we neglect the $\mu$ term and the ground state must be expressed as a superposition of states with $N$ particles.

When $J = 0$ the ground state of the hamiltonian is the one where each lattice site has exactly one particle:[8]

$$\begin{aligned} |\mathrm{MI}\rangle &= \ldots |j_1\rangle_{n_1}|j_2\rangle_{n_2}|j_3\rangle_{n_3}\cdots + \ldots |j_1\rangle_{n_1}|j_2\rangle_{n_3}|j_3\rangle_{n_2}\ldots \\ &+ \ldots |j_1\rangle_{n_2}|j_2\rangle_{n_1}|j_3\rangle_{n_3}\cdots + \ldots |j_1\rangle_{n_2}|j_2\rangle_{n_3}|j_3\rangle_{n_1}\ldots \\ &+ \ldots |j_1\rangle_{n_3}|j_2\rangle_{n_2}|j_3\rangle_{n_1}\cdots + \ldots |j_1\rangle_{n_3}|j_2\rangle_{n_1}|j_3\rangle_{n_2}\cdots + \ldots \ . \end{aligned} \tag{3.15}$$

We see that in this state fluctuations in the occupation numbers are absent and the state is a pure Fock state. This implies that $|\mathrm{MI}\rangle$ describes and insulator. Upon increasing the hopping $J$, the ground state will no more be the state (3.15), since now atoms are allowed, even if weakly, to move across the lattice, thus causing double (or multiple) occupancy. In this state moving particles will walk only a few lattice sites and, until the repulsion energy $U$ dominates, the state will remain insulating; but, for a sufficient high value of $J$, for the system will be energetically favorable to delocalize the atoms all over the lattice. When $U = 0$ the ground state of the hamiltonian is then

$$\begin{aligned} |\mathrm{BEC}\rangle &= \ldots(\ldots|j_1\rangle_{n_1} + |j_2\rangle_{n_1} + |j_3\rangle_{n_1}\ldots) \\ &\quad \times(\ldots|j_1\rangle_{n_2} + |j_2\rangle_{n_2} + |j_3\rangle_{n_2}\ldots) \\ &\quad \times(\ldots|j_1\rangle_{n_3} + |j_2\rangle_{n_3} + |j_3\rangle_{n_3}\ldots)\ldots \ . \end{aligned} \tag{3.16}$$

Upon expanding out the products above, we see that the number of bosons in any given site fluctuates considerably, as demonstrated by the term $|j_1\rangle_{n_1}|j_1\rangle_{n_2}|j_1\rangle_{n_3}$ in which all three of the bosons $n_1, n_2, n_3$ are in the site $j_1$ and none in the sites $j_2$ or $j_3$. Finally, note that all terms in the state (3.15) are also present in the state (3.16): the difference between the two is that $|\mathrm{BEC}\rangle$ has many more terms present in its quantum superposition representing the number fluctuations.

In the thermodynamic limit the two fundamental states can be rewritten in terms of creation operators as

$$|\mathrm{MI}\rangle = \prod_{j=1}^{V} b_j^\dagger |0\rangle \ , \tag{3.17}$$

$$|\mathrm{BEC}\rangle = \prod_{j=1}^{V} \exp\left(\sqrt{N/V}\, b_j^\dagger\right)|0\rangle \ . \tag{3.18}$$

From these expressions we see that, both in the $J \to 0$ and $U \to 0$ limits, the ground state of the Bose-Hubbard model takes the form

$$|\mathrm{GS}\rangle = \prod_j \left(\sum_{n=0}^{\infty} c_n |n\rangle_j\right) \ . \tag{3.19}$$

Since the $c_n$ coefficients do not depend on the site $j$, our products have a local nature (which can also be used as the starting point for a variational approximation [29, 72]). The associated atom number probability distribution $p_n = |c_n|^2$ is either a pure Fock or a full Poissonian distribution. This dramatic change reflects the basically different nature of the superfluid and insulating phases. Since the compressibility $\kappa = \partial\rho/\partial\mu$ vanishes when passing from a superfluid to an insulator, a divergence is present in the observable $\kappa^{-1}$, marking the onset of a phase transition.

[8] Any one of the terms above suffices to describe the configuration of the particles in the ground state because the particles are indistinguishable and we can never tell which particular particle is residing in any given site: we need all the permutations simply to ensure that physical results are independent of our arbitrary numbering of the particles.

Let us now consider instead the case $\bar{n}$ is not an integer. For $J \gg U$ the states are still superfluid but, upon decreasing the value of this ratio, particles will tend be pinned at a particular lattice site. If $\bar{n}$ is slightly larger than an integer value then there will be a little number of particles which is free to move over the top of a substantially frozen background. For the situation in which $\bar{n}$ is slightly lower than an integer, the same argument applies to holes rather than particles. We conclude that for non-integer values of the density a superfluid state can exist also in the limit $J \to 0$.

The considerations made so far demonstrate the existence of a phase transition in the ground state of the Bose-Hubbard model and the more general analysis of the grand canonical ensemble leads to the phase diagram of figure 3.1. We now briefly describe its main physical features. For $J \gg U$ the system is a perfect Bose-Einstein condensate where all the atoms are in the Bloch $\mathbf{q} = \mathbf{0}$ state for any value of $\mu$. For $J = 0$ the system is a Mott-insulator whose number density is fixed by the chemical potential according to $n = \text{integer}[\mu/U] + 1$. As $J$ is increased at fixed $\mu$ (but $\mu \neq -nU$), the insulating state persists until the superfluid state is formed. The phase boundaries of this transition have the typical lobe-shape depicted in figure 3.1.

There are two qualitative different ways in passing from a superfluid to a Mott-insulator: either at constant density or at varying density. Increasing $J$ at a constant chemical potential corresponding to non-integer filling, the onset on superfluidity occurs at varying density and the mechanism at the origin is the following: when some sites are occupied by $n$ bosons and others by $(n + 1)$ bosons, the extra particle can hop around the lattice without energy cost condensing for arbitrarily small $J$. Instead, when increasing $J$ at a constant chemical potential corresponding to integer filling, the onset on superfluidity occurs at the tip of the Mott lobe and the density stays constant. In this case what drives the transition is not the appearance of new particles, which can hop around, but the fact that the large hopping coupling enables bosons to overcome the repulsion energy. This qualitative difference in the onset of superfluidity will be reflected in the different field theories which rule the scaling properties of the transitions.

Given the physical relevance, both theoretical and experimental, of a phase transition driven by the quantum nature of the interaction among particles, much effort has been devoted, even with computational simulations, to the study of this fascinating phenomenon [38, 39, 44, 63, 79, 80, 94, 95, 96, 97, 99, 100, 122]. However, we know that the natural physical conditions for investigating bosonic quantum particles are those where a confining potential is present. In this case, as we will describe in more detail in Section 3.3, the interplay of quantum degeneracy and confinment leads to a modified phenomenology, which is characterized by the coexistence of Mott-insulator and superfluid regions [33, 42, 43, 51, 52, 53, 54, 55, 56, 57, 58, 59, 93, 104, 123].

### 3.2.1 The hard-core limit

In this work we will not study the Bose-Hubbard model in its generality but we will focus on the so-called *hard-core* limit, that is the limit $U \to \infty$.[9] In this case the hamiltonian becomes

$$H = -\frac{J}{2} \sum_{\langle ij \rangle} (b_i^\dagger b_j + b_j^\dagger b_i) + \mu \sum_i n_i \ , \tag{3.20}$$

where now each density number operator $n_i$ can take only the values $0, 1$. The lattice degrees of freedom are still bosonic, in the sense that relation (2.40) still applies and that coniugate operators acting on different lattice sites still commute. But, in order to algebraically improve the hard-core constraint, the original commutation relation (2.41) for standard bosonic operators must be modified, and the new commutation relation now reads

$$[b_i, b_j^\dagger] = \delta_{ij}(1 - 2n_i) \ , \tag{3.21}$$

[9] The reason for this choice will be explained in Section 4.3.

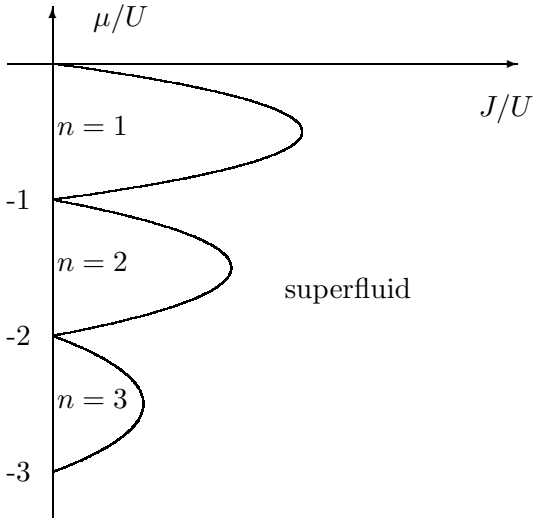


Figure 3.1: A qualitative sketch of the $T = 0$ phase diagram of the Bose-Hubbard model in the $\mu J$ plane (in units of $U$).

which applies to hard-core bosonic operators.[10]

Fixing the energy unit with $J$, the only control parameter for the system is the chemical potential $\mu$. It is possible to demonstrate that the hard-core Bose-Hubbard model is characterized by two quantum phase transitions at $\mu = +dJ$ and $\mu = -dJ$ from a superfluid to a Mott-insulator. When $\mu < -dJ$ the ground state is fully occupied so that $\langle n_i \rangle = 1$ while for $\mu > +dJ$ the ground state is completely empty so that $\langle n_i \rangle = 0$. We note that, through the change of variables

$$\sigma_i^x = b_i^\dagger + b_i \ , \tag{3.24}$$

$$\sigma_i^y = i(b_i^\dagger - b_i) \ , \tag{3.25}$$

$$\sigma_i^z = 1 - 2b_i^\dagger b_i \ , \tag{3.26}$$

where $\sigma^a$ are the usual Pauli matrices, the hamiltonian (3.20) becomes the hamiltonian of the so-called XX-model:

$$H_{\rm XX} = -J \sum_i \left( S_i^x S_{i+1}^x + S_i^y S_{i+1}^y \right) - \mu \sum_i S_i^z \ , \tag{3.27}$$

where $S_a = \sigma_a/2$.

These results hold in any dimension. In the one-dimensional case it is possible to solve exactly the model by the following method [20]. Applying the well know Jordan-Wigner transformation

$$\sigma_i^x = \prod_{j<i} (1 - 2c_j^\dagger c_j)(c_i^\dagger + c_i) \ , \tag{3.28}$$

$$\sigma_i^y = \prod_{j<i} (1 - 2c_j^\dagger c_j)(c_i^\dagger - c_i) i \ , \tag{3.29}$$

$$\sigma_i^z = 1 - 2c_i^\dagger c_i \ \ , \tag{3.30}$$

[10] The reason for this modification is due to the fact that the standard commutation relation allows the occupation numbers to be any non-negative integer. Instead, applying equation (3.21), we get

$$b_i b_j^\dagger - b_j^\dagger b_i = 0 \quad \text{for} \ \ i \neq j \ , \tag{3.22}$$

$$b_i b_i^\dagger + b_i^\dagger b_i = 1 \ . \tag{3.23}$$

The last "anticommutation" relation realizes the hard-core constraint.

$H_{\rm XX}$ becomes

$$H_c = \sum_i \left( -\frac{J}{2}(c_{i+1}^\dagger c_i + c_i^\dagger c_{i+1}) + \mu c_i^\dagger c_i \right) . \tag{3.31}$$

The new operators $c_i$, which are non-local combinations of the original degrees of freedom $b_i$, satisfy anticommutation relations, so that they support a fermion representation of the model. Furthermore these modes are easily seen to be spinless. In this representation the hamiltonian can be diagonalized by a standard Fourier transform of the fermionic variables:

$$\eta_k = \sum_j e^{-ikx_j} c_j . \tag{3.32}$$

The final result is

$$H_\eta = \sum_k \epsilon_k \eta_k^\dagger \eta_k , \tag{3.33}$$

where $\epsilon(k) = \mu - J\cos k$. In this way we see that the independent modes of the hard-core Bose-Hubbard model are the new $\eta$-pseudoparticles. Since the empty state has zero energy, the ground state is obtained by filling with unity occupation all the modes whose energy is negative. For $\mu > J$ the energy of all $\eta$-modes is positive and the ground state is empty: this is the Mott-insulator with $\bar{n} = 0$. For $\mu < -J$ all the fermions have negative energy and every fermion state is occupied: this is the Mott-insulator with $\bar{n} = 1$. At intermediate values of $\mu$ there will be a partial occupation.

We now compute the ground state density, which will be of great interest for the analyses of subsequent chapters. Recalling that in a homogeneous system $\rho = \langle n_i \rangle$ independently on the site $i$ and that $\langle b_i^\dagger b_i \rangle = (1 - \langle \sigma_i^z \rangle)/2 = \langle c_i^\dagger c_i \rangle$, we obtain

$$\rho(\mu) = \begin{cases} 0 & \text{for } \mu > 1 , \\ 1/\pi \arccos(\mu/J) & \text{for } -1 \le \mu \le 1 , \\ 1 & \text{for } \mu < -1 , \end{cases} \tag{3.34}$$

### 3.2.2 Quantum field theory of the Bose-Hubbard model

In view of future developments, we now consider the continuum field limit of the Bose-Hubbard model [20], which is given by

$$\mathcal{L} = K_1 \phi^* \frac{\partial \phi}{\partial \tau} + K_2 \left| \frac{\partial \phi}{\partial \tau} \right|^2 + K_3 |\nabla \phi|^2 + \bar{r} |\phi|^2 + u |\phi|^4 + \dots , \tag{3.35}$$

where $\phi(r, \tau)$ is a $c$-number field, the parameters $K_1, K_2, K_3, \bar{r}, u$ are complicated functions of the original system parameters and the dots represent higher order contributions which are irrelevant for the critical behavior. Equation (3.35) is valid in any number of dimensions and for any value of the system parameters while the operator $|\phi|^2$ is the continuum limit of the density number operator and $\bar{r} \sim (\mu - \mu_c)$.

Changing the hamiltonian parameters in a continuous way leads to a path in the system phase diagram. Sometimes this brings to points of non analyticity and this corresponds to a phase transition. Depending on the way the path is taken and the point is reached, the phase transition shows peculiar behaviors and the universal features are described by different effective continuum field theories. For the Bose-Hubbard model, as we have seen at the beginning of this section, there are two qualitatively distinctive ways of undergoing a phase transition: passing from a Mott insulating phase to the superfluid phase, the local density may change or stay constant at the insulator value. Phase transitions driven by the chemical potential are of course of the first type, since this implies a change in the density value. We now discuss the general results known for both types of transitions.

- The low-energy properties of the transitions driven by the chemical potential $\mu$ are described by a *non*-relativistic $U(1)$-symmetric bosonic field theory, whose relevant lagrangian density is given by

$$\mathcal{L} = \phi^* \partial_\tau \phi + \frac{1}{2m} |\nabla \phi|^2 + \bar{r} |\phi|^2 + u |\phi|^4 \ . \tag{3.36}$$

  The upper critical dimension of this bosonic theory is $d = 2$. Thus its critical behavior is mean field for $d > 2$. For $d = 2$ the field theory is essentially free, apart from logarithmic corrections, thus the dynamic critical exponent is $z = 2$ and the renormalization group dimension of the coupling $\mu$ is $y_\mu = 2$. In $d = 1$ the theory turns out to be equivalent to a free field theory of nonrelativistic spinless fermions, from which one infers the renormalization group exponents $z = 2$ and $y_\mu = 2$.

- The special transitions at fixed integer density, that is at fixed $\mu$, belong to a universality class described by a relativistic $U(1)$-symmetric bosonic field theory, whose relevant lagrangian density is

$$\mathcal{L} = |\partial_\tau \phi|^2 + v^2 |\nabla \phi|^2 + \bar{r} |\phi|^2 + u |\phi|^4 \ , \tag{3.37}$$

  for which $z = 1$ and $y_\mu = 1/\nu_{XY}$ where $\nu_{XY}$ is the correlation length exponent of the $D = d + 1$ XY universality class. Thus $\nu_{XY} = 1/2$ for $d = 3$, that is mean-field behavior apart from logarithms, $\nu_{XY} = 0.6717(1)$ in the $d = 2$ case and formally $\nu = \infty$ for the Kosterlitz-Thouless transition [34, 125] at $d = 1$.

We finally mention that the gapless superfluid phase is instead described by a free massless bosonic field theory with dynamical critical exponent $z = 1$ [8].

## 3.3 Trap-size scaling of quantum phase transitions

In this section we use the renormalization group theory to obtain an effective description of the scaling behavior of trapped bosonic particles, as described by the full Bose-Hubbard hamiltonian (2.46). We call such a description *trap-size scaling* since we will show that its predictions resemble some aspects of the well known theory of finite-size scaling [1, 4, 5]. The theory of trap-size scaling has been developed by Campostrini and Vicari [101] and applied by the authors to the study of quantum phase transitions, both in equilibrium [35, 60, 61] and off-equilibrium [62] conditions. Moreover, the theory has been used also for the study of phase transitions at finite-temperature, both in classical [36, 64] and quantum [66, 67, 81, 82] systems.

We start rewriting the last (trapping) term of equation (2.46) as

$$V(r) = v^p r^p \ . \tag{3.38}$$

We take the origin of coordinates in the zero of $V(r)$ so that the distance of site $i$ from the center of the trap is $r_i$. The exponent $p$ is clearly a positive number. The parameter $v$, which is related to the strength of $V(r)$, has units of energy divided the $p$th power of a length. The external potential can be recast in the form

$$V(r) = J \left( \frac{r}{l} \right)^p \ , \tag{3.39}$$

where we introduced the new parameter

$$l \equiv \frac{J^{1/p}}{v} \tag{3.40}$$

which has the dimension of length. The parameter $l$ will be called the *trap size*. The trapping potential (3.38), in the harmonic case, is conventionally expressed as $V(r) = \frac{1}{2} m \omega^2 r^2$, thus we get

$$l = \frac{1}{\omega} \sqrt{\frac{2J}{m}} = \gamma \frac{h}{m \omega \lambda} \ , \tag{3.41}$$

where, in the last equality, we used equation (2.47) and the relation between the coupling $J$ and the lattice depth $V_0$ (see Section II.B of Ref. [119]).[11] If we fix the unit of energy by setting $J = 1$ then $l = 1/v$.

Let us consider the case in which the system parameters are tuned to values corresponding to the critical regime of the unconfined system. In the presence of a confining potential, the critical behavior of the homogeneous (unconfined) system can be observed around the middle of the trap only in a window where the length scale $\xi$ of the critical modes is much smaller than the trap size, but sufficiently large to show the universal scaling behavior. If $\xi$ is large, but not much smaller than the trap size, the critical behavior gets somehow distorted by the trap, although it may still show universal effects controlled by the universality class of the phase transition of the unconfined system. The confining potential gives rise to a space inhomogeneity, thus changing the scaling behavior of the homogeneous system, which could be only recovered in the limit of large trap size (keeping fixed the other parameters of the system).

Our starting point is then a scaling Ansatz which includes all these ingredients and extends the scaling laws of homogeneous systems at quantum transitions to allow for the presence of a confining potential like (3.38). We write the scaling law of the singular part of the free energy density at the quantum transition as

$$F(\bar{\mu}, T, v, r) = b^{-(d+z)} F(\bar{\mu} b^{y_\mu}, T b^z, v b^{y_v}, r b^{-1}) \,, \tag{3.42}$$

where $b$ is again any positive number, $\bar{\mu} = \mu - \mu_c$ and $y_v$ is the renormalization group dimension of the trap parameter $v$. Repeating the steps of Section 3.1, we fix $v b^{y_v} = 1$ and introduce the trap size $l = v^{-1}$, obtaining the following quantum trap-size scaling

$$F = l^{-\theta(d+z)} \mathcal{F}(\bar{\mu} l^{\theta/\nu}, T l^{\theta z}, r l^{-\theta}) \,, \tag{3.43}$$

where as usual $\nu \equiv 1/y_\mu$ while $\theta \equiv 1/y_v$ is the new *trap exponent*.

The correlation length $\xi$ around the middle of the trap, or any generic length scale associated with the critical modes, behaves as

$$\xi = l^\theta \mathcal{X}(\bar{\mu} l^{\theta/\nu}, T l^{\theta z}) \,, \tag{3.44}$$

where $\mathcal{X}(y, 0) \sim y^{-\nu}$ for $y \to 0$. This implies that, at the $T = 0$ quantum critical point, the trap induces a finite length scale, given by $\xi \sim l^\theta$, which clarifies the physical meaning of the trap exponent. Analogously one can derive the trap-size scaling formulas of other observables. Any low-energy scale at $T = 0$, and in particular the gap, is expected to behave as

$$\Delta = l^{-\theta z} \mathcal{D}(\bar{\mu} l^{\theta/\nu}) \,, \tag{3.45}$$

with $\mathcal{D}(y) \sim y^{z\nu}$ for $y \to 0$ to match the scaling $\Delta \sim \bar{\mu}^{z\nu}$ in the absence of the trap. In the case of a generic local operator $O(r)$, with renormalization group dimension $y_o$, we expect that its expectation value and equal-time correlator behave as

$$\langle O(r) \rangle = \mathcal{A}(r, \mu, l, T) + l^{-\theta y_o} \mathcal{O}(\bar{\mu} l^{\theta/\nu}, T l^{\theta z}, r l^{-\theta}) \,, \tag{3.46}$$

$$\langle O(r) O(0) \rangle_c = l^{-2\theta y_o} \mathcal{G}(\bar{\mu} l^{\theta/\nu}, T l^{\theta z}, r l^{-\theta}) \tag{3.47}$$

where $\mathcal{A}$ is a possible analytic contribution.

The trap-size scaling has a high degree of generality: the trap-size exponent is determined only by the analytical shape of the external potential, the way it is coupled to the microscopic degrees of freedom and, of course, the universality class of the phase transition of the homogeneous system. Thus, let us compute the critical exponent $\theta$ for the case of the Bose-Hubbard model in a trapping potential. We recall that the low-energy properties of quantum phase transitions driven by the chemical

[11] The constant $\gamma$ is a slowly decreasing function of $V_0$: at $V_0 = 3E_r$ we get $c = 0.5$ and at $V_0 = 20E_r$ we have $c = 0.1$. For typical experimental values we get $l/d$ in the range 10 to 100, where $d = \lambda/2$ is the lattice spacing. As a reference, in the experiment reported in Ref. [37] we have $l/d = 20$.

potential, that is at varying density, are described by the lagrangian density (3.36) which represent a non-relativistic $U(1)$-symmetric bosonic field theory. Thus the corresponding renormalization group perturbation is

$$\int V(r)|\phi(r)|^2\, d^3r\, dt \tag{3.48}$$

where $\phi(r)$ is the order parameter of the corresponding $\phi^4$ theory. Using the well known relations between a scaling field and the corresponding operator

$$y_V + y_{|\phi|^2} = d + z\ , \tag{3.49}$$

$$y_\mu + y_{|\phi|^2} = d + z\ , \tag{3.50}$$

where $y_\mu$ and $y_V$ are the renormalization group dimensions of the coupling $\bar{r}$ which enters the lagrangian density (3.36) with the $\phi(r)$ term and of the trapping potential $V(r)$, we obtain

$$py_v - p = y_\mu\ , \tag{3.51}$$

where we have used the relation $y_V = py_v - p$ which relates the scaling exponents $y_v$, $y_V$ of the trap parameter $v$ and the trapping potential $V$. As a consequence, recalling the definition $\nu = 1/y_\mu$, for the Bose-Hubbard model we obtain

$$\theta = \frac{p\nu}{1 + p\nu}\ . \tag{3.52}$$

We observe that, as expected, in the $p \to \infty$ limit we get $\theta \to 1$, corresponding to confining the homogeneous system into a finite-size box of length $L = 2l$ with open boundary conditions. Moreover, recalling the positivity of $p$ and $\nu$, we see that $\theta$ is an increasing function of $p$ between the values 0 and 1.

Finally, we discuss the question of the robustness of the trap-size scaling with respect to a variation of the trapping potential from a simple power law. Considering for instance the potential

$$V(r) = \left(\frac{r}{l}\right)^p + c\left(\frac{r}{l}\right)^q\ , \tag{3.53}$$

where $c$ is a positive constant and $q > p$, we take the trap-size limit: $r, l \to \infty$ while keeping $R = r/l^\theta$ fixed (see Section 4.1.1). The resulting potential is thus

$$V(R) = \frac{R^p}{l^{p(1-\theta)}}\left(1 + c\,\frac{R^{q-p}}{l^{(1-\theta)(q-p)}}\right)\ . \tag{3.54}$$

We clearly see that in the trap-size limit, if $\theta < 1$ as in our case, the first term dominates over the second one. Of course this gives rise to scaling corrections, which turn out to be of order $O[l^{-(1-\theta)(q-p)}]$. We conclude that in the trap-size scaling the leading power is the smallest one and the relevant behavior is given by the small-$r$ form of the potential. In agreement with this, if we consider a harmonic confinement in the presence of a box – $V(r) = (r/l)^2 + (r/l)^q$ with $q \to \infty$ – it is clear that the leading term in the scaling behavior must be the quadratic one.

# Chapter 4

# Scaling of the Mott-insulator to superfluid transition

In this chapter we start to study the effects of a trapping potential on the phenomenology of continuous quantum phase transitions; in particular we consider the superfluid to Mott-insulator transitions of the hard-core Bose-Hubbard model (see Section 3.2). These issues have been analyzed in Refs. [60, 61] for the one dimensional system at $T = 0$, using the density matrix renormalization group technique. We now extend the study to the effects of finite temperatures considering the model in one and two dimensions near its quantum critical points. For this purpose we present the results of numerical quantum Monte Carlo simulations, whose details are reported in the Appendix. The content of this chapter is taken from Refs. [66, 67] and we here explicitly write the system hamiltonian:

$$H = -\frac{J}{2}\sum_{\langle ij\rangle}(b_i^\dagger b_j + b_j^\dagger b_i) + \mu\sum_i n_i + \sum_i V(r_i)n_i \ . \tag{4.1}$$

where, as usual, $V(r_i)$ is the external harmonic confinement and the values of $n_i$ are restricted to 0 and 1 only.

The phase diagram of the homogeneous system is reported in figure 4.1, both for the one-dimensional and two-dimensional case. We recall that for the one-dimensional model there are three phases at $T = 0$: two Mott-insulator phases for $\mu < -1$ (where $n = 1$) and $\mu > +1$ (where $n = 0$) which are separated by a superfliud region for $|\mu| < 1$; no phase transition is present for $T > 0$ and the system is a normal fluid. For the two dimensional model the $T = 0$ line is qualitatively analogous (with two Mott-insulator phases, for $\mu < -2$ where $n = 1$ and $\mu > +2$ where $n = 0$, separated by a superfliud region, for $|\mu| < 2$) but the superfluid phase also extends at finite temperatures and a phase transition from a superfluid to a normal fluid takes place. The superfluid phase is characterized by the dynamical

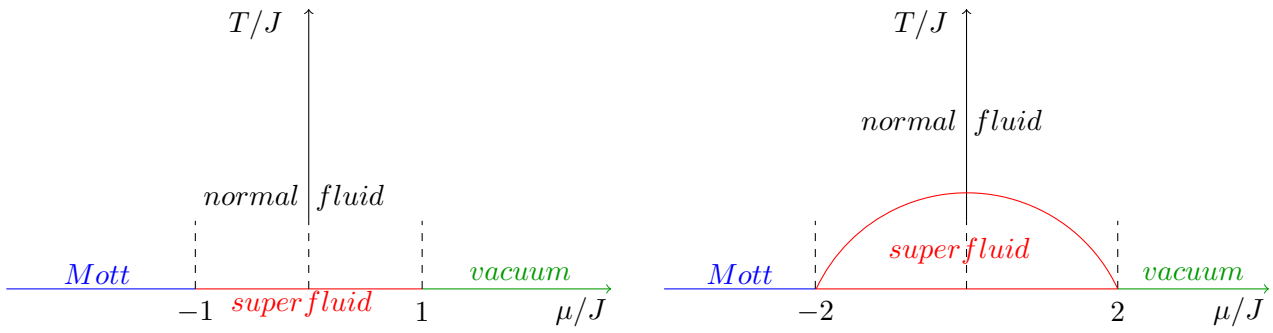


Figure 4.1: A qualitative sketch of the phase diagram of the hard-core Bose-Hubbard model in the $\mu T$ plane in one (left) and two (right) dimensions.

exponent $z = 1$. For the quantum transitions (both at positive and negative chemical potential) we have $z = 2$ and $\nu = 1/2$. Finally, specializing equation (3.52), the trap exponent for these transitions (driven by the chemical potential) is

$$\theta = \frac{p}{2+p} \ . \tag{4.2}$$

We want to investigate the existence of a non trivial trap-size limit as the confining potential is removed and the system approaches its $T = 0$ transition points. To this end, look at the path taken following the dashed lines of figure 4.1: it never intercepts a phase transition; this is achieved tuning the chemical potential at the fixed critical values $\mu_c$ of the unconfined systems and letting the temperature vary. Strictly speaking, we will simulate the trapped system: as the temperature is decreased, the trap size $l$ is increased so that, in this way, we can approach in a smooth fashion the critical points (on the $T = 0$ axis) of the superfluid to Mott-insulator transitions. Thus, we can study the interplay of thermal and quantum fluctuations in the quantum critical region described in Section 3.1.2.

We focus our attention on two standard observables: the particle density profile and the density-density correlation function. They are defined as follows:

$$\rho(\mathbf{x}) \equiv \langle n_{\mathbf{x}} \rangle \ , \tag{4.3}$$

$$G(\mathbf{x}, \mathbf{y}) \equiv \langle n_{\mathbf{x}} n_{\mathbf{y}} \rangle - \langle n_{\mathbf{x}} \rangle \langle n_{\mathbf{y}} \rangle \ , \tag{4.4}$$

where $\mathbf{x}$ and $\mathbf{y}$ are the coordinates of lattice sites. The scaling relations for the singular part of the free energy density, for the density and for the density-density correlation function are[1]

$$F(\mu, T, l, \mathbf{x}) = g_{\mathrm{reg}}(\mathbf{x}) + l^{-\theta(d+z)} \mathcal{F}(\bar{\mu} l^{\theta/\nu}, T l^{\theta z}, \mathbf{x} l^{-\theta}) \ , \tag{4.5}$$

$$\rho(\mathbf{x}) = f_{\mathrm{reg}}(\mathbf{x}) + l^{-d\theta} \mathcal{D}(\bar{\mu} l^{\theta/\nu}, T l^{z\theta}, \mathbf{x} l^{-\theta}) \ , \tag{4.6}$$

$$G(\mathbf{x}, \mathbf{y}) = l^{-2d\theta} \mathcal{G}(\bar{\mu} l^{\theta/\nu}, T l^{z\theta}, \mathbf{x} l^{-\theta}, \mathbf{y} l^{-\theta}) \ , \tag{4.7}$$

where, in agreement with standard theoretical results [12], $g_{\mathrm{reg}}(\mathbf{x})$ and $f_{\mathrm{reg}}(\mathbf{x})$ are supposed to be regular (analytic) functions.[2]

Equations (4.5, 4.6, 4.7) are our trap-size scaling predictions: they relate the behavior of our observables for different values of the system parameters. More precisely, considering the system at $T = 0$, the free energy density, depending on the rescaled coordinate $\mathbf{x} l^{-\theta}$, is a function of the variable $\bar{\mu} l^{\theta/\nu}$ only. Analogously, considering the homogeneous system at criticality ($\bar{\mu} = 0$), the free energy density depends only on the combination $\tau = T l^{z\theta}$. Similar considerations also apply to $\rho$ and $G$. Specializing equations (4.5, 4.6, 4.7) to the proper values of $d, z, \theta$ (recalling that $\nu$ and $p$ enter through $\theta$) of the different transitions will lead to a series of specific scaling predictions. In the following we will demonstrate that these predictions show a very good agreement with our numerical simulations.

## 4.1 One-dimensional model

### 4.1.1 Analytic results

In the presence of an external coupling potential, the one-dimensional hard-core Bose-Hubbard model, following the same steps of Section 3.2.1, can be mapped into

$$H_c = \sum_{ij} c_i^\dagger h_{ij} c_j \ , \tag{4.8}$$

[1] All scaling relations are written neglecting contributions from irrelevant scaling operators and corrections of higher order in $l^{-\theta}$.

[2] In deriving equations (4.6, 4.7) from equations (3.46, 3.47) we used the renormalization group dimension $y_\rho = d$ for the particle density operator.

where

$$h_{ij} = \delta_{ij} - \frac{1}{2}\delta_{i,j-1} - \frac{1}{2}\delta_{i,j+1} + [\bar{\mu} + V(x_i)]\delta_{ij} \tag{4.9}$$

with $\bar{\mu} \equiv \mu - 1$. In the fermion representation this hamiltonian can be easily diagonalized by introducing new canonical fermionic variables $\eta_k = \sum_i \phi_{ki} c_i$ , where $\phi$ satisfies the equation

$$\sum_j h_{ij}\phi_{kj} = \omega_k \phi_{ki} \ , \tag{4.10}$$

obtaining $H_c = \sum_k \omega_k \eta_k^\dagger \eta_k$.

We now discuss in more detail our knowledge of the ground state. Since the $\eta$-modes are fermionic and without spin, for each pair of values of the parameters $\mu$ and $l$, the ground state is obviously obtained filling all levels with a negative energy $\omega_k < 0$. The number of filled energy levels is designed with $N$. Using the unitarity of the Jordan-Wigner transformation, we can see that the number $N$ of $\eta$-excitations is also the number of bosonic $b$-particles present in the chain. In case $\omega_k > 0$ for all states, the ground state is obviously the vacuum state with no excitation. When a specific $\omega_\kappa$ equals zero, we have a degeneration, since the state with all negative levels filled and the state which also has $\langle \eta_\kappa^\dagger \eta_\kappa \rangle = 1$ have the same energy.

The picture which in general emerges is thus the following. For a fixed value of $\mu$ we have an infinite set (labelled by $k$) of increasing energy levels $\omega_k(l)$ which depends on the trap size $l$. Removing the trapping potential, the particle number will tend to the homogeneous limit so that, in the partially or totally filled phases (that is for $\mu < 1$) where the ground state has a finite density, we get $N \to \infty$ (because of the previous relation among $b$-bosons and spinless $\eta$-fermions). It is now clear that, in the $l \to \infty$ limit, an infinite number of $\omega_k(l)$ must pass from positive values to negative ones, since only in this way the corresponding level in the ground state can be populated. But this implies that, for a fixed $k$ value, there must be a specific value of $l$ for which $\omega_k(l) = 0$. When this happens we say that a level crossing has verified: we stress that level crossing is essentially related to the fact that the particle number is conserved even in the presence of the trap.[3]

Let us now consider a fixed value of $\mu$ and start from a value of $l$ such that $\omega_k(l)$ is negative for $k < \kappa$ and positive otherwise. Increasing $l$ will shift the energy spectrum until $\omega_\kappa$ will equal zero. When this happens, the gap vanishes, the ground state is doubly degenerate and a level crossing has taken place. In general we denote the values of $l$ at which the gap vanishes by $l_0^{(k)}$ with $k = 1, 2, \ldots$. This implies

$$l = l_0^{(k)} \Leftrightarrow \omega_k(l) = 0 \ . \tag{4.11}$$

Further increasing $l$, we note that $\omega_\kappa(l)$ becomes more and more negative, thus raising the gap, while the smallest positive eigenvalue $\omega_{\kappa+1}(l)$ progressively moves to zero, where the next level crossing will take place, thus lowering the gap: it is then clear that this competition will lead to a value of $l_{\rm peak}$ where the energy gap is maximum and level crossings of the lowest states occur in the $\mu l$ plane separating the regions with $N = k$ and $N = k + 1$. In general we denote the values of $l$ at which the gap is maximum by $l_{\rm peak}^{(k)}$ with $k = 1, 2, \ldots$. Consequently we have

$$l = l_{\rm peak}^{(k)} \Leftrightarrow \omega_{k-1}(l) + \omega_k(l) = 0 \ . \tag{4.12}$$

Until now all considerations have been general and no approximation has been assumed. We now take the continuum limit setting $\phi_k(x) \equiv \phi_{kx}$ and rewriting equations (4.9, 4.10) as

$$\phi_k(x) - \frac{1}{2}\phi_k(x+1) - \frac{1}{2}\phi_k(x-1) + [\bar{\mu} + V(x)]\phi_k(x) = \omega_k \phi_k(x) \ . \tag{4.13}$$

[3]The phenomenon of level crossing has emerged in a natural way looking at the fermionic spinless description, but we know from the general theory that a level crossing can occur when the hamiltonian can be written as $H = H_0 + gH_1$, where $H_0$ and $H_1$ commute while $g$ is a parameter. In this case the eigenvalues depend on $g$ while the eigenvectors do not. The trapped Bose-Hubbard model falls under this condition since the number operator, which is the $H_1$ part of the total hamiltonian, commutes with the remaining part $H_0$, while $\mu$ plays the role of the $g$ parameter.

By expressing the discrete differences in terms of derivative expansions we obtain

$$\left[\bar{\mu} + \left(\frac{x}{l}\right)^p - \sum_{m=1}^{\infty} \frac{1}{(2m)!} \frac{d^{(2m)}}{dx^{(2m)}}\right] \phi_k(x) = \omega_k \phi_k(x) \ , \tag{4.14}$$

where we used the parity properties of the Taylor series coming from equation (4.13).[4] Introducing the rescaled quantities

$$X = x l^{-p/(2+p)} \ , \quad \mu_r = \bar{\mu} l^{2p/(2+p)} \ , \quad \Omega_k = \omega_k l^{2p/(2+p)} \ , \tag{4.15}$$

and then neglecting terms which are suppressed in the large-$l$ limit, we arrive to the equation

$$\left(-\frac{1}{2}\frac{d^2}{dX^2} + X^p\right) \varphi_k(X) = e_k \varphi_k(X) \ , \tag{4.16}$$

where $e_k \equiv \Omega_k - \mu_r$ and $\varphi_k(X) \equiv \phi_k(l^{p/(2+p)}X)$. These results make it possible to define the trap-size limit. Equation (4.16) is a Schrödinger-like equation which formally involves no parameter related to the system: we say it is universal. The trap-size limit is consequently defined as the limit in which $l \to \infty$ while all the other scaling quantities, like the coordinate $X$, the eigenenergies $e_k$ and the rescaled chemical potential $\mu_r$, stay constant.[5] Using the result (4.2), we infer the behavior $\mu_r = \bar{\mu} l^{2\theta}$ and $X = x l^{-\theta}$ for the control parameter of the transition and the rescaled coordinate: thus the predictions of trap-size scaling fully coincide with the analytical results (4.15).

In view of subsequent analyses, we now specialize the solutions of equation (4.16) to the cases of the harmonic trapping potential and the hard-wall limit.

- In the case of a harmonic potential ($p = 2$) we have $\theta = 1/2$ and

$$\begin{aligned} e_k &= 2^{1/2}(k + 1/2) \qquad k \geq 0 \ , \\ \varphi_k(X) &= \frac{2^{1/8} H_k(2^{1/4}X)}{\pi^{1/4} 2^{k/2} (k!)^{1/2}} \exp(-X^2/\sqrt{2}) \ , \end{aligned} \tag{4.17}$$

  where $H_k(x)$ are Hermite's polynomials.

- In the case of the hard-wall limit ($p \to \infty$) equation (4.16) becomes equivalent to the Schrödinger equation of a free particle in a box of size $L = 2l$ with boundary conditions $\varphi(-1) = \varphi(1) = 0$ so that $\theta = 1$ and

$$\begin{aligned} e_k &= \frac{\pi^2}{8}(k+1)^2 \qquad k \geq 0 \ , \\ \varphi_k(X) &= \sin\left[\frac{\pi}{2}(k+1)(X+1)\right] \ . \end{aligned} \tag{4.18}$$

Until now we considered only the $T = 0$ ground state. We are going to extend these results to the case of finite temperatures. The fermion two-point function, according to the rules of statistical quantum mechanics, is given by the standard average

$$\langle c_x^\dagger c_y \rangle = \sum_{ab} \phi_{ax} \phi_{by} \langle \eta_a^\dagger \eta_b \rangle = \sum_{k=0}^{\infty} \frac{\phi_{kx}\phi_{ky}}{1 + \exp(\omega_k/T)} \ . \tag{4.19}$$

[4] The smoothness hypothesis underlying the continuum limit requires that only functions with a slowly varying behavior on the scale of the lattice spacing $d$ are relevant: this is equivalent to having functions with a Fourier spectrum whose non-zero components satisfies $k < 1/d$.

[5] For this we must impose $\bar{\mu} \to 0$ (that is $\mu \to 1$) and $\omega_k \to 0$: these requirements consistently select the superfluid to vacuum transition.

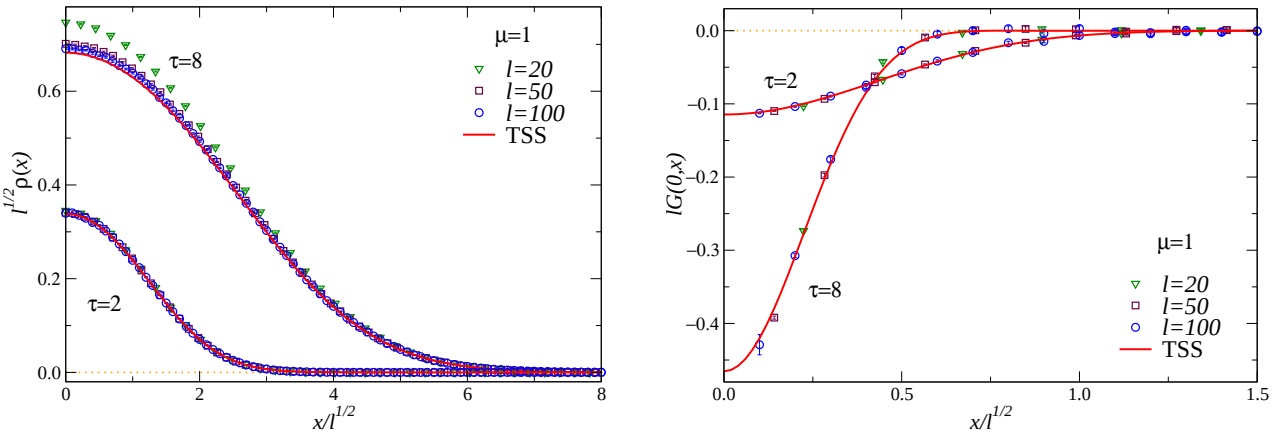


Figure 4.2: The particle density (left) and the density-density correlator (right) in the presence of a harmonic potential at $\mu = +1$ for some values of the trap size $l$ at $\tau = 2$ and $\tau = 8$ with $\tau \equiv Tl$. The full lines show the trap-size scaling functions.

Its trap-size scaling limit can be written in terms of the eigensolutions of equation (4.16) as

$$\langle c_x^\dagger c_y \rangle = l^{-\theta} \sum_{k=0}^{\infty} \frac{\varphi_k(X)\varphi_k(Y)}{1+\exp[(e_k+\mu_r)/\tau]} \,, \tag{4.20}$$

where we have introduced the scaling variable

$$\tau \equiv T l^{2\theta} \,, \tag{4.21}$$

since in this case $z = 2$ while $\theta$ still depends on $p$. Then straightforward calculations allow us to obtain

$$\rho(x) = l^{-\theta} \mathcal{D}(\bar{\mu} l^{2\theta}, T l^{2\theta}, x l^{-\theta}) \,, \tag{4.22}$$

$$\mathcal{D}(\mu_r, \tau, X) = \sum_{k=0}^{\infty} \frac{\varphi_k(X)^2}{1+\exp[(e_k+\mu_r)/\tau]} \,, \tag{4.23}$$

and

$$G(x,y) = l^{-2\theta} \mathcal{G}(\bar{\mu} l^{2\theta}, T l^{2\theta}, x l^{-\theta}, y l^{-\theta}) \,, \tag{4.24}$$

$$\mathcal{G}(\mu_r, \tau, X, Y) = -\left[ \sum_{k=0}^{\infty} \frac{\varphi_k(X)\varphi_k(Y)}{1+\exp[(e_k+\mu_r)/\tau]} \right]^2 \,, \tag{4.25}$$

which holds for $x \neq y$.[6] The above scaling functions describe the asymptotic large trap-size behavior and corrections are suppressed by a further $l^{2\theta}$ power. Practically exact results for the trap-size scaling functions of the harmonic potential and the hard-wall limit, for any $\mu_r$ and $\tau$, can be easily obtained using equations (4.17, 4.18) because the series are rapidly converging. We observe that our computation naturally leads to results of the form (4.6, 4.7) for the density and the density-density correlation function, from which we can infer $f_{\rm reg} \equiv 0$.

### 4.1.2 Low-density transition

As already mentioned, in order to verify the correctness of the trap-size scaling theory, we must simulate systems for some values of the parameters which make the arguments of the scaling functions stay constant. For this purpose we rewright equations (4.6, 4.7) as

$$l^{1/2}\rho(x) = \hat{\mathcal{D}}(Tl, X) \,, \tag{4.26}$$

$$lG(0,x) = \hat{\mathcal{G}}(Tl, X) \,, \tag{4.27}$$

[6] Note that $G(x,y) < 0$ for $x \neq y$ but $G(x,x) \equiv \langle n_x^2 \rangle - \langle n_x \rangle^2 > 0$ and indeed $\sum_{xy} G(x,y) > 0$.

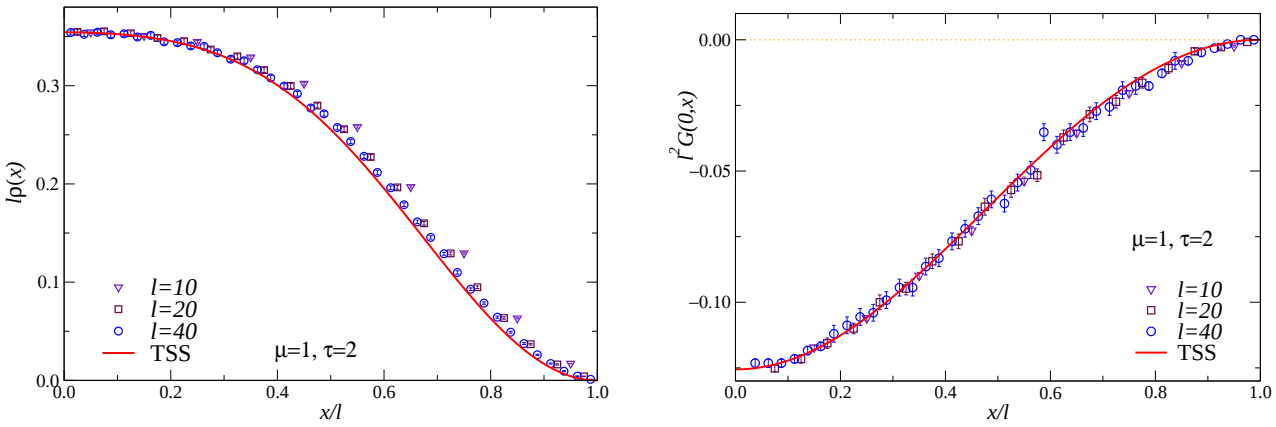


Figure 4.3: The particle density (left) and the density-density correlator (right) in the limit $p \to \infty$ at $\mu = +1$ for some values of the trap size $l$ at $\tau = 2$ with $\tau \equiv Tl^2$. The full lines show the trap-size scaling functions.

where we used the values $\theta = 1/2$ for the harmonic potential and $z = 2$, $X = xl^{-1/2}$ is the scaling coordinate and for the density-density function we considered only the correlation with the center of the trap. We thus see that the constraint on the scaling variable $\tau = constant$ now reads $Tl = constant$.

In figure 4.2 we show the behavior of the density profile and the correlator plotted against the analytic prediction: it is apparent that, apart from scaling corrections for low values of $l$, the data nicely collapse on a universal curve, thus demonstrating the correctness of trap-size scaling for the neighborhood of this transition.

To further check the theory, we considered the hard-wall limit. This limit is obtained with the substitution $p \to \infty$ in equation (3.52) which sets $\theta = 1$. Since still $z = 2$ at the low-density transition, simulations are made at $Tl^2 = constant$. In figure 4.3 we show that the agreement with the analytic prediction still persists also in the hard-wall limit.

### 4.1.3 Local density approximation

Before discussing the behavior of the superfluid and the $n = 1$ Mott phases in the presence of the trap, we address the important question of the *local density approximation*. Since in these phases we know that, even in the large-$l$ limit, a non zero filling contribution arises, a nontrivial influence of the mean density on the transition is expected.

Let us consider a homogeneous system whose ground state density as a function of a certain parameter (in our case the chemical potential $\mu$) is known. Turning on a local interaction, we want to obtain the ground state density profile in the new context. When the external coupling is slowly varying, we expect to get a slowly varying density profile too. We assume that the region around a certain point is characterized by a substantially constant density whose mean value depends on how strong is the potential in that neighborhood. The final result is that the local region we are focusing on is equivalent to a locally homogeneous system whose mean density is not given by $\mu$ only but also by the value of the external interaction. On these footings the local density approximation estimates the density at position $x$ in a trapped system as the density of the unconfined one provided with an effective chemical potential given by

$$\mu_{\rm eff}(x) \equiv \mu + \left(\frac{x}{l}\right)^p . \tag{4.28}$$

The local density approximation of the particle density thus reads

$$\langle n_x \rangle_{\rm LDA} \equiv \rho_{\rm LDA}(xl^{-1}) = \begin{cases} 0 & \text{for } \mu_{\rm eff}(x) > 1 , \\ 1/\pi \arccos \mu_{\rm eff}(x) & \text{for } -1 \le \mu_{\rm eff}(x) \le 1 , \\ 1 & \text{for } \mu_{\rm eff}(x) < -1 , \end{cases} \tag{4.29}$$

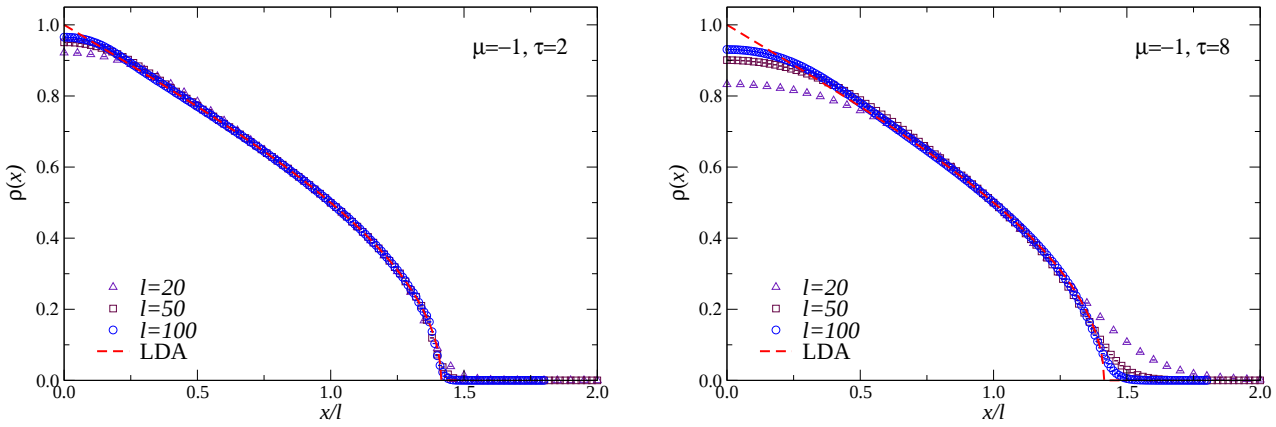


Figure 4.4: The particle density at $\mu = -1$ in the presence of a harmonic potential for some values of the trap size $l$ at $\tau = 2$ (left) and $\tau = 8$ (right) with $\tau \equiv Tl$.

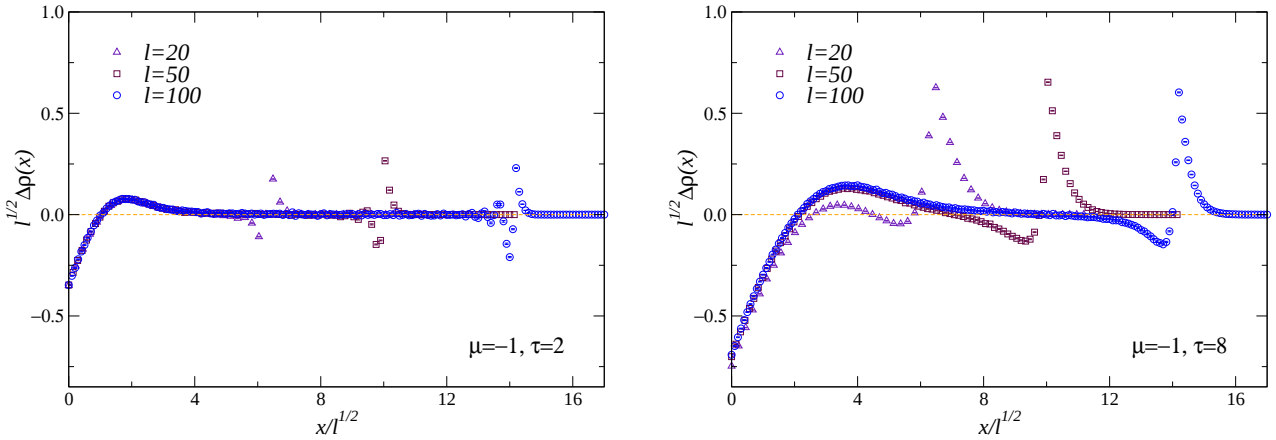


Figure 4.5: The subtracted particle density at $\mu = -1$ in the presence of a harmonic potential for some values of the trap size $l$ at $\tau = 2$ (left) and $\tau = 8$ (right) with $\tau \equiv Tl$.

Equation (4.29) makes it possible to obtain an insight into the particle distribution of the inhomogeneous system. We see that in a region near the center of the trap things are not very much distorted and a substantially homogeneous filling is expected. At fixed $\mu$, starting from the origin, we have a density which equals the one of the homogeneous system and moving outwards we see a decrease until zero. This would imply the presence of a plateau at $n = 1$ when $\mu_{\text{eff}} \leq -1$ for $x \leq l(-1-\mu)^{1/p}$ and a vanishing particle density when $\mu_{\text{eff}} \geq 1$ for $x \geq l(1-\mu)^{1/p}$.

We want to study the emergence of criticality as we remove the trapping potential and to this end we must take the $l \to \infty$ limit. We first observe from equation (4.6) that only the analytic contribution $f_{\text{reg}}(x)$ in this case survives. Moreover, working at fixed $\tau$, implies $T \to 0$ so that the particle density should approach the $T = 0$ result. It has been verified that, for the one dimensional system, the $T = 0$ density in the trap-size limit is exactly given by (4.29); thus we conclude that $f_{\text{reg}}(x) = \rho_{\text{LDA}}(x/l)$.

### 4.1.4 Mott insulator to superfluid transition at $n = 1$

We recall that the quantum critical behavior around $\mu = -1$ of the homogeneous hard-core Bose-Hubbard model without trap is essentially analogous to that at $\mu = +1$ because of the invariance under the particle-hole exchange. At the $n = 1$ Mott-insulator to superfluid transition the critical exponents $\nu$ and $z$ and the trap-size exponent $\theta$ are the same as those at for $\mu = +1$ and consequently simulations have been made keeping $Tl = constant$. However the particle-hole symmetry does not hold in the presence of the trapping potential and the asymptotic trap-size dependence at $T = 0$

appears more complicated at the $n = 1$ Mott transition, the main difference being the existence of a non zero analytic contribution to the particle density.

In figure 4.4 we can see that the trapped model at $\mu = -1$ indeed approaches its local density approximation in the large-$l$ limit but there are corrections that are suppressed as the trap size increases and, as we will show below, present a nontrivial trap-size scaling behavior. In two regions differences from a pure local density approximation are observed: near the origin, where the observed density is less than the expected one, and near the point $x = \sqrt{2}l$, where peculiar peaks arise. In the $l \to \infty$ limit the peaks disappear, living only the profile close to the center of the trap. We will study the criticality around the peaks in the following Section 4.1.5 and we now analyze the particle density near the origin.

The scaling laws for the density and the correlator which we derive putting the critical exponents for the present case are

$$l^{1/2}\Delta\rho(x) = \hat{\mathcal{D}}(Tl, X) \ , \tag{4.30}$$

$$lG(0, x) = \hat{\mathcal{G}}(Tl, X) \ . \tag{4.31}$$

where $X = xl^{-1/2}$ and $\Delta\rho \equiv \rho - \rho_{\rm LDA}$ is the subtracted density and corresponds to the scaling part of the particle density. In figure 4.5 we show how these relations are nicely verified.

In Ref. [60] it was observed that the spatial dependence of the particle density and its correlator turns out to be described by the following scaling behavior at large trap size:

$$\rho(x) = \rho_{\rm LDA}(xl^{-1}) + l^{-\theta} f(X, \phi) \ , \tag{4.32}$$

$$G(0, x) = l^{-2\theta} g(X, \phi) \ , \tag{4.33}$$

where $X = xl^{-\theta}$ while $f$ and $g$ are universal scaling functions. The phase-like variable $\phi$ measures the distance from the closest even level crossing and is defined as $\phi = (l - l_0^{(k)})/(l_0^{(k+1)} - l_0^{(k)})$. An interesting question is whether this scenario persists at finite temperature, where the effects of the level crossings of the lowest states are expected to be weaker. The same figures 4.4 and 4.5 give a clear evidence that trap-size scaling is fully verified, in its simplest form without periodic corrections, for the finite temperature one-dimensional hard-core Bose-Hubbard model. In particular we conclude that the modulation phenomenon observed at zero temperature, due to an infinite number of level crossings, is effectively averaged out by thermal fluctuations.

In order to further verify the trap-size scaling theory, we considered the hard-wall limit ($p \to \infty$ and $\theta = 1$). Simulations are made with the scaling variable fixed to $\tau \equiv Tl^2 = constant$ (recall $z = 2$). Moreover, since $V(x) = 0$ in all the sites, we get $\rho_{\rm LDA} = 1$. In figure 4.7 we show that also for the $\mu = -1$ transition the theory is in good agreement with numerical results.

Finally we mention that there is an unexpected similarity between the scaling of the $\mu = +1$ and $\mu = -1$ correlation functions. In fact the functions of $\mu = -1$ collapse on the same analytic curves of $\mu = +1$ and this can be considered a manifestation of the old (homogeneous) particle-hole symmetry.

### 4.1.5 Superfluid phase

We now analyze the trap-size dependence within the gapless superfluid phase, whose corresponding continuum theory is a conformal field theory with $z = 1$. We stress that no phase transition is expected to be seen and we are only testing how the predictions of trap-size scaling can be generalized. The asymptotic behavior within the superfluid phase turns out to be characterized by two length scales with different power-law divergence in the large trap-size limit [60]: the first scales as $\xi \sim l$ ($\theta = 1$) and describes the behavior of observables related to smooth modes, such as the half-lattice entanglement; the second scales as $\xi \sim l^{p/(1+p)}$ ($\theta = p/(p+1)$) and it is found in observables involving the modes at the Fermi scale $k_F = \pi f$, where $f$ is the filling of the homogeneous system.

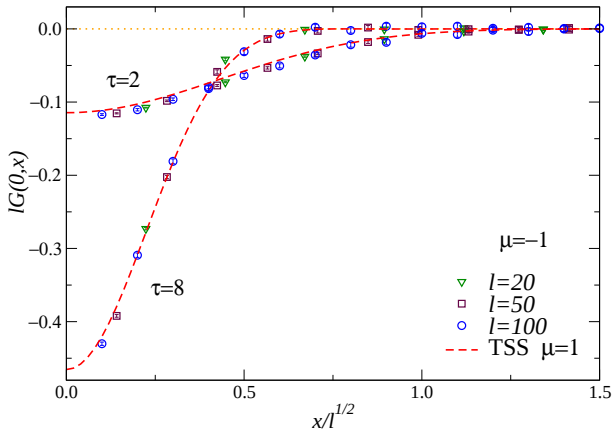


Figure 4.6: The density-density correlator in the presence of a harmonic potential at $\mu = -1$ for some values of the trap size $l$ at $\tau = 2$ and $\tau = 8$ with $\tau \equiv Tl$. The full lines show the trap-size scaling functions.

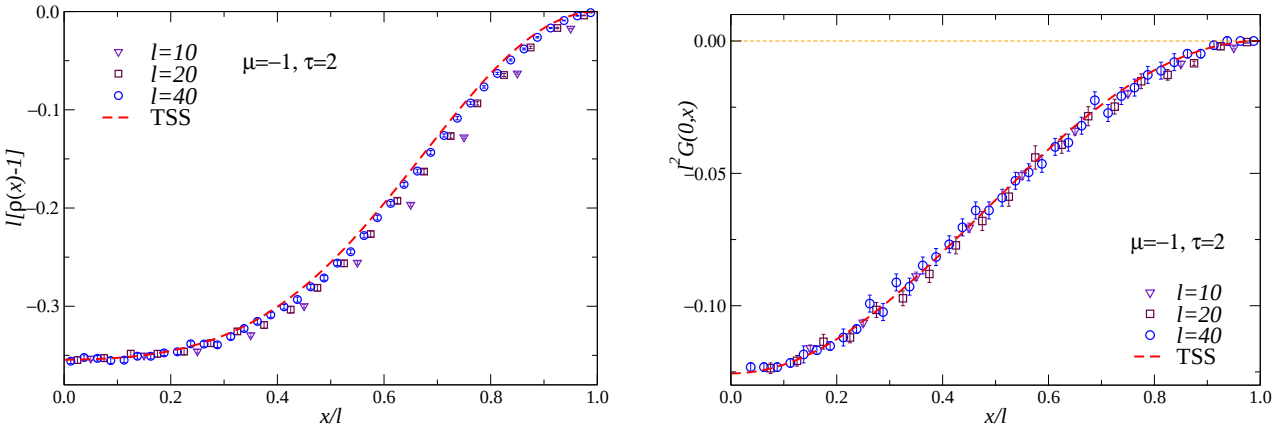


Figure 4.7: The particle density (left) and the density-density correlator (right) in the limit $p \to \infty$ at $\mu = -1$ for some values of the trap size $l$ for $\tau = 2$ with $\tau \equiv Tl$. The full lines show the trap-size scaling functions.

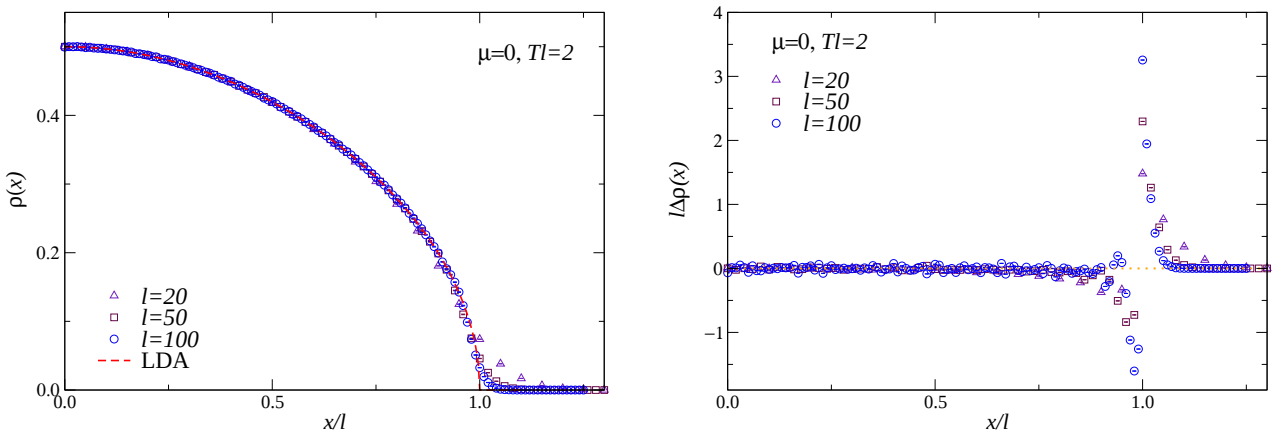


Figure 4.8: The particle density (left) and the subtracted density (right) in the presence of a harmonic potential at $\mu = 0$for some values of the trap size $l$ at $\tau = 2$ with $\tau \equiv Tl$.

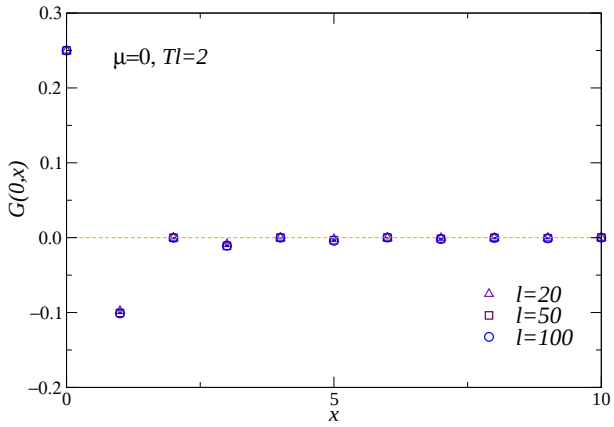


Figure 4.9: The density-density correlator in the presence of a harmonic potential at $\mu = 0$ for some values of the trap size $l$ at $\tau = 2$ with $\tau \equiv Tl$.

In figure 4.8 we show results for the particle density and various values of the trap size with $Tl = 2$. We choose this scaling of the temperature because the trap exponent associated with the smooth modes is expected to be $\theta = 1$. The main feature of the results is that they are clearly converging toward the corresponding local density approximation. Only around $x = l$ we observe some significant differences which decrease with increasing $l$. Finally, we see that the density-density correlator does not show any evidence of scaling and it vanishes in a few lattice spacing.

We now study the origin of the transition-like peaks we found in figures 4.5 and 4.8. When $\mu < 1$, the region where the particle density appears to rapidly vanish corresponds to the region where the effective chemical potential $\mu_{\rm eff}(x) = \mu + V(x)$ approaches the value $\mu_{\rm eff} = 1$, which is the value of the chemical potential corresponding to the transition between the superfluid phase and the empty state, where the particle density of the ground state gets suppressed. We thus expect that, for generic values of $\mu$ and $p$, the region around $x_c = l(1-\mu)^{1/p}$, where $\mu_{\rm eff}(x_c) = 1$, develops critical modes related to the superfluid to vacuum transition. Substituting $\mu = -1$ and $\mu = 0$ into the expression for the critical distance $x_c$ we obtain respectively $x_c = \sqrt{2}l$ and $x_c = l$, which are in perfect agreement with the observed pictures. The effective chemical potential can be expanded around $x_c$ as

$$\mu_{\rm eff}(x) = 1 + p(1-\mu)^{1-1/p}\,\frac{x - x_c}{l} + O[(x-x_c)^2]\,. \tag{4.34}$$

Therefore the behavior around $x_c$ is essentially analogous to that arising at $\mu = +1$ in the presence of a linear potential $V_l \sim (x - x_c)/l$. This means that the effective critical exponents, even in this superfluid phase, should be $z = 2$ and $\nu = 1/2$. Around $x_c$ the trap exponent governing critical modes, putting $p = 1$ into equation (3.52), turns out to be $\theta = 1/3$. We then expect that around $x = x_c$

$$l^{1/3}\Delta\rho(x) = \hat{\mathcal{D}}(Tl^{2/3}, Y)\,, \tag{4.35}$$

$$l^{2/3}G(x_c, x) = \hat{\mathcal{G}}(Tl^{2/3}, Y)\,, \tag{4.36}$$

where $Y = (x - x_c)l^{-1/3}$. Figure 4.10 fully supports this scenario, as expected without evidence of modulations, both because of finite-temperature effects and because of the relationship with the low-density transition.

## 4.2 Two-dimensional model

In this section we analyze the scaling behavior of the two-dimensional hard-core Bose-Hubbard model at finite temperature in a neighborhood of the two Mott-insulator to superfluid phase transitions at $\mu = +2$ and $\mu = -2$. The analyses of this section will closely follow those of Section 4.1. We saw in Section 4.1.1 that for the one-dimensional system the particle density and the density-density correlator

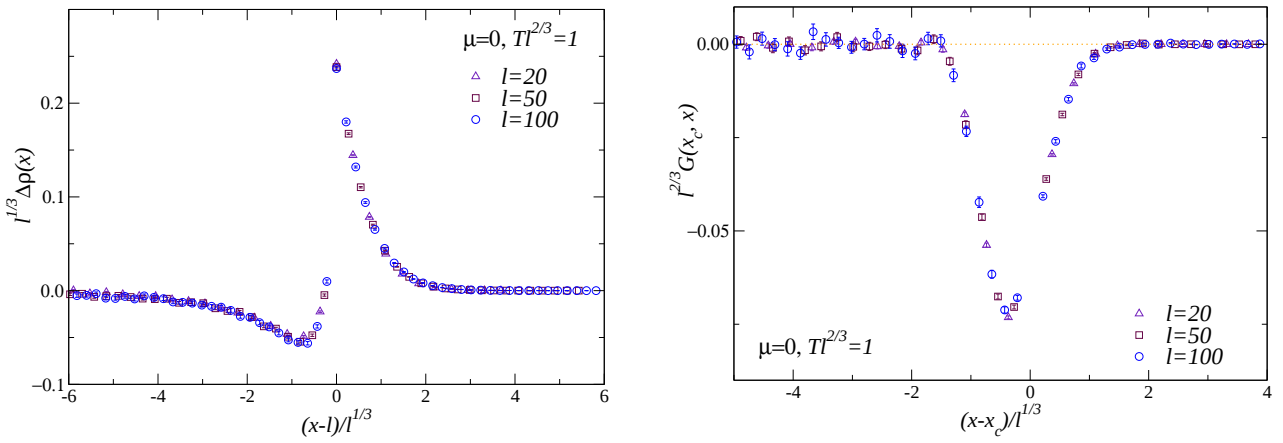


Figure 4.10: The particle density (left) and the density-density correlator (right) in the presence of a harmonic potential at $\mu = 0$ for some values of the trap size $l$ near $x_c$ at $\tau \equiv Tl^{2/3} = 1$.

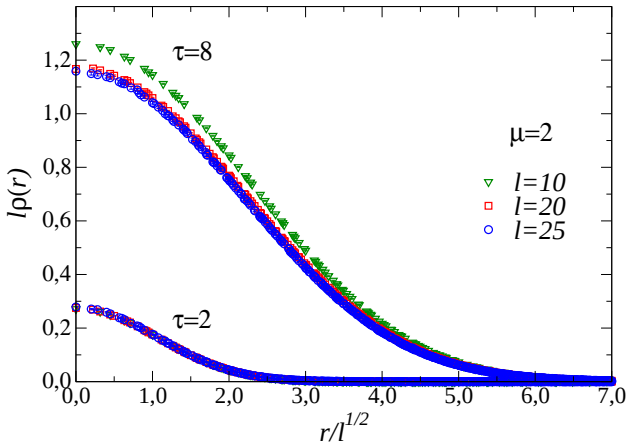


Figure 4.11: The rescaled particle density at $\mu = +2$ with $\tau = 2$ and $\tau = 8$ where $\tau \equiv Tl$ for different values of the trap size $l$.

could be treated analytically, both at zero and finite temperature, so that numerical outcomes could be compared with their analytical values. Instead, for the two-dimensional case, no exact solution is available and we must completely rely on numerical results.

### 4.2.1 Low-density transition

We start with the results for the superfluid to vacuum transition where the density vanishes. Since we are dealing with a two-dimensional system where the external potential has a radial symmetry, our scaling relations involving only one coordinate will be functions of $r = |\mathbf{x}|$. After setting $d = 2$, introducing the scaling coordinates $R = rl^{-\theta}$, $\mathbf{X} = \mathbf{x}l^{-\theta}$, $\mathbf{Y} = \mathbf{y}l^{-\theta}$ and considering the system at criticality ($\bar{\mu} = 0$), equations (4.6) and (4.7) can be rewritten as

$$l^{2\theta}\rho(r) = \hat{\mathcal{D}}(\tau, R) \,, \tag{4.37}$$

$$l^{4\theta}G(\mathbf{x}, \mathbf{y}) = \hat{\mathcal{G}}(\tau, \mathbf{X}, \mathbf{Y}) \,, \tag{4.38}$$

being $\tau \equiv Tl^{2\theta}$ the scaling variable that controls the critical behavior of the system (recall $z = 2$ for this transition). Simulations at $\tau = constant$ are performed working at fixed $Tl$ since the presence of a quadratic $p = 2$ confinement implies $\theta = 1/2$. For the scaling of the density we put the analytical contribution to zero because, if the local density approximation is correct, as we expect from the one-dimensional case, then $f_{\rm reg}$ must vanish also in two dimensions.

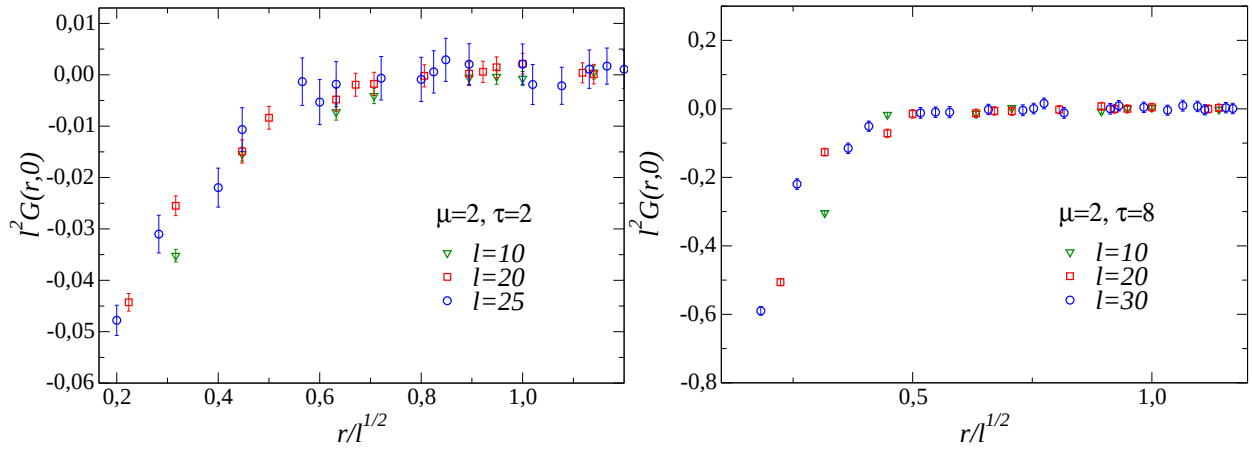


Figure 4.12: The density-density correlator at $\mu = +2$ with $\tau = 2$ (left) and $\tau = 8$ (right) where $\tau \equiv Tl$ different values of the trap size $l$.

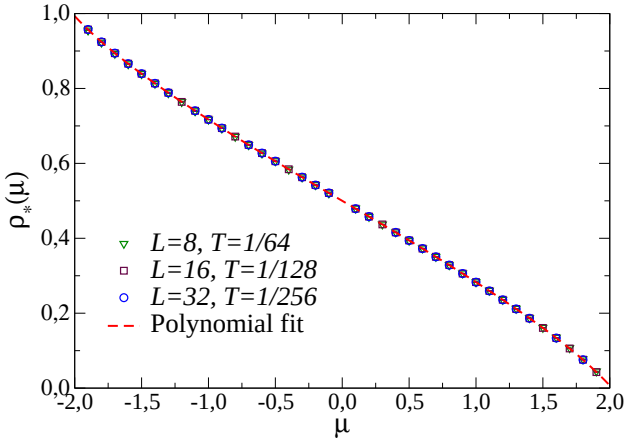


Figure 4.13: Numerical outcomes for $\rho_*(\mu)$ vs. $\mu$ for different values of the lattice extent $L$ and temperature $T$: data were collected in the homogeneous system with periodic boundary conditions. The dotted line represents the polynomial fit of the data corresponding to the larger extent.

Figure 4.11 shows the rescaled particle density. Data in it are divided into two groups corresponding to simulations performed with fixed $\tau = 2$ and $\tau = 8$. Since $\tau \equiv Tl$ and since the values of $l$ are essentially the same in both groups, sets with $\tau = 2$ are generally related to lower temperatures than those with $\tau = 8$. While the latter shows scaling corrections at small $l$, it is evident that the former have a more pronounced tendency to collapse on a universal curve. This comes with no surprise, since universality is a feature appearing in proximity of a phase transition, which occurs at $T = 0$ when working with chemical potential fixed at $\mu = +2$ as in the present case.

Figure 4.12 contains the rescaled density-density correlator at fixed $\tau = 2$ and $\tau = 8$ as a function of $R$. In this case we are considering the correlation with the center of the trap so that $G(r, 0) = l^{-4\theta}\hat{\mathcal{G}}(\tau, R)$. In analogy with the particle density, also for this observable, numerical outcomes after the prescribed rescaling display a tendency to collapse on a unique curve when increasing $l$, in agreement with the Ansatz in equation (4.38). Once again, corrections can be noticed only at small values of the trap size.

### 4.2.2 Local density approximation

Throughout the study of the Bose-Hubbard model, the local density approximation has played a dominant role, both for $T = 0$ and for $T > 0$. In the previous cases analytical results were obtained and this was heavily used in extracting the scaling part of observables whose behavior would be otherwise

obscured by the leading non-critical order. For the present two-dimensional situation, however, exact results are not available and so, to proceed further, we are forced to consider numerical simulations in order to test to which extent the reliability of the local density approximation works also in the two-dimensional case at finite $T$.

In analogy with the one-dimensional model, we assume that the local density approximation of the two-dimensional trapped system equals

$$\rho_{\rm LDA}(r) = \begin{cases} 0 & \text{for } \mu_{\rm eff}(r) > 2 \ , \\ \rho_*(\mu_{\rm eff}) & \text{for } -2 \leq \mu_{\rm eff}(r) \leq 2 \ , \\ 1 & \text{for } \mu_{\rm eff}(r) < -2 \ , \end{cases} \tag{4.39}$$

where $\rho_*(\mu)$ is the unknown $T = 0$ density of the two-dimensional homogeneous system provided with a given value of the chemical potential $\mu$. In order to obtain an estimate for $\rho_*(\mu)$, we performed simulations of the two-dimensional system without the trap and with periodic boundary conditions, since this is expected to reduce finite-size corrections, in the low-temperature regime for different values of the chemical potential. In particular we employed a set of equally-spaced values covering the range from $-2$ to $+2$. This setup is easily obtained by setting to zero the trap parameter $v$ in our quantum Monte Carlo code and by implementing the specific topology, all other features of the simulation remaining the same.

More specifically, we performed simulations with $L = 8$ at $T = 1/64$, with $L = 16$ at $T = 1/128$ and with $L = 32$ at $T = 1/256$, being $L$ the extent of a square lattice. Following the same criteria of [75], we checked that the data were consistent within errorbars so that we could safely assume that the results at $T = 1/256$ correspond effectively to the zero-temperature values. Figure 4.13 displays $\rho_*(\mu)$ for the three sets of simulation parameters mentioned above: data basically overlap.

Finally, we fitted the $T = 1/256$ outcomes to a generic polynomial function of degree $n$:

$$\rho_*(\mu) = \sum_{i=0}^{n} c_i \, \mu^i \ , \tag{4.40}$$

where $n$ was chosen by truncating this Taylor expansion when the $\chi^2$ of the fit stabilized. This was the case with $n = 7$ (the reduced $\chi^2$ being approximately 1.5), though truncations at higher order were also considered without showing meaningful deviations. As expected on theoretical grounds, it turned out that the constant term $c_0$ read $1/2$ (within $10^{-7}$) while even terms were negligible; thus, the only non-trivial contributions are given by the odd powers for which the following estimates were obtained:

$$\begin{aligned} c_1 &= -0.20779(1) \quad , \ c_3 = -0.01323(1) \\ c_5 &= +0.00441(1) \quad , \ c_7 = -0.00093(1) \ . \end{aligned} \tag{4.41}$$

The function in equation (4.40) with $n = 7$ and coefficients as given above is plotted in figure 4.13 and was used for the data analysis reported in the following sections.

### 4.2.3 Mott-insulator to superfluid transition with $n = 1$

As in one dimension, the invariance under the particle-hole exchange entails a similar behavior of the homogeneous model at the transitions with $\mu = +2$ and $\mu = -2$. However the trap-size scaling at the $n = 1$ transition is expected to be different than in the superfluid to vacuum one because the particle-hole symmetry does not hold for a trapped system.

In analogy with the previous results for the one-dimensional system, we expect the density profile to approach in the large-$l$ limit its local density approximation, so that ($\theta = 1/2$ and $z = 2$)

$$\begin{aligned} \rho(r) &= \rho_{\rm LDA}(rl^{-1}) + l^{-d\theta}\hat{\mathcal{D}}(Tl^{\theta z}, rl^{-\theta}) \ = \\ &= \rho_{\rm LDA}(rl^{-1}) + l^{-1}\hat{\mathcal{D}}(Tl, R) \ , \end{aligned} \tag{4.42}$$

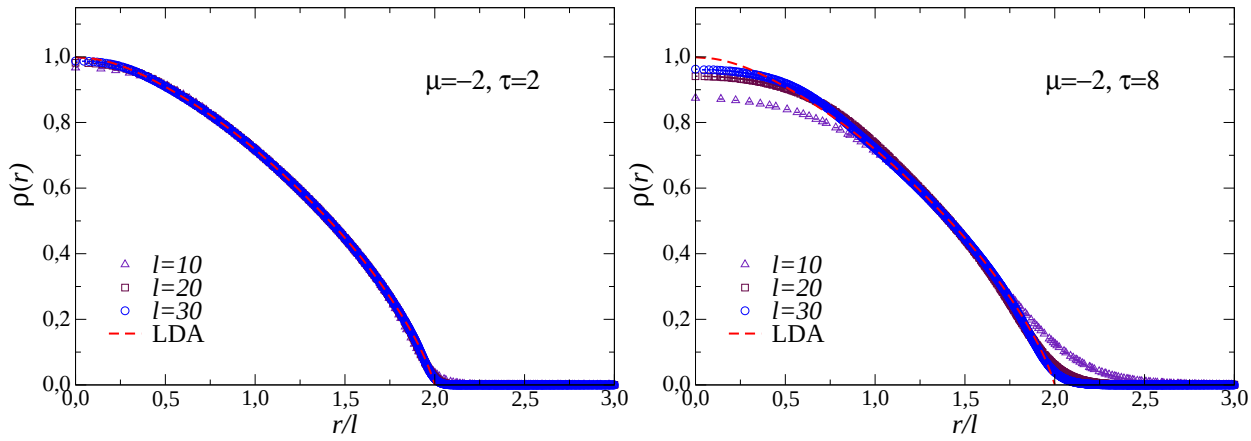


Figure 4.14: The particle density at $\mu = -2$ with $\tau = 2$ (left) and $\tau = 8$ (right) where $\tau \equiv Tl$ for different values of the trap size $l$. The dotted line shows the numerical estimates of the local density approximation.

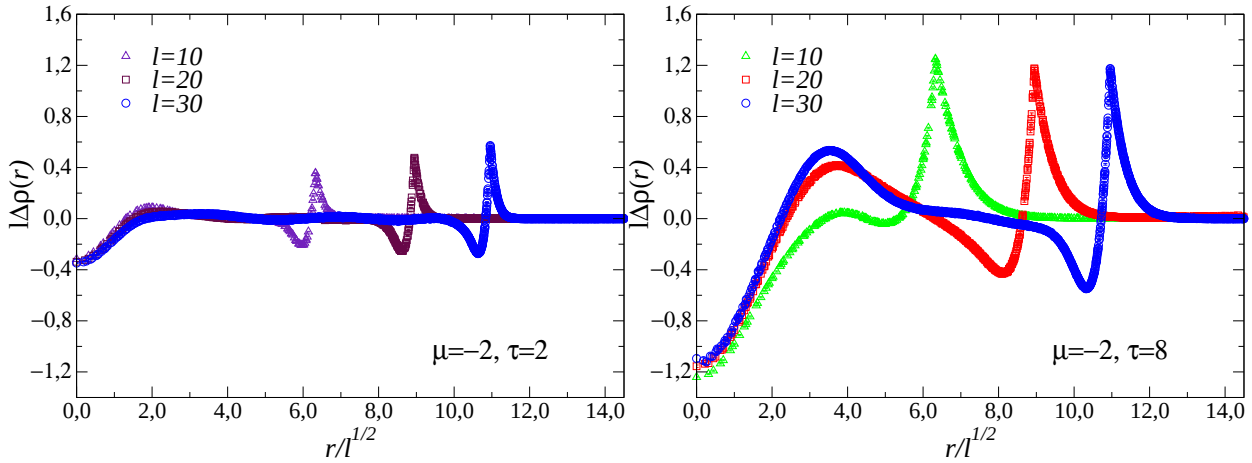


Figure 4.15: The rescaled particle density at $\mu = -2$ with $\tau = 2$ (left) and $\tau = 8$ (right) where $\tau \equiv Tl$ for different values of the trap size $l$.

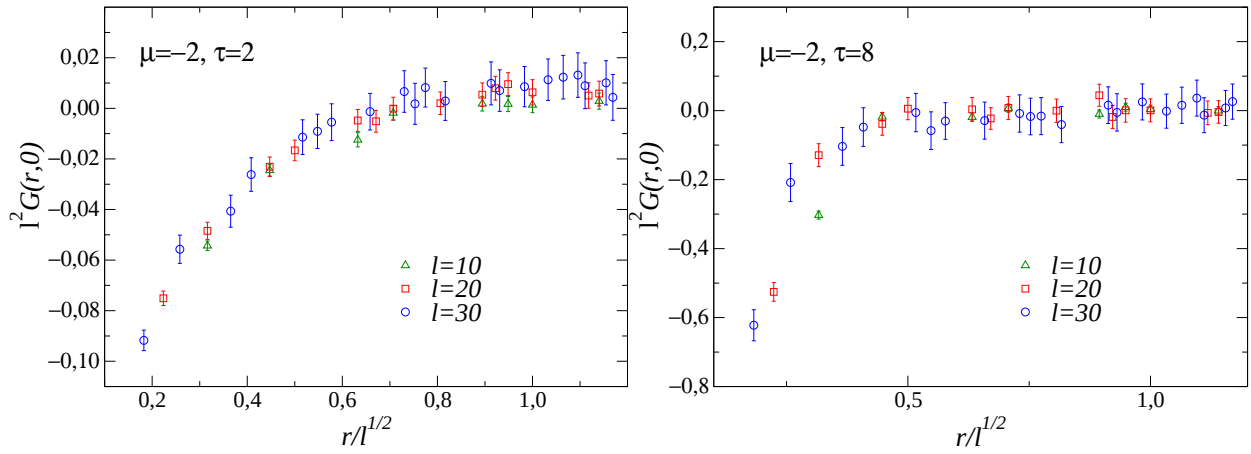


Figure 4.16: The density-density correlator at $\mu = -2$ with $\tau = 2$ (left) and $\tau = 8$ (right) where $\tau \equiv Tl$ for different values of the trap size $l$.

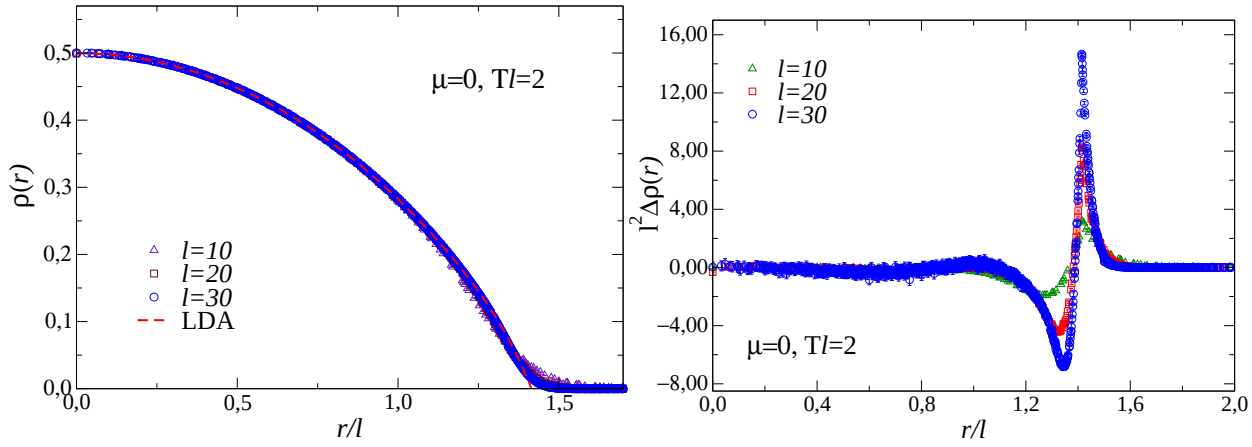


Figure 4.17: The density (left) and the substracted density (right) at $\mu = 0$ with $\tau = 2$ where $\tau \equiv Tl$.

leading to

$$l\Delta\rho(r) = \hat{\mathcal{D}}(Tl, R) \tag{4.43}$$

for the scaling quantity. Figure 4.14 shows how the particle density converges to the local density approximation in the two-dimensional model. Since $\tau \equiv Tl$ as in Section 4.2.1, once again data sets with $\tau = 2$ correspond to temperatures lower than those of the sets with $\tau = 8$, given the common values of the trap size. Besides improving with increasing $l$, in agreement with equation (4.42), the convergence to the local density approximation is better at small $T$, since local density approximation itself is approached at $T \to 0$.

Figure 4.15 illustrates the behavior of $\Delta\rho(r)$ for $\tau = 2$ and $\tau = 8$ after the rescaling suggested by equation (4.43) has been performed: a tendency to collapse on a universal curve is evident in a region close to the origin while some transition-like peaks appear at a distance $r \approx 2l$ from the center (in the large-$l$ limit only the region with the universal curve is left). The deviations from the expected scaling at finite $l$ will be treated in Section 4.2.4.

Finally, figure 4.16 show the rescaling for the density-density correlation function according to equation (4.38). Within the precision of the data and besides scaling corrections at small trap size, results for $\tau = 2$ and $\tau = 8$ show the universal expected behavior. Moreover we recall that in the one-dimensional hard-core Bose-Hubbard model a striking result was the universality for the correlator between the Mott-insulator to superfluid transitions with $n = 0$ and $n = 1$. A closer inspection at figures 4.12 and 4.16 reveals how this feature seems to hold also for the two-dimensional system.

### 4.2.4 Superfluid phase

We now study the model at $\mu = 0$. Since this corresponds to the deep interior of the superfluid phase, no transition is expected.

In figures 4.17 (left) and 4.18 we show the behavior of the particle density and its correlator and we observe a trivial situation where non particular scaling appears: the density profile collapse on the local density function while the correlation vanishes after a few lattice spacing. The scaling variable $\tau = Tl$ was determined by choosing $z = 1$ and $\nu = 1$ for the same reasons explained in Section 4.1.5. The only relevant signal, disappearing in the large trap limit, is seen in the density profile near the distance $r = \sqrt{2}l$, as shown in figure 4.17 (right). An analogous evidence has already appeared in Section 4.2.3. We now conjecture that this anomalous behavior has the same origin of that observed in Sections 4.1.4 and 4.1.5 for the one-dimensional model.

Following the same steps of Section 4.1.5, we define the critical distance $r_c$ as $\mu_{\text{eff}}(r_c) = 2$, since now the Mott-insulator to vacuum transition takes place at $\mu_c = +2$. Substituting $\mu = -2$ and $\mu = 0$ we get exactly the values $r_c = 2l$ and $r_c = \sqrt{2}l$ where the peaks appear, see figures 4.15 and 4.17 (right). In order to study the scaling near the critical distance, the expansion of $\mu_{\text{eff}}(r)$ around $r_c$ is

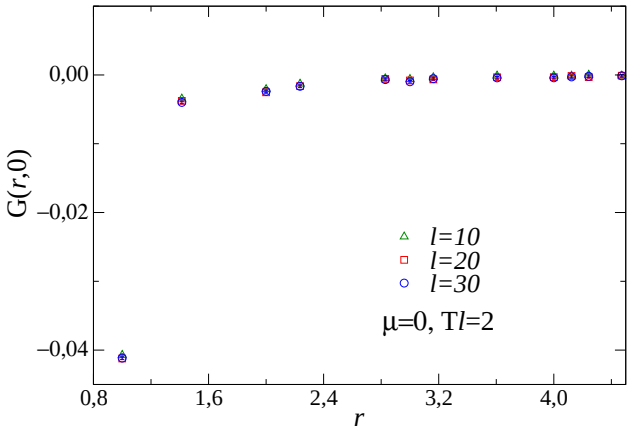


Figure 4.18: The density-density correlator at $\mu = 0$ with $\tau = 2$ where $\tau \equiv Tl$.

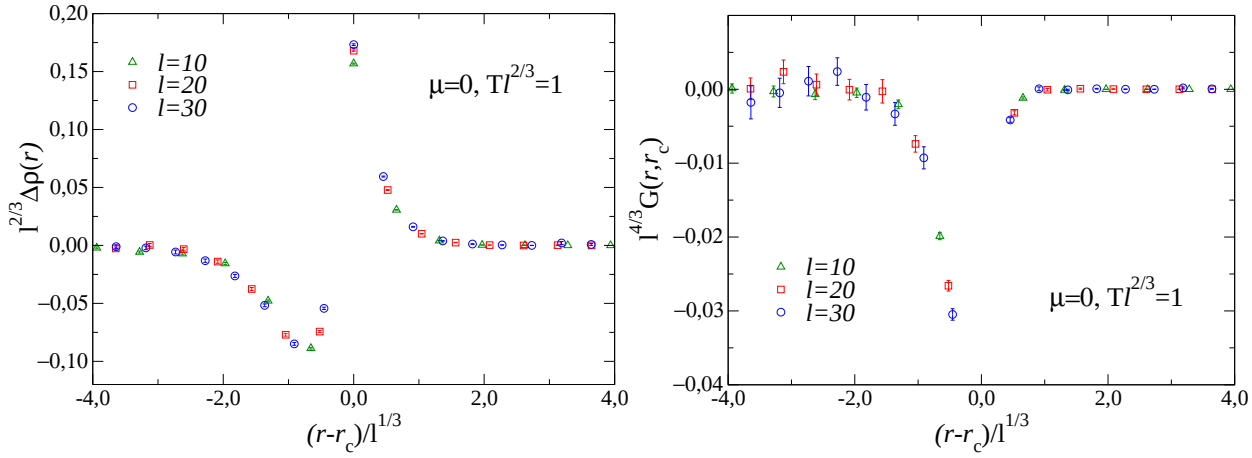


Figure 4.19: The subtracted density and the density-density correlator at $\mu = 0$ with $Tl^{2/3} = 1$ around the distance $r_c$ where $\mu_{\text{eff}} = 2$.

needed:

$$\mu_{\text{eff}}(r) = 2 + p(2-\mu)^{1-1/p}\,\frac{r - r_c}{l} + O[(r - r_c)^2]\ . \tag{4.44}$$

The appearance of the critical modes is effectively driven by the superfluid to vacuum transition in the presence of a linear potential for which $p = 1$. Thus the exponent ruling the divergence of the correlation length, from (4.2), is $\theta = 1/3$. The final scaling law (using $z = 2$) is

$$l^{2/3}\Delta\rho(r) = \hat{\mathcal{D}}(\tau, R)\ , \tag{4.45}$$

$$l^{4/3}G(r, r_c) = \hat{\mathcal{G}}(\tau, R)\ , \tag{4.46}$$

where $R$ and $\tau$ correspond now to $R = (r - r_c)/l^{1/3}$ and $\tau \equiv Tl^{2/3}$. Figure 4.19 shows the behavior of $\Delta\rho(r)$ and $G(r, r_c)$ vs. $(r - r_c)/l^{1/3}$ at $Tl^{2/3} = 1$ after these observables have been rescaled according to equations (4.45) and (4.46). The collapsing of both quantities on a single curve proves the foreseen scaling clearly right.

## 4.3 Relationship with experiments

In this chapter we studied how the theory of trap-size scaling predicts the behavior of typical observables in the neighborhood of a quantum phase transition. Before discussing how this study can be used to understand possible experimental results, we mention that the low-dimensional systems here considered have been experimentally realized [94, 97, 99, 106].

First of all, we considered the Bose-Hubbard model in its hard-core limit $U \to \infty$. This fact does not constitute a restriction for the following reason. In the spirit of the renormalization group theory, we are interested in describing the universal features of the model, that is critical parameters and scaling functions. What determines the universal behavior is not the detailed form of the hamiltonian but some general aspects (as the range and the symmetries of the interactions, the dimensionality, the coupling of external fields, ...). In the context of the Bose-Hubbard model the relevant aspect is the competition between an hopping term and a repulsive one, whose strength is expected not to play any role in determining the universal behavior. So, as long as the interaction remains repulsive, that is as long as $U > 0$, we expect that the universal observables can be described by the same scaling laws. Thus, working in the hard-core limit make us get the desired results. Of course, when studying the general Bose-Hubbard model at finite $U$, we must recall that the universal behavior settles only in a neighborhood of the transition, so that our results apply near the critical value $\mu_c(U)$, which is a function of the on-site energy.

The particle density and the density-density correlator are standard observables that are routinely measured with great accuracy, for example using *in situ* imaging techniques, both in the case of finite-temperature and quantum transitions [40, 41, 45, 46, 65, 68, 102, 104, 105]. We stress that the leading (non-universal) contribution to the particle density depends on the repulsion $U$ and, before using equation (4.6) and its specializations to the various transitions, the analytical contribution must be subtracted: in turn this requires a very precise determination of the density profile. The scaling equations reported in this chapter are expected to describe the universal behavior near the center of the trap, in particular the interplay of temperature and trap effects. They can be used to infer the experimental parameters of the system simply by probing the collapse of experimental data on the universal scaling functions. This procedure is tightly connected with the analogous one used in homogeneous systems where the finite-size scaling theory is used to get accurate estimates of the system parameters [48].

# Chapter 5

# Scaling of the normal to superfluid transition

In this chapter we study the phase transition from a normal fluid to a superfluid present in the three-dimensional Bose-Hubbard model, which belongs to the 3D XY universality class, and the effects that arise from the confinement of an external potential. In particular we will use the trap-size scaling theory to determine the physical parameters of the system.

## 5.1 $U(1)$-symmetry breaking transitions

The content of this chapter is taken from Ref. [81] and the details of the quantum Monte Carlo results here presented are discussed in the Appendix. The hamiltonians for the unconfined and confined systems are still given respectively by equations (3.20) and (4.1).

We start recalling the phase diagram of the homogeneous three-dimensional hard-core model in figure 5.1. The $T = 0$ line is characterized by two quantum critical points at $\mu = +3$ and $\mu = -3$, separating the superfluid phase from the Mott-insulating ones respectively at filling $n = 0$ and $n = 1$. For chemical potential values in the range $-3 < \mu < +3$, there exists a finite-temperature region where superfluidity still persists and then a phase transition to a normal fluid state occurs. As already explained in Section 3.1.2, the phenomenology of such a transition can be accounted for by the classical theory, and we now discuss this point in more detail.

We know from Chapter 2 that, under appropriate physical conditions, a finite (macroscopic) number of particles can accommodate in a single quantum state. When this happens, we can identify a

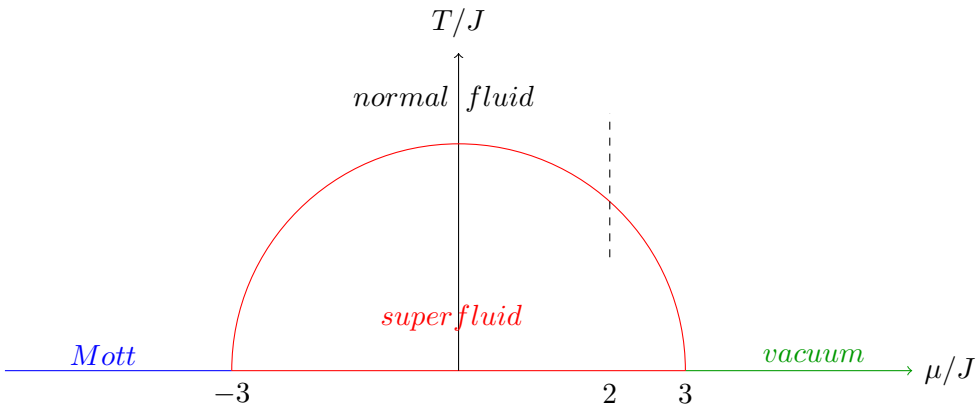


Figure 5.1: A qualitative sketch of the phase diagram of the three-dimensional hard-core Bose-Hubbard model in the $\mu T$ plane.

wave function $\Phi(\mathbf{r}) = n(\mathbf{r})e^{i\theta(\mathbf{r})}$ whose modulus squared gives the particle density $\rho(\mathbf{r}) = |n(\mathbf{r})|^2$ while the phase $\theta(\mathbf{r})$ is substantially related to the kinematic properties of the ensemble. However we can think to the existence of the phase as the manifestation of the coherence of the occupation of a single quantum state: this would be impossible if $n(\mathbf{r}) = 0$, that is in the absence of macroscopic occupation. Thus, when a Bose-Einstein condensate is formed, the mechanism which drives the transition leads to the appearance of a well defined phase: this can consistently be interpreted as the order parameter for the transition. In the spirit of the renormalization group theory, the main consequence is that all systems having a form of order accounted for by an angle belong to the same universality class. Since our transition is characterized by a common angle in each point of a three-dimensional space, the universality class is clearly the one of the classical 3D XY spin model.

The critical behavior described by the 3D XY universality class is characterized by the two relevant parameters $\tau$ and $h$, associated with the temperature $T$, that is $\tau \sim T/T_c - 1$, and the external field $h$ coupled to the order parameter. Their renormalization group dimensions, $y_\tau = 1/\nu$ and $y_h = (5-\eta)/2$ respectively, are related to the critical exponent $\nu$ of the correlation length and to the exponent $\eta$ describing the power-law decay of the two-point function of the order parameter at $T_c$. The critical exponents $\nu$ and $\eta$ are known with great accuracy from theoretical calculations [32, 48] and experiments at the $^4$He superfluid transition [76, 90]. Recent theoretical estimates of the critical exponents are [77, 78]

$$\nu = 0.6717(1) \ , \qquad \eta = 0.0381(2) \ . \tag{5.1}$$

In order to obtain the critical exponent $\theta$, which rules the emergence of the critical modes in the presence of the trap, we follow the same reasoning of Section 3.3. We start from the well known 3D $\Phi^4$ quantum field theory which represents the 3D XY univerality class [11]. The coupling of the complex field with the confining potential is

$$\int d^3r V(r)|\Phi(r)|^2 \tag{5.2}$$

and the scaling dimension $y_n$ of the density/energy operator $|\Phi(r)|^2$ is $y_n = 3 - 1/\nu$. We eventually obtain

$$\theta = \frac{p\nu}{1 + p\nu} \tag{5.3}$$

and, using our value of $\nu$ for a harmonic confinement ($p = 2$), we get

$$\theta = 0.57327(4) \ . \tag{5.4}$$

The observables that will be used to investigate the scaling properties of the transition are the following.

- The local density

$$\rho(\mathbf{x}) \equiv \langle n_{\mathbf{x}} \rangle \tag{5.5}$$

  for the trapped system, which is of course site-dependent, and the mean density

$$\rho \equiv \frac{\langle \hat{N} \rangle}{V} \tag{5.6}$$

  for the homogeneous system, where $\hat{N} = \sum_i n_i$ is the total particle number operator and $V$ is the total volume.

- The density-density correlation function

$$G_n(\mathbf{x}, \mathbf{y}) \equiv \langle n_{\mathbf{x}} n_{\mathbf{y}} \rangle - \langle n_{\mathbf{x}} \rangle \langle n_{\mathbf{y}} \rangle \tag{5.7}$$

  and the one-particle density matrix (or Green function)

$$G_b(\mathbf{x}, \mathbf{y}) \equiv \langle b^\dagger_{\mathbf{x}} b_{\mathbf{y}} \rangle \ . \tag{5.8}$$

In homogeneous conditions, due to translational invariance, $G_n$ and $G_b$ only depend on $\mathbf{x}-\mathbf{y}$, so that we can write them as $G(\mathbf{x},\mathbf{y}) \equiv G(\mathbf{x}-\mathbf{y})$. It is then possible to write the Fourier transform for the homogeneous model as

$$\tilde{G}_b(\mathbf{k}) = \sum_{\mathbf{x}} e^{i\mathbf{k}\mathbf{x}} G_b(\mathbf{x}) \ . \tag{5.9}$$

- The homogeneous compressibility

$$\kappa \equiv -\frac{\partial \rho}{\partial \mu} \ . \tag{5.10}$$

The sign is needed to make $\kappa$ a positive definite quantity. In fact, recalling the sign convention for $\mu$ in equation (3.20), $\kappa$ can be rewritten as

$$\kappa = \frac{1}{L^3}\left(\langle \hat{N}^2 \rangle - \langle \hat{N} \rangle^2\right) \ . \tag{5.11}$$

Moreover, taking advantage of translational invariance, we get

$$\kappa = \sum_{\mathbf{x}} G_n(\mathbf{x}) \ , \tag{5.12}$$

which is the space integral of the density-density correlator.

- The susceptibility for the homogeneous system

$$\chi = \sum_{\mathbf{x}} G_b(\mathbf{x}) \ , \tag{5.13}$$

which is the zero-momentum component of the Fourier transform of the Green function. Instead, for trapped systems, we consider the trap susceptibility defined as

$$\chi_t = \sum_{\mathbf{x}} G_b(\mathbf{0},\mathbf{x}) \ . \tag{5.14}$$

We note that $\chi_t$ is related only to the integral of the correlation with the center of the trap.

- The second moment correlation length for the homogeneous system

$$\xi^2 \equiv \frac{1}{4\sin^2(\pi/L)} \frac{\widetilde{G}_b(\mathbf{0}) - \widetilde{G}_b(\mathbf{p})}{\widetilde{G}_b(\mathbf{p})} \ , \tag{5.15}$$

where $\mathbf{p} = (2\pi/L, 0, 0)$. The analogous quantity in the presence of the trap is

$$\xi_t^2 = \frac{1}{6\chi_t} \sum_{\mathbf{x}} |\mathbf{x}|^2 G_b(0,\mathbf{x}) \ . \tag{5.16}$$

- The helicity modulus $\Upsilon$, which is related to the winding number (see Appendix), defined as

$$\Upsilon \equiv -\frac{1}{L} \frac{\partial^2 Z}{\partial \phi^2}(\phi)|_{\phi=0} \ , \tag{5.17}$$

where $Z$ is the partition function under a twist $\phi$ of the boundary conditions in one direction.

## 5.2 Scaling relations for three-dimensional systems

In order to study the phenomenology of the transition, we will apply to the previous observables the theory of finite-size scaling (in the homogeneous case) and trap-size scaling (in the trapped case). First of all we fix the value of the chemical potential at $\mu = +2$, which lies in the region where a phase transition is possible.[1] Then we determine with great accuracy the critical temperature $T_c(\mu = +2)$ according a standard to finite-size analysis of quantum Monte Carlo data, moving along the dashed line of figure 5.1 We verify that this transition of the Bose-Hubbard model lies in the expected universality class. Finally we investigate a neighborhood of $T_c$ when the external confinement is turned on. Improving the trap-size scaling analysis of Chapter 4 to the new observables, we give evidence of the reliability of the theory in extracting critical parameters from a matching with scaling predictions. The experimental relevance of our approach will be discussed in Section 5.5.

Let us now discuss the theoretical predictions. First of all, finite-size scaling predicts the following asymptotic scaling laws of the one-particle and particle density correlation functions for $r \equiv |\mathbf{x}| > 0$:

$$G_b(\mathbf{x}) = L^{-1-\eta}\mathcal{G}_b(r/L, \tau L^{1/\nu}) + \dots \ , \tag{5.18}$$

$$G_n(\mathbf{x}) = L^{-2y_n}\mathcal{G}_n(r/L, \tau L^{1/\nu}) + \dots \ , \tag{5.19}$$

where $\tau \equiv T/T_c - 1$. Thus, the susceptibility $\chi$ behaves as

$$\chi = L^{2-\eta}\left[g(\tau L^{1/\nu}) + L^{-\omega} g_\omega(\tau L^{1/\nu}) + ...\right] \ , \tag{5.20}$$

where we have also included the leading $O(L^{-\omega})$ scaling corrections, and $\omega = 0.785(20)$ is the critical exponent controlling the leading scaling corrections in the 3D XY universality class. The dots indicate further scaling corrections suppressed by higher powers of $1/L$. The scaling functions $g$ and $g_\omega$ are universal apart from a multiplicative constant (since $\chi$ is not invariant under the renormalization group, $g(0)$ is not universal) and a rescaling of the argument.

We consider the dimensionless renormalization group invariant quantities

$$R_\xi \equiv \xi/L \ , \qquad R_\Upsilon \equiv \Upsilon L \ . \tag{5.21}$$

According to the finite-size scaling theory they behave as [78]

$$R = f(\tau L^{1/\nu}) + L^{-\omega} f_\omega(\tau L^{1/\nu}) + \dots \tag{5.22}$$

around $T_c$ and in the large $L$ limit. $f$ and $f_\omega$ are scaling functions. In particular the leading one $f$ is universal (although it depends on the shape of the volume and the choice of the boundary conditions), that is it is independent of the particular model within the universality class, apart from a trivial rescaling of the argument; thus, $R^* \equiv f(0)$ is universal. For cubic-shaped lattices with periodic boundary conditions, the universal infinite-volume limit of $R_\xi$ and $R_\Upsilon$ at $T = T_c$ are known with great accuracy [78]:

$$R_\xi^* = 0.5924(4) \ , \qquad R_\Upsilon^* = 0.516(1) \ . \tag{5.23}$$

Moving to trap-size scaling, the equations for the observables and correlation functions provide an effective description of the critical behavior around the center of the trap and in particular of the interplay between the temperature and the confining potential. At the superfluid transition and around the center of the trap the one-particle correlation function $G_b$ behaves as

$$G_b(\mathbf{x}, \mathbf{y}) = l^{-(1+\eta)\theta}\mathcal{G}_b(\mathbf{x}l^{-\theta}, \mathbf{y}l^{-\theta}, \tau l^{\theta/\nu}) + \dots \tag{5.24}$$

and the particle-density correlation $G_n$ as

$$G_n(\mathbf{x}, \mathbf{y}) = l^{-2y_n\theta}\mathcal{G}_n(\mathbf{x}l^{-\theta}, \mathbf{y}l^{-\theta}, \tau l^{\theta/\nu}) + \dots \ , \tag{5.25}$$

[1] We could have chosen a negative value as well: the main line of reasoning would have been the same, even if a bigger computational effort is expected in this case. A different approach instead is needed when considering the transition at the tip of the phase boundary, as explained in Ref. [82].

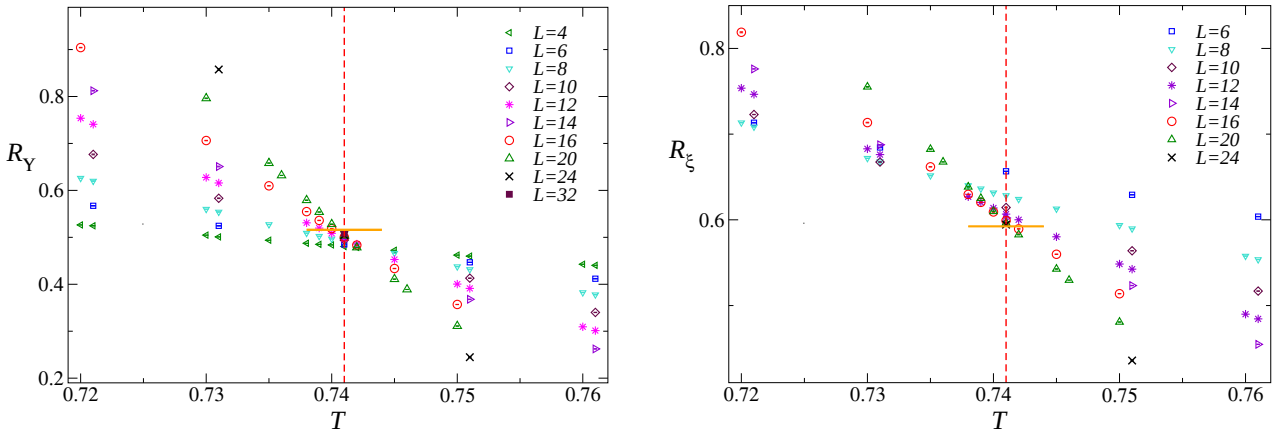


Figure 5.2: Data of $R_\xi \equiv \xi/L$ (left) and $R_\Upsilon \equiv \Upsilon L$ (right) for the homogeneous model with periodic boundary conditions. The vertical dotted line shows our final estimate of $T_c = 0.7410(1)$. The horizontal segments around the crossing point indicate the universal asymptotic values [78] $R_\xi^* = 0.5924(4)$ and $R_\Upsilon^* = 0.516(1)$ at $T_c$.

where $y_n$ is the renormalization group dimension of the density operator

$$y_n = 3 - 1/\nu = 1.5112(2) \; . \tag{5.26}$$

Analogous scaling relations can be inferred for other correlations. According to trap-size scaling, the trap susceptibility and the second moment correlation with the center of the trap are expected to behave as

$$\chi_t = l^{(2-\eta)\theta} \mathcal{X}(\tau l^{\theta/\nu}) + \dots \; , \tag{5.27}$$

$$\xi_t = l^{\theta} \mathcal{R}(\tau l^{\theta/\nu}) + \dots \; . \tag{5.28}$$

Note however that any length scale $\xi$ extracted from the critical modes is expected to show the same trap-size scaling as $\xi_t$.

The above trap-size scaling equations provide the asymptotic dependence on the trap size $l$. Scaling corrections are generally expected to be $O(l^{-\omega\theta})$ where $\omega = 0.785(20)$ is the scaling-correction exponent of the 3D XY universality class, thus

$$\omega\theta = 0.45(1) \; . \tag{5.29}$$

## 5.3 Finite-size scaling of the homogeneous model

### 5.3.1 Invariant quantities

In figure 5.2 we show the quantum Monte Carlo results for $R_\xi$ and $R_\Upsilon$. Their sets of data for different lattice sizes show a clear evidence of a crossing point, whose location is expected to converge to $T_c$ in the large-$L$ limit, according to equation (5.22). Moreover, the values of $R_\xi$ and $R_\Upsilon$ at the crossing point are consistent with the asymptotic universal values $R_\xi^*$ and $R_\Upsilon^*$ reported above. The small deviations appear to decrease with increasing the lattice size; they are explained by the presence of $O(L^{-\omega})$ corrections, according to equation (5.22).

In order to derive an estimate of $T_c$, we fit the data to the Ansatz

$$R = R^* + \sum_{i=1}^{n} a_i \tau^i L^{i/\nu} + L^{-\omega} \sum_{j=0}^{m} b_j \tau^j L^{j/\nu}, \tag{5.30}$$

obtained by expanding equation (5.22) around $\tau = 0$. The best estimate of $T_c$ is obtained from the data of $R_\Upsilon$. Sufficiently close to $T_c$, the first terms of the sums, that is setting $n = 1$ and $m = 0$ in

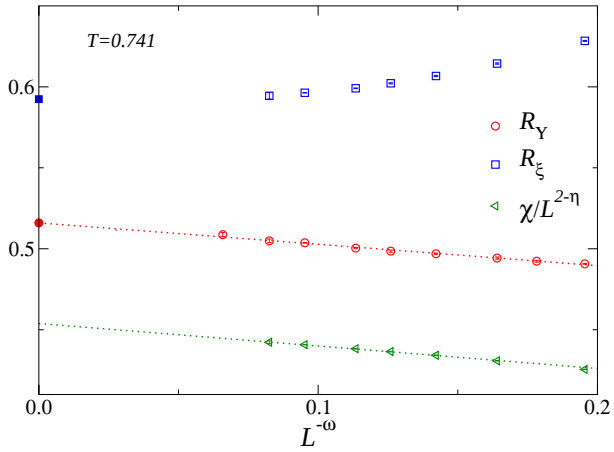


Figure 5.3: Data of $R_\Upsilon$, $R_\xi$ and $\chi/L^{2-\eta}$ at $T_c$ vs. $L^{-\omega}$ with $\omega = 0.785$. In the case of $R_\Upsilon$ and $R_\xi$ we also show (by full symbols) their universal $L \to \infty$ limit: $R^*_\Upsilon = 0.516(1)$ and $R^*_\xi = 0.5924(4)$. The dotted lines show linear fits of the data of $R_\Upsilon$ and $\chi/L^{2-\eta}$. In the case of $R_\xi$, higher-order scaling corrections appear also important.

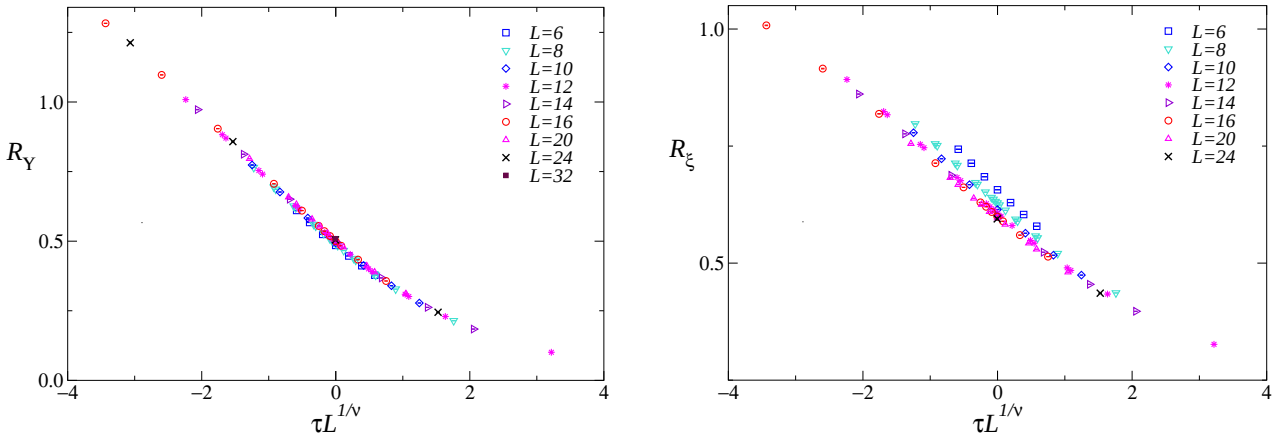


Figure 5.4: $R_\Upsilon$ (left) and $R_\xi$ (right) vs. $\tau L^{1/\nu}$ with $\tau \equiv T/T_c - 1$ and $T_c = 0.7410$ for the homogeneous model with periodic boundary conditions.

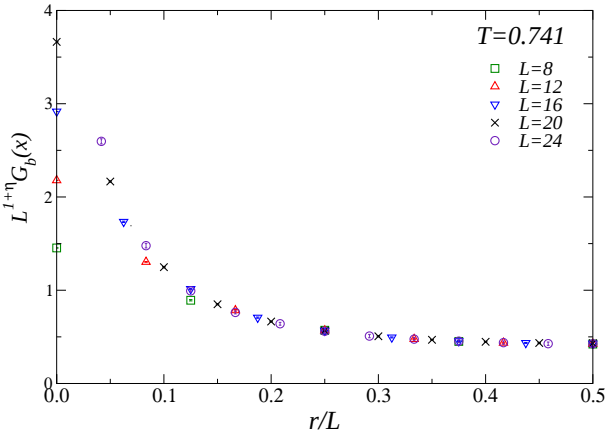


Figure 5.5: $L^{1+\eta}G_b(\mathbf{x})$ vs. $r/L$ (where $r \equiv |\mathbf{x}|$) at $T = T_c$ for homogeneous Bose-Hubbard systems with periodic boundary conditions. The data show the expected scaling behavior (5.18).

equation (5.30), provide already good fits keeping the known universal quantities $\nu$, $\omega$, $R^*_\Upsilon$ fixed: in this respect the $O(L^{-\omega})$ scaling correction term is necessary to achieve fits with acceptable $\chi^2$/dof. For example the fit of the data for $L \geq 10$ gives $T_c = 0.74103(1)$ with $\chi^2/\mathrm{dof} \approx 1.4$. We consider

$$T_c = 0.7410(1) \qquad (\mu = +2) \tag{5.31}$$

as our final estimate of $T_c$, where the error includes the statistical errors of the fits, and takes into account the dependence of the results on the choice of the Ansatz and the interval of values of $T$ around the transition allowed in the fit. Further subleading scaling corrections are controlled by increasing the minimum value $L_{\min}$ of $L$ of the data allowed in the fits. The analysis of the data of $R_\xi$ gives consistent results, but less precise because they are apparently affected by larger scaling corrections.

Figure 5.3 shows data of $R_\xi$, $R_\Upsilon$ and $\chi/L^{2-\eta}$ at $T_c = 0.741$ plotted versus $L^{-\omega}$, which is the expected order of the leading scaling corrections. As expected $R_\xi$ and $R_\Upsilon$ converge to their universal values $R^*_\Upsilon$ and $R^*_\xi$. The approach of $R_\Upsilon$ and $\chi/L^{2-\eta}$ is approximately linear with respect to $L^{-\omega}$, while in the case of $R_\xi$ also higher-order scaling corrections appear significant for the available lattice sizes. Figure 5.4 reports the data of $R_\Upsilon$, $R_\xi$ and $\chi/L^{2-\eta}$ versus $\tau L^{1/\nu}$ with $\tau \equiv T/T_c - 1$. They show the asymptotic collapse of the data along a universal curve, apart from small scaling corrections which get suppressed with increasing $L$.

Figure 5.5 shows the data of the one-particle correlation function $G_b$ at $T_c$, which are consistent with the expected asymptotic scaling behavior reported in equation (5.18). In conclusion, the above finite-size scaling analysis of the quantum Monte Carlo data of the homogeneous hard-core Bose-Hubbard model at $\mu = +2$ definitely confirms that its superfluid transition belongs to the 3D XY universality class and provides an accurate determination of the (non-universal) critical temperature, given by equation (5.31).

### 5.3.2 Compressibility, particle density and its correlator

The behaviors of the particle density, the compressibility and the density-density correlator around the transition are particularly interesting because they can be directly investigated experimentally [123], for example by *in situ* density image techniques.

The behavior of the mean particle number around the transition point is analogous to that of the energy density in spin systems, so that[2]

$$\rho = f_a(\tau) + L^{-y_n} f_s(\tau L^{1/\nu}) \tag{5.32}$$

[2]In the following, unless explicitly written, higher order scaling corrections will be omitted.

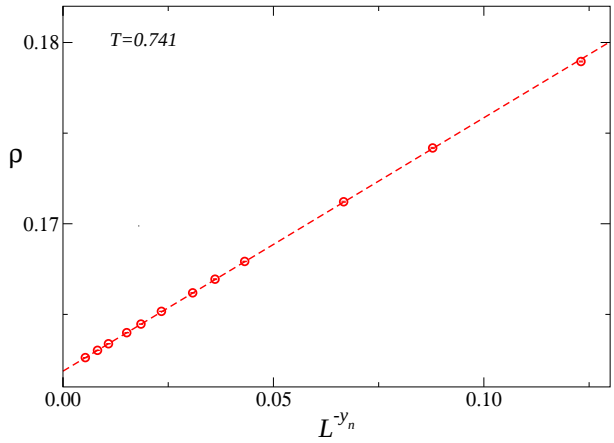


Figure 5.6: The particle density at $T_c$ of the homogeneous model. The dashed line shows a linear fit of the data to $\rho_0 + c\,L^{-y_n}$, with $\rho_0 = 0.16187(1)$ and $c = 0.140(1)$.

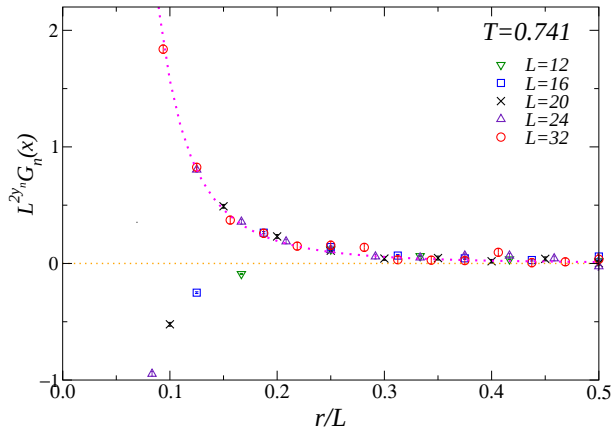


Figure 5.7: $L^{2y_n}G_n(x)$ vs. $r/L$ at $T = T_c$ for homogeneous systems with periodic boundary conditions. The dotted line sketches the expected asymptotic behavior $G_n(\mathbf{x}) \sim r^{-2y_n}$ at small $r \equiv |\mathbf{x}|$.

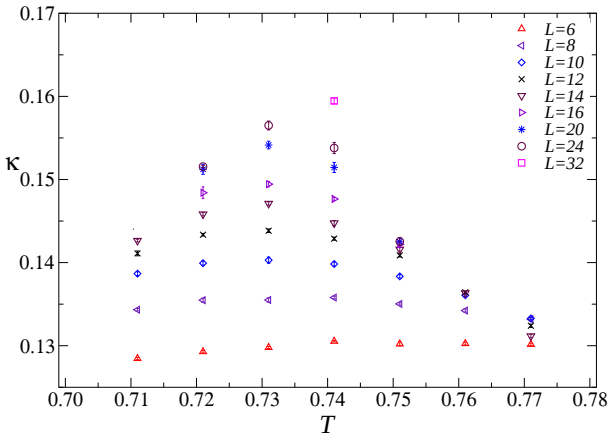


Figure 5.8: Data of the compressibility $\kappa$ (5.10).

at fixed chemical potential, where $f_a$ is a nonuniversal analytic function of $\tau$ (and $\mu$), $y_n$ is the renormalization group dimension of the particle density operator $n_x$ of equation (5.26) and $f_s$ is a universal function apart from a factor and a rescaling of its argument. This behavior is clearly shown by the data at $T_c$, which are well approximated by the asymptotic formula

$$\rho = \rho_0 + cL^{-y_n} , \tag{5.33}$$

as shown in figure 5.6. A linear fit to equation (5.33) gives $\rho_0 = 0.16187(1)$.

Figure 5.7 reports data of the particle-density correlation function at $T_c$. They show the expected scaling behavior, obtainable from equation (5.19) setting $\tau = 0$. Note that it develops for positive values of $G_n$, while the negative data at small distance are pushed toward the origin, not contributing to the scaling behavior.

The scaling behavior of the compressibility (5.10) is complicated by the sum around $\mathbf{x} = 0$, which gives rise to a nonuniversal analytic contribution, analogously to the specific heat in $^4$He [48]. Indeed, we expect

$$\kappa = g_a(\tau) + L^{\alpha/\nu} g_s(\tau L^{1/\nu}), \tag{5.34}$$

where $\alpha$ is the specific heat exponent $\alpha = -0.0151(3)$, $g_a$ is a nonuniversal analytic function of $\tau$ and $g_s$ is a universal function apart from a factor and a rescaling of the argument. Notice that, since $\alpha < 0$, the nonuniversal analytic term provides the leading behavior for $L \to \infty$. Figure 5.8 shows the data of the compressibility. They hint at the typical $\lambda$ shape expected in the infinite-volume limit, which also characterizes the specific heat at the superfluid transition of $^4$He [120]. At $T_c$ they show the asymptotic scaling behavior

$$\kappa = a + b\, L^{\alpha/\nu} , \tag{5.35}$$

as shown in figure 5.9. Linear fits of the available data at $T_c$, up to $L = 32$, gives $a \approx 0.90$ and $b \approx -0.80$.

## 5.4 Critical parameters from trap-size scaling

We now consider the three-dimensional Bose-Hubbard model in the presence of a trapping potential, as described by the hamiltonian (4.1). We present results of our simulations of the hard-core model at $\mu = +2$ for several values of the trap size $l$.

### 5.4.1 Finite-size effects with the trap

We start analyzing the finite-size effects in the presence of the trap, that is when considering the trap within a finite box of size $L$ (with open boundary conditions). They can be taken into account by

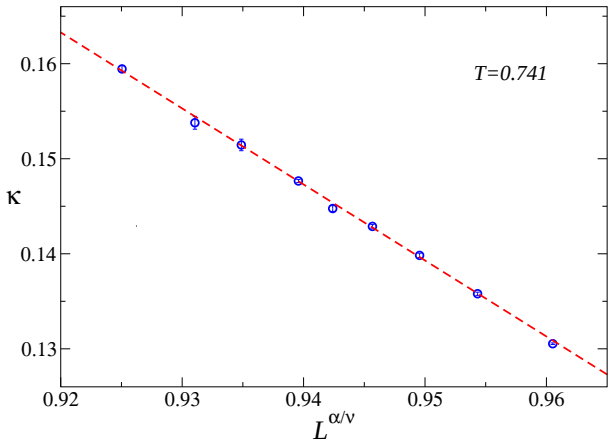


Figure 5.9: Data of the compressibility $\kappa$ at $T_c$. The dashed line shows a linear fit to the predicted asymptotic behavior $a+bL^{\alpha/\nu}$. Data for $L \geq 8$ give $a = 0.90(1)$ and $b \approx -0.80(1)$ with $\chi^2$/d.o.f. $\approx 1.1$.

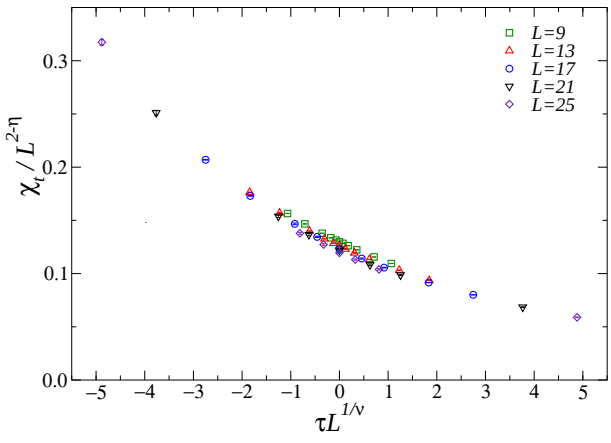


Figure 5.10: Finite-size scaling of the trap dependence of the data of $\chi/L^{2-\eta}$ in the presence of the trap from simulations keeping $L/l^{\theta} = 2$ fixed and using open boundary conditions.

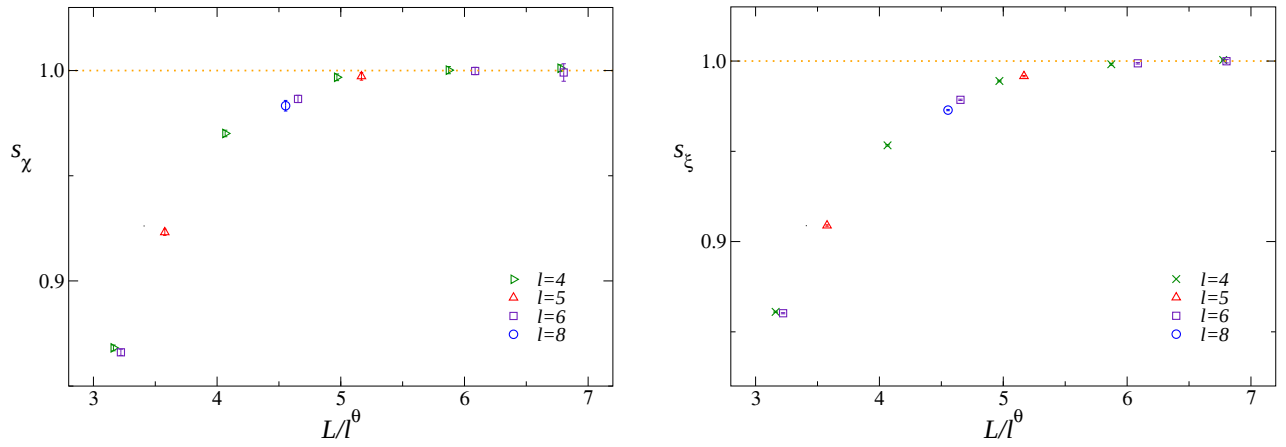


Figure 5.11: Finite-size scaling curves of the trap susceptibility $\chi_t$ and correlation length $\xi_t$ at $T_c$ equations (5.38) and (5.39).

adding a further dependence on $Ll^{-\theta}$ in the trap-size scaling predictions of equations (5.24, 5.25) [87]. For example the finite-size and trap-size scaling of the trap susceptibility $\chi_t$ and the correlation length $\xi_t$ of equations (5.14, 5.16) can be written as

$$\chi_t = L^{2-\eta}\mathcal{X}(\tau L^{1/\nu}, L/l^\theta) \,, \tag{5.36}$$

$$\xi_t = L\mathcal{R}(\tau L^{1/\nu}, L/l^\theta) \,. \tag{5.37}$$

The above scaling is confirmed by the data of $\chi_t$ shown in figure 5.10, obtained by quantum Monte Carlo simulations keeping $L/l^\theta = 2$ fixed.

For the future analysis, that is in order to study pure trap-size effects, the lattice size $L$ must be taken sufficiently large to effectively reproduce the infinite-volume limit, that is so that the residual finite-size effects can be considered negligible compared with the statistical errors. In this respect, we start noting that finite-size and trap-size scaling also implies that at $T_c$ the ratio of quantities computed in box of size $L$ and for $L \to \infty$ becomes a function of $L/l^\theta$ only, that is

$$s_\chi \equiv \frac{\chi_t(l,L)}{\chi_t(l,L\to\infty)} = f_\chi(L/l^\theta) \,, \tag{5.38}$$

$$s_\xi \equiv \frac{\xi_t(l,L)}{\xi_t(l,L\to\infty)} = f_\xi(L/l^\theta) \,. \tag{5.39}$$

Their data at $T_c$ support this scaling behavior, as shown in figure 5.11.

Finally, they tell us that around the transition the finite-size effects on $\chi_t$ and $\xi_t$ get smaller than one per mille when $L/l^\theta > 7$. All data reported in Section 5.4.2, which were supposed to correspond to the infinite size limit, were obtained by simulations of systems satisfying this condition.

### 5.4.2 Trap-size scaling analyses of the Monte Carlo data

We now show that a trap-size scaling analysis of the data for trapped systems allows us to determine the critical parameters, analogously to the finite-size scaling analysis presented in the previous section.

In order to determine the critical temperature from the trap-size scaling predictions (5.27, 5.28), we may exploit the fact that at $T = T_c$, that is for $\tau = 0$, the ratios $\chi_t/l^{\theta(2-\eta)}$ and $\xi_t/l^\theta$ become independent of the trap size $l$ in the large-$l$ limit. Therefore, we expect that sets of data for different trap sizes cross each other at one value of the temperature (apart from scaling corrections), providing an estimate of $T_c$. This is indeed observed in figure 5.12, which shows the available data of $\chi_t/l^{\theta(2-\eta)}$ and $\xi_t/l^\theta$ versus $T$. The apparent crossing point of the trap-size scaling data indicates $T_c \approx 0.74$. A more accurate estimate is achieved by fitting the data to the simple Ansatz

$$a + b(T - T_c)l^{\theta/\nu} \,, \tag{5.40}$$

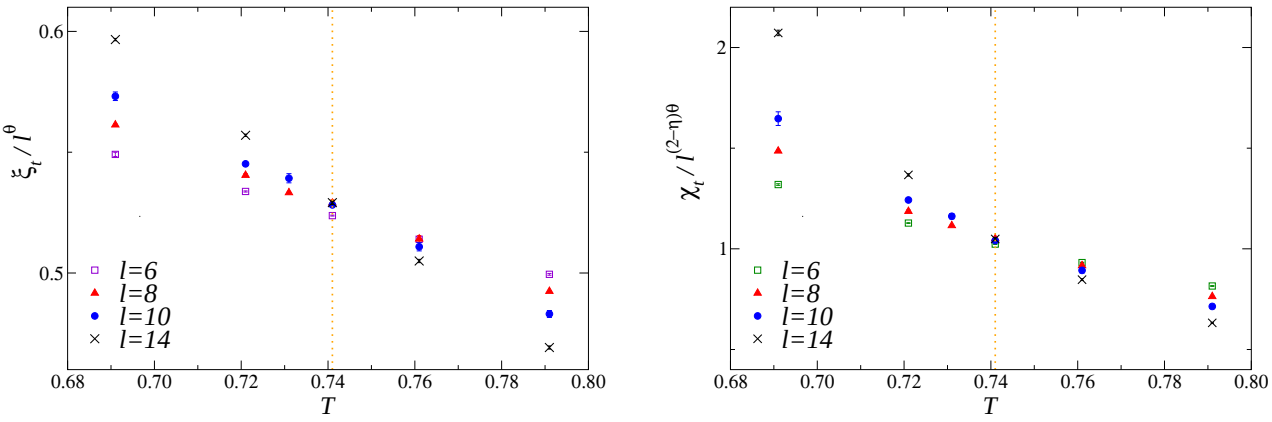


Figure 5.12: Data of $\xi_t/l^\theta$ (left) and $\chi_t/l^{(2-\eta)\theta}$ (right) in the presence of the trap. The vertical dotted line indicates the critical temperature $T_c = 0.7410$ obtained from the FSS analysis of Section 5.3.

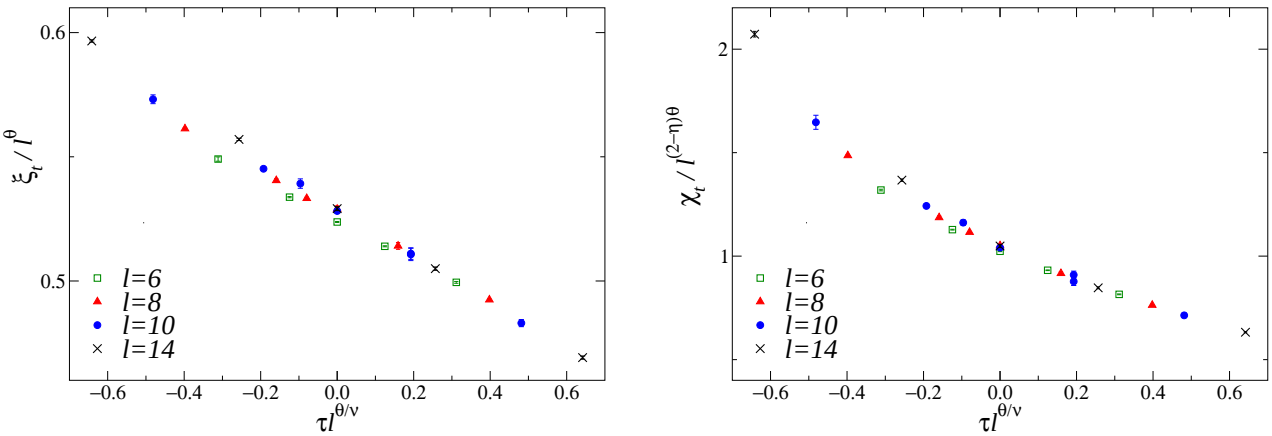


Figure 5.13: Data of $\xi_t/l^\theta$ (left) and $\chi_t/l^{(2-\eta)\theta}$ (right) in the presence of the trap vs. $\tau l^{\theta/\nu}$ with $\tau \equiv T/T_c - 1$ and $T_c = 0.741$.

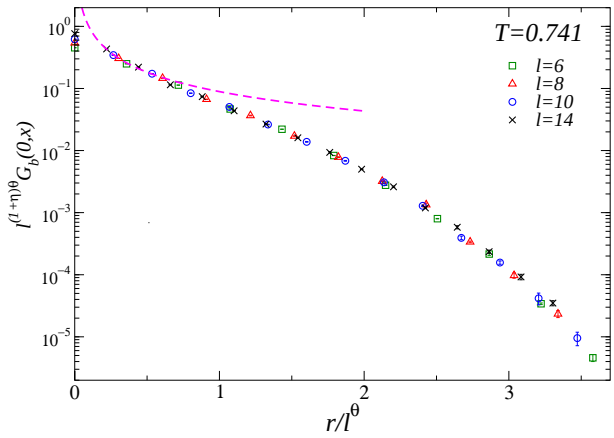


Figure 5.14: The one-particle correlation function $G_b(0,\mathbf{x})$ at $T_c$. The dashed line shows the expected small-distance behavior $G_b(0,\mathbf{x}) \sim r^{-(1+\eta)}$.

considering data sufficiently close to the crossing point to avoid higher powers of $\tau l^{\theta/\nu}$.

We obtain $T_c = 0.741(2)$ and $T_c = 0.742(2)$ respectively from the data of $\xi_t/l^\theta$ and $\chi_t/l^{(2-\eta)\theta}$ (in both cases from data for $l \geq 8$). The error takes also into account results from different intervals of values of $T$ around $T_c$. The expected $O(l^{-\omega\theta})$ scaling corrections of equation (5.29) appear quite suppressed, at least for $l \geq 8$. Although the available data come from moderately large trap sizes, their analysis shows a clear evidence of the expected trap-size scaling, which allows us to accurately estimate the critical temperature $T_c$ with a precision of a few per mille, in good agreement with the estimate of $T_c$ by the standard finite-size scaling analysis of Section 5.3, that is $T_c = 0.7410(1)$. In figure 5.13 we plot the data of of $\chi_t/l^{\theta(2-\theta)}$ and $\xi_t/l^\theta$ versus $\tau l^{\theta/\nu}$. They are consistent with the scaling behavior predicted by equations (5.27) and (5.28), approaching a universal curve in the large-$l$ limit.

The trap-size scaling of the one-particle correlation function $G_b(0,\mathbf{x})$ at $T_c$, that is

$$G_b(0,\mathbf{x}) = l^{-(1+\eta)\theta} g_b(X) \ , \quad X \equiv r/l^\theta \ , \tag{5.41}$$

is nicely reproduced by the data shown in figure 5.14. At small distance $r$ the two-point function $G_b$ is expected to show the power-law behavior of the homogeneous system, tha is $G_b(0,\mathbf{x}) \sim 1/r^{1+\eta}$.

### 5.4.3 Trap-size dependence of the particle density

Finally, we discuss the trap-size dependence of the particle density, which has been considered in the literature as a possible probe of critical behavior, due to the experimental capability of measuring it quite accurately. Analogously to the finite-size scaling of homogeneous systems, the scaling behavior of the particle density is more involved, because it is dominated by an analytical contribution. In the presence of the trap, its behavior is further complicated by the fact that the particle density depends on the distance from the center of the trap. To begin with, we consider the particle density at the center of the trap, that is at $\mathbf{x} = 0$. Its asymptotic trap-size dependence is expected to be

$$\rho(0) = g_a(\tau) + l^{-y_n\theta} g_s(\tau l^{\theta/\nu}) \ , \tag{5.42}$$

where $y_n\theta = 0.8664(3)$, $g_a$ is a nonuniversal analytical function and $g_s$ is a scaling function. Moreover the local-density approximation suggests that the leading analytical term $g_a(\tau)$ is identical to that of equation (5.32) for homogeneous systems. This is supported by the data at $T_c$ shown in figure 5.15, which are consistent with the asymptotic formula

$$\rho(0) = \rho_0 + b\, l^{-y_n\theta} \tag{5.43}$$

with $\rho_0$ equal to the leading constant term of homogeneous systems of equation (5.33) with $\rho_0 = 0.16187(1)$. Indeed, a linear fit of the data to equation (5.43) gives $\rho_0 = 0.1617(3)$ and $b = -0.027(1)$ with $\chi^2/\mathrm{dof} \approx 0.4$.

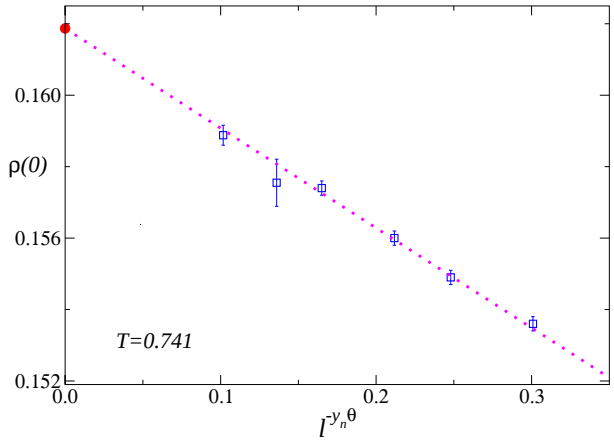


Figure 5.15: The particle density at $T_c$ and at the center of the trap. The full circle along the $y$-axis shows the value $\rho_0 = 0.16187$ of the leading asymptotic term obtained for homogeneous systems, see figure 5.6. The dotted line shows a linear fit to $\rho_0 + b\, l^{-\theta y_n}$, which gives $\rho_0 = 0.1617(3)$ and $b = -0.027(1)$.

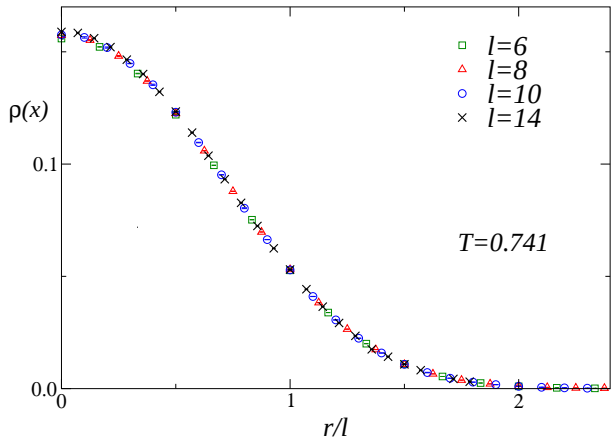


Figure 5.16: The space dependence of the particle density $\rho(x)$ at $T_c$ in the presence of the trap.

Concerning the space-dependence of the particle density and using rotational invariance, we expect that its large trap-size behavior is

$$\rho(\mathbf{x}) = f_a(rl^{-1}, T) + l^{-y_n\theta} f_s(r/l^\theta, \tau l^{\theta/\nu}) \; , \tag{5.44}$$

where $f_a$ is again an analytic function. Its analytic dependence on the ratio $r/l$ is quite natural, because we expect it to be a smooth function of

$$\mu_{\rm eff}(rl^{-1}) \equiv \mu + V(r) = \mu + \left(\frac{r}{l}\right)^2 \; , \tag{5.45}$$

as suggested by the local density approximation. The asymptotic dependence on $r/l$ is shown by the plot of figure 5.16. We expect that the leading analytic function $f_a(rl^{-1}, T)$ is provided by the local density approximation, that is by the particle density $\rho_{\rm homo}(\mu_{\rm eff}, T)$ of the homogeneous system in the infinite-volume limit. The asymptotic validity of the local density approximation was also found at the $T = 0$ quantum transitions of one-dimensional and two-dimensional models (see Chapter 4).

The above results show that the behavior of the particle density around the center of the trap and across the transition is quite nontrivial. We finally write it as

$$\rho(\mathbf{x}) = \rho_{\rm homo}[\mu_{\rm eff}(rl^{-1}), T] + l^{-y_n\theta} f_s(r/l^\theta, \tau l^{\theta/\nu}) \; . \tag{5.46}$$

Let us consider the trap-size scaling limit at $T = T_c$ (that is $\tau = 0$) of this asymptotic behavior, in other words the $l \to \infty$ limit while keeping the ratio $X \equiv r/l^\theta$ fixed. In this limit we get $r/l = X/l^{1-\theta} \to 0$ so that

$$\mu_{\rm eff} = \mu + \left(\frac{X}{l^{1-\theta}}\right)^2 \tag{5.47}$$

and we can expand the analytical term near the point of value $\mu$. We finally obtain

$$\rho(\mathbf{x}) = \rho_{\rm homo}(\mu, T_c) - l^{-2(1-\theta)} \kappa_{\rm homo}(\mu, T_c) X^2 + O(l^{-4(1-\theta)}) + l^{-y_n\theta} f_s(X) + O(l^{-(y_n+\omega)\theta}) \; , \tag{5.48}$$

where $\kappa_{\rm homo}(\mu, T_c) \equiv -\partial\rho_{\rm homo}(\mu, T_c)/\partial\mu$ and the critical temperature corresponds to the specific value of $\mu$. Note that the $O(l^{-2(1-\theta)})$ term cannot be neglected with respect to the scaling term because

$$2(1-\theta) < y_n\theta < 4(1-\theta) \; . \tag{5.49}$$

Indeed $2(1-\theta) = 0.8535(1)$ and $y_n\theta = 0.8664(3)$. Therefore, in order to determine the universal scaling term, we must subtract the terms containing $\rho_{\rm homo}(\mu)$ and $\kappa_{\rm homo}(\mu)$. They may be evaluated from calculations within the homogeneous model at $\mu$ and $T$ fixed, for example considering their large-$L$ limit using periodic boundary conditions. Using the corresponding results at $T_c$ for the finite-size scaling of homogeneous systems (see Section 5.3.2), we estimate $\rho_{\rm homo}(\mu = 2, T_c) \approx 0.16187$ and $\kappa_{\rm homo}(\mu = 2, T_c) \approx 0.90$. Then we define the subtracted particle density

$$\begin{aligned} \rho_{\rm sub}(\mathbf{x}) &\equiv \rho(\mathbf{x}) + \rho_{\rm homo}(\mu, T) - l^{-2(1-\theta)} \kappa_{\rm homo}(\mu, T) X^2 \\ &= l^{-y_n\theta} f_s(X) + \dots \; , \qquad X \equiv r/l^\theta \; . \end{aligned} \tag{5.50}$$

Its scaling behavior is nicely confirmed by the corresponding data plotted in figure 5.17.

Finally in figure 5.18 we show our data for the density-density correlation $G_n$, which vanish at relatively small distance and do not apparently show scaling behaviors, likely because the trap size of the available data is still too small. Indeed the finite-size scaling data of figure 5.7 begin showing scaling at relatively large values of the size, essentially because the correlation function is significantly nonzero only at small distance.

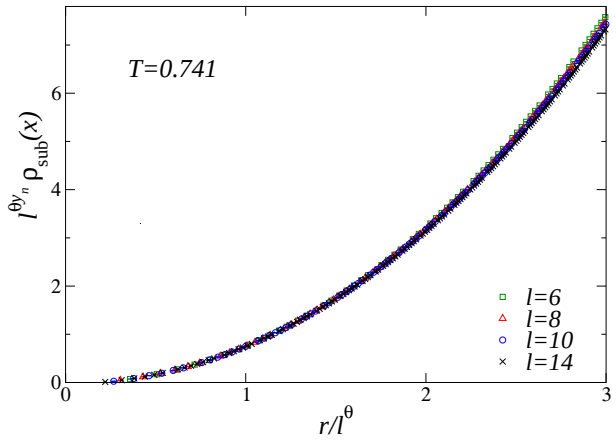


Figure 5.17: The subtracted particle density $\rho_{\rm sub}(x)$ at $T_c$, cf Eq. (5.50). The data of $l^{y_n\theta}\rho_{\rm sub}$ versus $r/l^\theta$ for different trap sizes collapse toward a unique curve, confirming the scaling behavior (5.50).

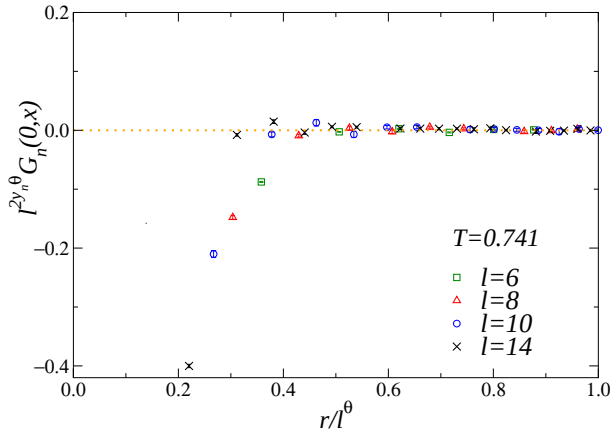


Figure 5.18: The density-density correlation $G_n(0,x)$ at $T_c$.

## 5.5 Relationship with experiments

In this chapter, as we have done in Chapter 4, we have shown that a good determination of the critical parameters and a precise study of the critical behavior of systems that are made inhomogeneous by the presence of an external space-dependent field can be achieved by matching the trap-size dependence of appropriate observables with the scaling laws predicted by the theory. Our approach is clearly similar to experiments probing the finite-size scaling behavior of homogeneous $^4$He systems at the superfluid transition [120]. We stress that the main advantage of this approach is that it is supposed to exactly converge to the critical parameters in the large trap-size limit. Since no further assumption or approximation, such as the local density approximation or mean field theory, is used, our method provides a scheme to improve the results, in particular with respect to the problem of controlling the various sources of uncertainty.

A few comments are now in order concerning the optimal observables to determine the critical parameters in trapped systems. Of course, they are those which are closely related to the critical modes around the center of the trap. In particular, the most convenient quantities are those whose leading behavior in the large trap-size limit is given by the universal trap-size scaling associated with the critical modes.

The dominant contribution to the particle density, as already noted in Chapter 4, in the large trap-size limit is given by an analytical background, which is related to the non-critical modes. Our numerical analysis of Section 5.4.3 shows that such leading background is well approximated (actually we conjecture that it is exactly given) by the corresponding local density approximation; thus trap-size scaling provides the leading behavior of the deviations. Of course this requires very precise data before one can apply the scaling relations, in order to observe the genuine critical term.

In the case of the superfluid transition or Bose-Einstein condensation, the optimal quantities are related to the one-particle correlation function of the bosonic field around the center $G_b(0, \mathbf{x})$. In particular we considered the susceptibility and the trap correlation length defined from the second moment of the Green function. Note that any length scale $\xi$ extracted from the critical modes is expected to show the same trap-size scaling behavior as $\xi_t$ and therefore to be effective to determine the critical parameters. Considering the trap susceptibility, we should note that $\chi_t$ is not proportional to the zero-momentum component of the momentum distribution, which is given by $n(\mathbf{k}) \equiv \sum_{\mathbf{x},\mathbf{y}} e^{i\mathbf{k}\cdot(\mathbf{x}-\mathbf{y})} G_b(\mathbf{x}, \mathbf{y})$, even in the presence of the trap, and which can be experimentally related to the interference patterns of absorption images after a time-of-flight period in the large-time ballistic regime [119]. Simple considerations show that $n(\mathbf{k})$, and in particular its zero-momentum component, is largely dominated by the non-critical regions of the trap, while the contribution of the critical modes are suppressed, roughly by a total volume factor of the system. Its critical scaling in trapped system in not clear, at least in the trap-size scaling framework, thus the global momentum distribution of the system does not appear promising to accurately determine the critical parameters. For a discussion of methods based on the measurement of the momentum distribution, see Refs. [68, 98, 104].

Finally, the particle-density correlations and compressibility are also working optical lattice observables [46, 97] An analogous trap-size scaling applies also to the connected particle-density correlation, for which we have $G_n(0, \mathbf{x}) = l^{-2\theta y_n} \hat{\mathcal{G}}_n(rl^{-\theta}, \tau l^{\theta/\nu})$. Thus, information on the critical behavior, can be achieved by matching the experimental data to this trap-size scaling formula. However, our numerical analysis shows that the universal scaling of $G_n$ at the superfluid transition turns out to appear at relatively small distance, as shown in figures 5.7 and 5.18, which may make an accurate determination of its scaling quite hard.

# Appendix A

# Quantum Monte Carlo simulations

Numerical techniques are very powerful tools in obtaining results about physical models when an analytic solution is not available, for example due to the complexity of the interactions. Such techniques can roughly be divided into two classes: (*i*) exact numerical computations and (*ii*) Monte Carlo simulations. The first class gives results which coincide with theoretical ones (if one would be able to get a solution in closed mathematical form) up to machine precision; the second class instead gives results which are affected by a statistical error, much like a real experimental measurement.

In this work all numerical results reported in the main chapters are obtained through Monte Carlo simulations. The general setting of a Monte Carlo simulation is now briefly reviewed. Let us consider a classical system which is defined by a given phase space and a given hamiltonian function. We select at random a state of the system and we define a set of rules according to which a new configuration is chosen, so that a dynamical sequence of states is generated. Of course this dynamics has nothing to do with the real dynamics of the system. The usefulness of this picture is that the phase space of the system is sampled according to a probability distribution which reflects the properties of the transition rules. If we are able to create a sequence whose distribution is exactly the one given by the Boltzmann probabilities then we can identify the thermal average of any observable with the mean of that observable computed on the states belonging to the dynamical sequence. A peculiarity of this scheme is that the generation of the dynamical sequence and the computation of the value of an observable are completely decoupled. This picture is very general and the great variety of classical Monte Carlo algorithms resides only in the particular set of transition rules chosen.

The system we are going to study is instead a quantum system. The main consequence is that the measurements of a general observable cannot be separated by the creation of the sequence of states, implying that we loose the great generality described for the classical situation, so that we must rely on more specific algorithms. In the following we describe the *stochastic series expansion* method, which is very useful for the simulations of quantum spin systems and bosonic particle models. It was first introduced by Kurkijärvi and Sandvik [31, 71] and then improved by Sandvik and Syljuasen [74, 84]. A general account of this method is given in the review article of Sandvik [21]. We mention that important extensions of this method have been explored in the literature [85, 86]. A review of recent developments in Monte Carlo methods in the field of ultracold gases has been given by Pollet [110].

The numerical code used for the present quantum Monte Carlo simulations has been developed in collaboration with Christian Torrero. The simulations were performed at the INFN Pisa GRID DATA center, using also the cluster CSN4.

## A.1 Stochastic series expansion

The starting point of our analysis is the exact partition function

$$Z = \mathrm{Tr}\left(e^{-\beta H}\right) = \sum_{\alpha} \sum_{n=0}^{\infty} \frac{\beta^n}{n!} \langle \alpha | (-H)^n | \alpha \rangle \ , \tag{A.1}$$

where $\{|\alpha\rangle\}$ is a basis. It is now convenient to rewrite the hard-core Bose-Hubbard hamiltonian in a more symmetric way as a sum over the bonds:

$$\begin{aligned} H &= -\frac{J}{2}\sum_{\langle ij\rangle}(b_i^\dagger b_j + b_j^\dagger b_i) + \mu\sum_i n_i + \sum_i V(r_i)n_i \\ &= \sum_{\langle ij\rangle}\left(-\frac{J}{2}(b_i^\dagger b_j + b_j^\dagger b_i) + (\mu+V_i)\frac{n_i}{\kappa_i} + (\mu+V_j)\frac{n_j}{\kappa_j}\right) \\ &\equiv -\sum_b H_b \ , \end{aligned} \tag{A.2}$$

where $\kappa_i$ is the number of links merging to site $i$ and we used the notation $V_i \equiv V(r_i)$ for the trapping potential. In equation (A.2) we have implicitly defined the single bond hamiltonians $H_b$. Moreover, since every hamiltonian is given up to an additive constant, we can use

$$\bar{H} = H - CN_{\text{bonds}} = -\sum_b (H_b + C) \equiv -\sum_b \bar{H}_b \ , \tag{A.3}$$

where the constant $C$ has been added to each $H_b$. In equation (A.3) we now further decompose the single bond hamiltonians $\bar{H}_b$ as the sum of a part $\bar{H}_{1b}$ which has only diagonal matrix elements and a part $\bar{H}_{2b}$ which has only off-diagonal matrix elements on the basis $\{|\alpha\rangle\}$:

$$\bar{H}_b = \bar{H}_{1b} + \bar{H}_{2b} \ , \tag{A.4}$$

where

$$\bar{H}_{1b} = C - \frac{n_i}{\kappa_i}(\mu + V_i) - \frac{n_j}{\kappa_j}(\mu + V_j) \ , \tag{A.5}$$

$$\bar{H}_{2b} = \frac{J}{2}(b_i^\dagger b_j + b_j^\dagger b_i) \ \ , \tag{A.6}$$

and where we have chosen the standard basis of the occupation numbers ($|0\rangle_i$ and $|1\rangle_i$ where $i$ is the lattice site). Thus, there are only the following six non-zero matrix elements:

$$\langle 0,0|\bar{H}_{1\,ij}|0,0\rangle = C \tag{A.7}$$

$$\langle 0,1|\bar{H}_{1\,ij}|0,1\rangle = C - \mu_j - m_j \tag{A.8}$$

$$\langle 1,0|\bar{H}_{1\,ij}|1,0\rangle = C - \mu_i - m_i \tag{A.9}$$

$$\langle 1,1|\bar{H}_{1\,ij}|1,1\rangle = C - \mu_i - \mu_j - m_i - m_j \tag{A.10}$$

$$\langle 1,0|\bar{H}_{2\,ij}|0,1\rangle = J/2 \tag{A.11}$$

$$\langle 0,1|\bar{H}_{2\,ij}|1,0\rangle = J/2 \tag{A.12}$$

where the numbers in the bras and the kets refer to the occupancy of the sites $i$ and $j$ which are connected by the bond $b$ and we defined $\mu_i \equiv \mu/\kappa_i$ and $m_i \equiv V_i/\kappa_i$. These formula for the matrix elements are valid ($i$) for any external coupling, ($ii$) in any dimension and ($iii$) with any topology (all these informations being accounted for by the $\kappa_i$).

Now observe that the power expansion in $n$ of the partition function (A.1), inserting equation (A.3), can be expressed as a sum of products of bond operators (A.5, A.6) of variable length. We denote as $S_n$ one of the sequences with $n$ operators (both diagonal and off-diagonal) and write it in the form

$$S_n = [a_1, b_1][a_2, b_2]\cdots[a_n, b_n] \ , \tag{A.13}$$

where $a_i$ corresponds to the type of operator (1, diagonal; 2, off-diagonal) and $b_i$ to the bond. The number $n$ is called *order* of the expansion term, each term being an ordered string of non-commutating bond hamiltonians. The final form for the partition function is thus

$$Z = \sum_\alpha \sum_{n=0}^{\infty} \sum_{S_n} \frac{\beta^n}{n!}\langle\alpha|\prod_{i=1}^{n} H_{a_i\,b_i}|\alpha\rangle \ . \tag{A.14}$$

We now see the rationale for the sings of equations (A.2, A.3, A.4): it is evident that the expansion for (A.1) is written as a sum of matrix elements which are positive (like $\bar{H}_{2b}$) or can be made positive by a suitable choice of the constant $C$ (like $\bar{H}_{1b}$). In order to sustain a probabilistic interpretation of the partition function, our matrix elements must be non-negative and the constant $C$ is thus constrained.

Until now we have only rewritten the partition function and no approximation has been made. Since equation (A.1) is a converging series, we can truncate it at an enough high value $M$ for $n$, so that the truncation error be negligible with respect to the statistical error which will emerge from the Monte Carlo simulation. Thus we can insert $(M-n)$ fill-in identity operators in the operator products in all possible ways, denoting them as $H_{0\,0}$ and adding the label $a_i = 0$ when a unit operator is placed at level $i$ in the operator sequence: this has the advantage of dealing with operator expansions of the same length. Taking into account the combinatorics factors stemming from the arbitrariness of placing the $H_{0\,0}$ among the $H_b$, we finally obtain

$$Z = \sum_{\alpha} \sum_{S_M} \frac{\beta^n (M-n)!}{M!} \langle \alpha | \prod_{i=1}^{M} H_{a_i\, b_i} | \alpha \rangle \ , \tag{A.15}$$

where now $n$, which depends on the particular operator string $S_M$, is the number of bond operators, that is the number of elements $[a_i, b_i] \neq [0, 0]$.

At this point we can describe the Monte Carlo procedure. For the moment let us forget of computing observables and think only to a stochastic sampling of $Z$: there are a lot of contributions arising from (A.15) and we want to select a dynamical sequence whose frequencies reflect the thermal probability distribution. The terms contributing to (A.15) are given by a state $|\alpha\rangle$ and an operator string $S_M$ that, after its application, gives back the same state $|\alpha\rangle$. The stochastic sampling which gives rise to the Monte Carlo dynamics is made of rules that select a new basis state $|\alpha'\rangle$ and a new operator string $S'_M$: thus, it naturally takes place in the extended space $\{|\alpha\rangle\} \otimes \{S_M\}$, and we will call the pair of a system state and an operator string a *configuration*. The configuration changes cannot be completely arbitrary but must satisfy some constrains: $(a)$ the new state and string must contribute to (A.15); $(b)$ the sequence must be ergodic, that is all possible (contributing) terms must be reachable; $(c)$ the dynamics must visit the configuration space consistently with the Boltzmann distribution.

The next question is then how to generate the required Monte Carlo sequence. Of course there are a lot of possibility to explore our configuration space. We now describe the prescriptions of the algorithm used in our simulations. Given a term contributing to (A.15), two types of updating are performed: $(A)$ identity operators are replaced by diagonal operators and vice versa; $(B)$ bond operators of different types are replaced by each other. Moreover, the consistency of the update implies that at the end also the state $|\alpha\rangle$ is changed. Constrains $(a)$ and $(b)$ are easily seen to be verified while, to satisfy $(c)$, the equations of the *detailed balance principle* must be fulfilled every time an operator substitution takes place.

Type $(B)$ can be realize both in a local form [31] or in a global form [74]: in the latter case it is called *operator loop* and the efficiency of the algorithm is greatly enhanced. However, there are still many solutions for the equations of detailed balance, even for the operator loop case, and they can be classified according to their bouncing probabilities. A *bounce* is an attempt to change a particular bond operator which fails and takes the algorithm a step behind. Minimizing the bouncing processes will generally improve the efficiency of creating decorrelated configurations. The present case of the hard-core Bose-Hubbard model can be resolved recalling the equivalence with the XXZ-model treated in Section 3.2.1; thus, we can use the procedure described in detail in Section III of Ref. [84]. The most simple way of solving the detailed balance equations is using the so-called heat-bath solution while a more involved solution is needed to minimize bounces; in the latter case the loop is called *directed operator loop*.

Using the symmetry properties of the matrix elements, it possible to divide all the detailed balance equations into eight independent groups, with three possible bounces for each group. Within each group we set the value of $C$ in such a way that the bouncing probabilities are minimized; in turn this is another constrain on $C$. For some values of the system parameters it is possible to eliminate all

bounces while in other cases some bouncing processes must be allowed. As a result, we allow for one bounce within each group for positive $\mu$ and $\mu = 0$ and two bounces for negative $\mu$, independently of the dimensionality.

A quantum Monte Carlo simulation of the hard-core Bose-Hubbard model starts choosing at random a state $|\alpha\rangle$ and the sequence $S_M$ filled only with identity operators, which of course give a non-zero contribution to $Z$. In homogeneous systems it is known that the average expansion order is $\langle n\rangle \sim \beta N_{\rm bonds}|\bar{H}_b|$, where $\bar{H}_b$ is a sort of mean of the matrix elements of the (unique) bond operator. Thus, for our trapped systems, we fix the value of $M$ at $a\cdot\beta N_{\rm bonds}|\bar{H}_{\rm max}|$, where $|\bar{H}_{\rm max}|$ is the highest (in absolute value) bond matrix element and $a$ is a control parameter (of order unity) which ensures that the configuration order $n$ does never exceed $M$. For our simulations we find $1.0 \leq a \leq 1.3$. Of course, during a simulation, we check that the order is safely less than $M$ and that its distribution is a gaussian with variance $\langle n\rangle^{1/2}$, as expected on theoretical grounds. Then we define a Monte Carlo step in the standard way as one Monte Carlo sweep of type $(A)$ followed by $N_{\rm loops}$ updates of type $(B)$. The number $N_{\rm loops}$ is fixed at run time in such a way that, at the end of a Monte Carlo step, the number of bond operators that have been touched by the updating loops is roughly $2M$. We stress that the choice of the above parameters $a$ and $N_{\rm loops}$ is not a fundamental point, as long as the consistency conditions are satisfied, since they act on the fine details of the efficiency of the algorithm. The only relevant point is that, during a simulation, any Monte Carlo step must have the same number of loops.

In our simulations the parameters can be divided into two groups: $(i)$ the parameters that are related to the physical conditions of the system (the temperature $T$, the chemical potential $\mu$, the linear extension $L$ of the $d$-dimensional lattice, the trap size $l$) and $(ii)$ the parameters that are related to the details of the stochastic sampling (the length of the series expansion $M$, the number $N_{\rm loops}$ of operator loops, the value for the additive constant $C$, the frequency of bouncing processes). In tables A.1, A.2, A.3, A.4, A.5, A.6 we give the values of the Monte Carlo parameters corresponding to some physical values of the system parameters. The chosen values for the system parameters approximately cover the range of the ones used in the simulations. According with the previous considerations, the values for the Monte Carlo parameters are approximated (within 10%). Of course, when simulating a homogeneous system, the parameter $l$ is absent while, for a trapped system, we must be sure that the ratio $L/l$ is sufficiently large so that finite-size effect are negligible. To this end, we give the values of $L$ for which finite-size effects for trapped systems of trap size $l$ can be considered negligible: $(i)$ for one-dimensional systems at $\mu = +1, 0$ we take $L = 4l + 1$ while at $\mu = -1$ we have $L = 9l + 1$; $(ii)$ for two-dimensional systems at $\mu = +2, 0$ we take $L = 3l + 1$ while at $\mu = -2$ we have $L = 5l + 1$; $(iii)$ for the three-dimensional case the details are given in Section 5.4.1.

## A.2 Observables

Until now we have described how to change the configurations of the system. When the expectation value of an observable is needed, the quantity to be sampled is not $Z$ but

$$\langle O\rangle \equiv \frac{\mathrm{Tr}\left(Oe^{-\beta H}\right)}{Z}\ . \tag{A.16}$$

This would result in a completely different sampling procedure, since in expansion (A.15) also the operator $O$ must enter together with $H_{a\,b}$ in the operator strings. However there are some operators for which it is possible to compute expectation values only from the knowledge of $Z$: these are operators that are diagonal in the basis $\{|\alpha\rangle\}$ or operators that are a combination of the bond hamiltonians (in particular the total energy) [21, 71].

- The particle density and the density-density correlator are given by

$$\langle n_{\mathbf{x}}\rangle = \langle\alpha(\mathbf{x})|\hat{n}|\alpha(\mathbf{x})\rangle\ , \tag{A.17}$$

$$\langle n_{\mathbf{x}} n_{\mathbf{y}}\rangle = \langle\alpha(\mathbf{x})|\hat{n}|\alpha(\mathbf{x})\rangle\,\langle\alpha(\mathbf{y})|\hat{n}|\alpha(\mathbf{y})\rangle\ , \tag{A.18}$$

where $\alpha(\mathbf{x})$ is the ket of site $\mathbf{x}$. It is clear that only the local occupancies are involved and these expectation values can be computed simply from the knowledge of the state $|\alpha\rangle$, so that the problem is substantially equivalent to a classical one.

- The mean value of the bond operator $H_b$ is

$$\langle H_b \rangle = C - \frac{\langle n_b \rangle}{\beta} , \tag{A.19}$$

where $n_b$ is the number of $H_b$ present in a given operator string and $C$ is the additive constant. Consequently the total energy of the system is given by

$$E = CN_{\text{bonds}} - \frac{\langle n \rangle}{\beta} , \tag{A.20}$$

where $n$ is the order of the actual configuration.

- One observable of great importance in homogeneous quantum systems is the linear winding number, which is defined as

$$W_i = \frac{N_i^+ - N_i^-}{L} , \tag{A.21}$$

where, for the present case of bosonic systems, $N_i^+$ and $N_i^-$ are respectively the number of off-diagonal operators which move a particle in the positive and negative $i$th direction [73]. The winding number is related to the spin stiffness $\rho_s$ of spin models [78] and to the helicity modulus $\Upsilon$ of particle systems [69] by the following relation:

$$\Upsilon = \frac{\langle W_i^2 \rangle}{L^{d-2}} . \tag{A.22}$$

Taking advantage of the homogeneity of the system, $\Upsilon$ is independent of $i$.
Since no temperature factor enters in (A.22) (as sometimes is found), we note that $\Upsilon$ has dimension of length in one dimension, is a pure number in two dimensions and is a linear density in three dimensions.

- Finally, we consider the one-particle density matrix defined by

$$G_b(\mathbf{x}, \mathbf{y}) = \langle b_{\mathbf{x}}^\dagger b_{\mathbf{y}} \rangle . \tag{A.23}$$

This observable is non-diagonal in the basis of occupation numbers and it is not reducible to a combination of operators which enter the system hamiltonian, thus an *ad hoc* algorithm for its computation must be considered. The details for the stochastic sampling of $G_b$ are explained by Dorneich and Troyer [83]. We mention that the great advantage of this sampling is that $G_b$ is computed simply taking track of the details of the dynamics of operator loops, so that no new construction is needed.

## A.3 Sampling and statistics

We now discuss the statistics of our sampling. After each Monte Carlo step we take a measure of an observable. In order to save hard disk memory, after $N_{\text{block}}$ Monte Carlo steps we record on an output file the mean value of these $N_{\text{block}}$ measurements. In the simulations we took $100 \leq N_{\text{block}} \leq 10000$. This was repeated $N_{\text{meas}}$ times (the number of printings), so that the final number of Monte Carlo steps of a single run was $N_{\text{run}} = N_{\text{block}} \cdot N_{\text{meas}}$.

We checked the thermalization of a single run basically in two different (but equivalent) ways, depending on the specific observable. First, dividing the run in $n$ parts and computing the mean within single blocks (each block being made of $\nu = N_{\text{meas}}/n$ printings and corresponding to $\nu \cdot N_{\text{block}}$

Monte Carlo steps): we checked that the block values were all consistent within error bars; this implies that the thermalization time, in Monte Carlo steps units, is less than $\nu \cdot N_{\rm block}$ (in our checks $2 \leq \nu \leq 10$). Second, computing the mean values obtained excluding part one, two, ... of the simulation and observing that the final estimates do not change within error bars.

Then, for each set of the system parameters, we launched a number $N_{\rm sim}$ of simulations which differ only for the seed of the random number generator. The number $N_{\rm sim}$ was chosen compatibly with the computing resources and so that the final statistical error was sufficiently small. In this way the total number of Monte Carlo steps is given by

$$N_{\rm MCS} = N_{\rm sim} \cdot N_{\rm run} = N_{\rm sim} \cdot N_{\rm block} \cdot N_{\rm meas} \ . \tag{A.24}$$

Of course, the effective independent measurements are $N_{\rm eff} = N_{\rm MCS}/\tau_{\rm auto}$ , where $\tau_{\rm auto}$ is the autocorrelation time at equilibrium. If we suppose that $\tau_{\rm auto}$ is of the same order of the thermalization time then we have the rough constrain $\tau_{\rm auto} \leq N_{\rm block}$ , where we must remember that significant differences can occur for different observables. The statistical error scales as $\epsilon_{\rm rel} \sim N_{\rm eff}^{-1/2}$ and, taking for instance $\tau_{\rm auto} \sim 10$ as expected from previous studies [21], we get $\epsilon_{\rm rel} \sim 10^{-3}$ for $N_{\rm MCS} \sim 10^7$ .

However, we observe that the mean values of an observable computed on two different simulations of length $N_{\rm run}$ can be considered as independent from a statistical point of view, due to the difference of the random seed. This implies that we can avoid a detailed study of autocorrelation and, in order to compute the expectation value of an observable and its statistical error for fixed values of the system parameters, we use the standard jackknife method, where in each bin we put the mean of a single run (or more suns).

Finally, we give the values of the statistics.

- 1D. Simulations made at $\mu = +1, 0, -1$ ranges from $10^6$ to $3 \cdot 10^6$ Monte Carlo steps in the presence of harmonic confinement while in the hard-wall limit we have $15 \cdot 10^6$. The total CPU time is about 40 years.

- 2D. Simulations made at $\mu = +2, -2$ have typical statistics of order $2.5 \cdot 10^6$ Monte Carlo steps while for $\mu = 0$ we have $7.5 \cdot 10^6$. The total CPU time is about 30 years.

- 3D. Simulations of the homogeneous system have statistics of order $10^6$ Monte Carlo steps while for the trapped system we have $5 \cdot 10^6$. The total CPU time is about 50 years.

| $T$ | $l$ | $\mu$ | $C$ | $M$ | $N_{\text{loops}}$ | bounce |
|---|---|---|---|---|---|---|
| 1 | 10 | +1 | 7.66 | 360 | 50 | 7 |
| 0.1 | 10 | +1 | 7.66 | 3700 | 100 | 5 |
| 0.1 | 100 | +1 | 7.73 | 37000 | 1000 | 5 |
| 0.01 | 100 | +1 | 7.73 | 370000 | 2500 | 4 |
| 1 | 10 | 0 | 6.06 | 300 | 40 | 4 |
| 0.1 | 10 | 0 | 6.06 | 3000 | 20 | 2 |
| 0.1 | 100 | 0 | 6.23 | 30000 | 180 | 2 |
| 0.01 | 100 | 0 | 6.23 | 300000 | 80 | 2 |
| 1 | 10 | -1 | 30.2 | 3300 | 140 | 3 |
| 0.1 | 10 | -1 | 30.2 | 33000 | 100 | 2 |
| 0.1 | 100 | -1 | 30.6 | 330000 | 1500 | 2 |
| 0.01 | 100 | -1 | 30.6 | 3300000 | 700 | 2 |

Table A.1: Parameters of the simulations for one-dimensional systems in the presence of harmonic confinement.

| $T$ | $L$ | $\mu$ | $C$ | $M$ | $N_{\text{loops}}$ | bounce |
|---|---|---|---|---|---|---|
| 0.02 | 10 | +1 | 1.75 | 950 | 20 | 15 |
| 0.001 | 40 | +1 | 1.75 | 82000 | 100 | 15 |
| 0.02 | 10 | -1 | 0.25 | 540 | 20 | 20 |
| 0.001 | 40 | -1 | 0.25 | 47000 | 85 | 20 |

Table A.2: Parameters of the simulations for one-dimensional systems in the hard-wall limit.

| $T$ | $l$ | $\mu$ | $C$ | $M$ | $N_{\text{loops}}$ | bounce |
|---|---|---|---|---|---|---|
| 1 | 10 | +2 | 5.57 | 13000 | 1000 | 8 |
| 0.1 | 10 | +2 | 5.57 | 130000 | 4000 | 6 |
| 0.1 | 30 | +2 | 5.63 | 1100000 | 12000 | 5 |
| 0.05 | 30 | +2 | 5.63 | 2200000 | 14000 | 5 |
| 1 | 10 | 0 | 3.90 | 8700 | 450 | 4 |
| 0.1 | 10 | 0 | 3.90 | 87000 | 10 | 3 |
| 0.1 | 30 | 0 | 3.97 | 750000 | 20 | 3 |
| 0.05 | 30 | 0 | 3.97 | 1500000 | 10 | 3 |
| 1 | 10 | -2 | 10.5 | 65000 | 2000 | 6 |
| 0.1 | 10 | -2 | 10.5 | 650000 | 1500 | 5 |
| 0.1 | 30 | -2 | 10.6 | 5800000 | 15000 | 5 |
| 0.05 | 30 | -2 | 10.6 | 11600000 | 8000 | 5 |

Table A.3: Parameters of the simulations for two-dimensional systems in the presence of harmonic confinement.

| $T$ | $L$ | $\mu$ | $C$ | $M$ | $N_{\text{loops}}$ | bounce |
|---|---|---|---|---|---|---|
| 0.1 | 8 | +2 | 1.9 | 3000 | 35 | 13 |
| 0.01 | 32 | +2 | 1.9 | 470000 | 250 | 13 |
| 0.1 | 8 | +1 | 1.1 | 1700 | 5 | 11 |
| 0.01 | 32 | +1 | 1.1 | 270000 | 5 | 11 |
| 0.1 | 8 | 0 | 0.25 | 1500 | 10 | 0 |
| 0.01 | 32 | 0 | 0.25 | 246000 | 10 | 0 |
| 0.1 | 8 | -1 | 0.25 | 1300 | 10 | 16 |
| 0.01 | 32 | -1 | 0.25 | 238000 | 150 | 16 |
| 0.1 | 8 | -2 | 0.25 | 1300 | 70 | 21 |
| 0.01 | 32 | -2 | 0.25 | 238000 | 900 | 21 |

Table A.4: Parameters of the simulations for two-dimensional homogeneous systems.

| $T$ | $L$ | $C$ | $M$ | $N_{\text{loops}}$ | bounce |
|---|---|---|---|---|---|
| 1 | 8 | 1.42 | 2600 | 75 | 12 |
| 0.741 | 8 | 1.42 | 3500 | 15 | 12 |
| 0.5 | 8 | 1.42 | 5200 | 10 | 12 |
| 1 | 16 | 1.42 | 21000 | 600 | 12 |
| 0.741 | 16 | 1.42 | 28000 | 30 | 12 |
| 0.5 | 16 | 1.42 | 42000 | 10 | 12 |
| 1 | 32 | 1.42 | 170000 | 4600 | 11 |
| 0.741 | 32 | 1.42 | 230000 | 55 | 11 |
| 0.5 | 32 | 1.42 | 330000 | 10 | 11 |

Table A.5: Parameters of the simulations for three-dimensional homogeneous systems at $\mu = 2$.

| $L$ | $l$ | $C$ | $M$ | $N_{\text{loops}}$ | bounce |
|---|---|---|---|---|---|
| 17 | 4 | 8.18 | 180000 | 5800 | 4 |
| 21 | 6 | 6.15 | 260000 | 6500 | 4 |
| 25 | 8 | 5.26 | 380000 | 7700 | 5 |
| 29 | 10 | 4.78 | 550000 | 9400 | 5 |
| 33 | 12 | 4.47 | 760000 | 11000 | 5 |

Table A.6: Parameters of the simulations for three-dimensional systems in the presence of harmonic confinement at $\mu = 2$ and at the critical temperature $T_c = 0.7410$.

# List of Figures


3.1 A qualitative sketch of the $T = 0$ phase diagram of the Bose-Hubbard model in the $\mu J$ plane (in units of $U$). . . . . 26

4.1 A qualitative sketch of the phase diagram of the hard-core Bose-Hubbard model in the $\mu T$ plane in one (left) and two (right) dimensions. . . . . 31
4.2 The particle density (left) and the density-density correlator (right) in the presence of a harmonic potential at $\mu = +1$ for some values of the trap size $l$ at $\tau = 2$ and $\tau = 8$ with $\tau \equiv Tl$. The full lines show the trap-size scaling functions. . . . . 35
4.3 The particle density (left) and the density-density correlator (right) in the limit $p \to \infty$ at $\mu = +1$ for some values of the trap size $l$ at $\tau = 2$ with $\tau \equiv Tl^2$. The full lines show the trap-size scaling functions. . . . . 36
4.4 The particle density at $\mu = -1$ in the presence of a harmonic potential for some values of the trap size $l$ at $\tau = 2$ (left) and $\tau = 8$ (right) with $\tau \equiv Tl$. . . . . 37
4.5 The subtracted particle density at $\mu = -1$ in the presence of a harmonic potential for some values of the trap size $l$ at $\tau = 2$ (left) and $\tau = 8$ (right) with $\tau \equiv Tl$. . . . . 37
4.6 The density-density correlator in the presence of a harmonic potential at $\mu = -1$ for some values of the trap size $l$ at $\tau = 2$ and $\tau = 8$ with $\tau \equiv Tl$. The full lines show the trap-size scaling functions. . . . . 39
4.7 The particle density (left) and the density-density correlator (right) in the limit $p \to \infty$ at $\mu = -1$ for some values of the trap size $l$ for $\tau = 2$ with $\tau \equiv Tl$. The full lines show the trap-size scaling functions. . . . . 39
4.8 The particle density (left) and the subtracted density (right) in the presence of a harmonic potential at $\mu = 0$for some values of the trap size $l$ at $\tau = 2$ with $\tau \equiv Tl$. . . . . 39
4.9 The density-density correlator in the presence of a harmonic potential at $\mu = 0$ for some values of the trap size $l$ at $\tau = 2$ with $\tau \equiv Tl$. . . . . 40
4.10 The particle density (left) and the density-density correlator (right) in the presence of a harmonic potential at $\mu = 0$ for some values of the trap size $l$ near $x_c$ at $\tau \equiv Tl^{2/3} = 1$. 41
4.11 The rescaled particle density at $\mu = +2$ with $\tau = 2$ and $\tau = 8$ where $\tau \equiv Tl$ for different values of the trap size $l$. . . . . 41
4.12 The density-density correlator at $\mu = +2$ with $\tau = 2$ (left) and $\tau = 8$ (right) where $\tau \equiv Tl$ different values of the trap size $l$. . . . . 42
4.13 Numerical outcomes for $\rho_*(\mu)$ vs. $\mu$ for different values of the lattice extent $L$ and temperature $T$: data were collected in the homogeneous system with periodic boundary conditions. The dotted line represents the polynomial fit of the data corresponding to the larger extent. . . . . 42
4.14 The particle density at $\mu = -2$ with $\tau = 2$ (left) and $\tau = 8$ (right) where $\tau \equiv Tl$ for different values of the trap size $l$. The dotted line shows the numerical estimates of the local density approximation. . . . . 44
4.15 The rescaled particle density at $\mu = -2$ with $\tau = 2$ (left) and $\tau = 8$ (right) where $\tau \equiv Tl$ for different values of the trap size $l$. . . . . 44

4.16 The density-density correlator at $\mu = -2$ with $\tau = 2$ (left) and $\tau = 8$ (right) where $\tau \equiv Tl$ for different values of the trap size $l$. . . . . 44
4.17 The density (left) and the substracted density (right) at $\mu = 0$ with $\tau = 2$ where $\tau \equiv Tl$. 45
4.18 The density-density correlator at $\mu = 0$ with $\tau = 2$ where $\tau \equiv Tl$. . . . . 46
4.19 The subtracted density and the density-density correlator at $\mu = 0$ with $Tl^{2/3} = 1$ around the distance $r_c$ where $\mu_{\rm eff} = 2$. . . . . 46

5.1 A qualitative sketch of the phase diagram of the three-dimensional hard-core Bose-Hubbard model in the $\mu T$ plane. . . . . 49
5.2 Data of $R_\xi \equiv \xi/L$ (left) and $R_\Upsilon \equiv \Upsilon L$ (right) for the homogeneous model with periodic boundary conditions. The vertical dotted line shows our final estimate of $T_c = 0.7410(1)$. The horizontal segments around the crossing point indicate the universal asymptotic values [78] $R_\xi^* = 0.5924(4)$ and $R_\Upsilon^* = 0.516(1)$ at $T_c$. . . . . 53
5.3 Data of $R_\Upsilon$, $R_\xi$ and $\chi/L^{2-\eta}$ at $T_c$ vs. $L^{-\omega}$ with $\omega = 0.785$. In the case of $R_\Upsilon$ and $R_\xi$ we also show (by full symbols) their universal $L \to \infty$ limit: $R_\Upsilon^* = 0.516(1)$ and $R_\xi^* = 0.5924(4)$. The dotted lines show linear fits of the data of $R_\Upsilon$ and $\chi/L^{2-\eta}$. In the case of $R_\xi$, higher-order scaling corrections appear also important. . . . . 54
5.4 $R_\Upsilon$ (left) and $R_\xi$ (right) vs. $\tau L^{1/\nu}$ with $\tau \equiv T/T_c - 1$ and $T_c = 0.7410$ for the homogeneous model with periodic boundary conditions. . . . . 54
5.5 $L^{1+\eta} G_b(\mathbf{x})$ vs. $r/L$ (where $r \equiv |\mathbf{x}|$) at $T = T_c$ for homogeneous Bose-Hubbard systems with periodic boundary conditions. The data show the expected scaling behavior (5.18). 55
5.6 The particle density at $T_c$ of the homogeneous model. The dashed line shows a linear fit of the data to $\rho_0 + c\, L^{-y_n}$, with $\rho_0 = 0.16187(1)$ and $c = 0.140(1)$. . . . . 56
5.7 $L^{2y_n} G_n(x)$ vs. $r/L$ at $T = T_c$ for homogeneous systems with periodic boundary conditions. The dotted line sketches the expected asymptotic behavior $G_n(\mathbf{x}) \sim r^{-2y_n}$ at small $r \equiv |\mathbf{x}|$. . . . . 56
5.8 Data of the compressibility $\kappa$ (5.10). . . . . 57
5.9 Data of the compressibility $\kappa$ at $T_c$. The dashed line shows a linear fit to the predicted asymptotic behavior $a + bL^{\alpha/\nu}$. Data for $L \geq 8$ give $a = 0.90(1)$ and $b \approx -0.80(1)$ with $\chi^2/\text{d.o.f.} \approx 1.1$. . . . . 58
5.10 Finite-size scaling of the trap dependence of the data of $\chi/L^{2-\eta}$ in the presence of the trap from simulations keeping $L/l^\theta = 2$ fixed and using open boundary conditions. . . 58
5.11 Finite-size scaling curves of the trap susceptibility $\chi_t$ and correlation length $\xi_t$ at $T_c$ equations (5.38) and (5.39). . . . . 59
5.12 Data of $\xi_t/l^\theta$ (left) and $\chi_t/l^{(2-\eta)\theta}$ (right) in the presence of the trap. The vertical dotted line indicates the critical temperature $T_c = 0.7410$ obtained from the FSS analysis of Section 5.3. . . . . 60
5.13 Data of $\xi_t/l^\theta$ (left) and $\chi_t/l^{(2-\eta)\theta}$ (right) in the presence of the trap vs. $\tau l^{\theta/\nu}$ with $\tau \equiv T/T_c - 1$ and $T_c = 0.741$. . . . . 60
5.14 The one-particle correlation function $G_b(0, \mathbf{x})$ at $T_c$. The dashed line shows the expected small-distance behavior $G_b(0, \mathbf{x}) \sim r^{-(1+\eta)}$. . . . . 61
5.15 The particle density at $T_c$ and at the center of the trap. The full circle along the $y$-axis shows the value $\rho_0 = 0.16187$ of the leading asymptotic term obtained for homogeneous systems, see figure 5.6. The dotted line shows a linear fit to $\rho_0 + b\, l^{-\theta y_n}$, which gives $\rho_0 = 0.1617(3)$ and $b = -0.027(1)$. . . . . 62
5.16 The space dependence of the particle density $\rho(x)$ at $T_c$ in the presence of the trap. . . 62
5.17 The subtracted particle density $\rho_{\rm sub}(x)$ at $T_c$, cf Eq. (5.50). The data of $l^{y_n\theta}\rho_{\rm sub}$ versus $r/l^\theta$ for different trap sizes collapse toward a unique curve, confirming the scaling behavior (5.50). . . . . 64
5.18 The density-density correlation $G_n(0, x)$ at $T_c$. . . . . 64

# List of Tables

A.1 Parameters of the simulations for one-dimensional systems in the presence of harmonic confinement. . . . . 73
A.2 Parameters of the simulations for one-dimensional systems in the hard-wall limit. . . . 73
A.3 Parameters of the simulations for two-dimensional systems in the presence of harmonic confinement. . . . . 73
A.4 Parameters of the simulations for two-dimensional homogeneous systems. . . . . 74
A.5 Parameters of the simulations for three-dimensional homogeneous systems at $\mu = 2$. . 74
A.6 Parameters of the simulations for three-dimensional systems in the presence of harmonic confinement at $\mu = 2$ and at the critical temperature $T_c = 0.7410$. . . . . 74

# Bibliography


[1] M.N. Barber, in *Phase Transitions and Critical Phenomena, Volume 8*, (ed) C. Domb, J.L. Lebowitz, Academic (1983) New York .

[2] L.D. Landau, E.M. Lifshitz, *Quantum mechanics, Volume 3*, Pergamon (1987) New York .

[3] K. Huang, *Statistical mechanics*, Wiley (1987) New York .

[4] J. Cardy, *Finite-Size Scaling*, North Holland (1988) Amsterdam .

[5] V. Privman, *Finite Size Scaling and Numerical Simulation of Statistical Systems* World Scientific (1990) Singapore .

[6] K.G. Wilson, in *Nobel Lectures in Physics 1981-1990*, (ed) G. Ekspong, World Scientific Publications (1993) Singapore .

[7] A. Griffin, D.W. Snoke, S. Stringari (ed), *Bose-Einstein condensation*, Cambridge University Press (1995) New York .

[8] A.M. Tsvelik, *Quantum field theory in condensed matter physics*, Cambridge University Press (1995) New York .

[9] W. Ketterle, N.J. van Druten, in *Advances in Atomic, Molecular and Optical Physics, Vol. 37*, (ed) B.Bederson, H. Walther, Academic (1996) San Diego .

[10] J.T.M. Walraven, in *Quantum Dynamics of Simple Systems*, (ed) G.L. Oppo, S.M. Barnett, E. Riis, M. Wilkinson, Institute of Physics (1996) London .

[11] J. Zinn-Justin, *Quantum Field Theory and Critical Phenomena*, Clarendon Press (1996) Oxford.

[12] J. Cardy, *Scaling and renormalization in statistical physics*, Cambridge University Press (1996) New York .

[13] G. Grosso, G. Pastori Parravicini, *Solid State Physics*, Academic Press (2000) London .

[14] L.P. Pitaevskii, S. Stringari, *Bose-Einstein condensation*, Oxford University Press (2003) New York .

[15] M. Greiner, *Ultracold quantum gases in three-dimensional optical lattice potentials*, PH.D. Theis (2003) München .

[16] J.F. Annett, *Superconductivity, superfluids and condensates*, Oxford University Press (2004) New York .

[17] C.J. Foot, *Atomic Physics*, Oxford University Press (2005) New York .

[18] C.J. Pethick, H. Smith, *Bose-Einstein condensation in dilute gases*, Cambridge University Press (2008) New York .

[19] A. Griffin, T. Nikuni, E. Zaremba, *Bose-condensed gases at finite temperatures*, Cambridge University Press (2009) New York .

[20] S. Sachdev, *Quantum phase transitions*, Cambridge University Press (2011) New York .

[21] A.W. Sandvik, *Computational methods in spins systems*, arXiv:1101.3281 (2013)

[22] S.N. Bose, *Z. Phys.*, **26** (1924) 178 .

[23] A. Einstein, *Sitzber. Kgl. Preuss. Akad. Wiss.*, (1924) 261 .

[24] A. Einstein, *Sitzber. Kgl. Preuss. Akad. Wiss.*, (1925) 3 .

[25] P.S. Jessen, I.H. Deutsch, *Adv. At. Mol. Opt. Phys.*, **37** (1996) 95 .

[26] R. Grimm, M. Weidemüller, Y.B. Ovchinnokov, *Adv. At. Mol. Opt. Phys.*, **42** (2000) 95 .

[27] C. Bruder, R. Fazio, G. Schön, *Annalen der Physik*, **14** (2005) 566 .

[28] D.R. Meacher, *Contemp. Phys.*, **39** (1998) 329 .

[29] K. Sheshadri, H.R. Krishnamurthy, R. Pandit, T.V. Ramakrishnan, *Europhys. Lett.*, **22** (1993) 257 .

[30] W. Zwerger, *J. Opt. B*, **5** (2002) S9 .

[31] A.W. Sandvik, *J. Phys. A*, **25** (1992) 3667 .

[32] R. Guida, J. Zinn-Justin, *J. Phys. A*, **31** (1998) 8103 .

[33] L. Urba, E. Lundh, A. Rosengren, *J. Phys. B*, **39** (2006) 5187 .

[34] J.M. Kosterlitz, D.J. Thouless, *J. Phys. C*, **6** (1973) 1181 .

[35] M. Campostrini, E. Vicari, *J. Stat. Mech.*, (2010) P08020; E04001 .

[36] G. Costagliola *J. Stat. Mech.*, (2011) L08001 .

[37] M. Greiner, I. Bloch, M.O. Mandell, T. Hänsch, T. Esslinger, *Nature*, **415** (2002) 39 .

[38] B. Paredes, A. Widera, V. Murg, O. Mandel, S. Fölling, I. Cirac, G. Shlyapnikov, R.W. Hänsch, I. Bloch, *Nature*, **429** (2004) 277 .

[39] Z. Hadzibabic, P. Krüger, M. Cheneau, B. Battelier, J. Dalibard, *Nature*, **441** (2006) 1118 .

[40] N. Gemelke, X. Zhang, C.-L. Hung, C. Chin, *Nature*, **460** (2009) 995 .

[41] W. Bakr, J. Gillen, A. Peng, S. Foelling, M. Greiner, *Nature*, **462** (2009) 74 .

[42] C.-L. Hung, X. Zhang, N. Gemelke, C. Chin, *Nature*, **470** (2011) 236 .

[43] T.-L. Ho, Q. Zhou, *Nat. Phys.*, **6** (2010) 131 .

[44] S. Trotzky, L. Pollet, F. Gerbier, U. Schnorrberger, I. Bloch, N.V. Prokofev, B. Svistunov, M. Troyer, *Nat. Phys.*, **6** (2010) 998 .

[45] X. Zhang, C.-L. Hung, S.-K. Tung, N. Gemelke, C. Chin, *New J. Phys.*, **13** (2011) 045011 .

[46] C.-L. Hung, X. Zhang, L.-C. Ha, S.-K. Tung, N. Gemelke, C. Chin, *New J. Phys.*, **13** (2011) 075019 .

[47] G. Grynberg, C. Robilliard, *Phys. Rep.*, **355** (2001) 335 .

[48] A. Pelissetto, E. Vicari, *Phys. Rep.*, **368** (2002) 549 .

[49] W. Kohn, *Phys. Rev.*, **115** (1959) 809 .

[50] Y.B. Band, B. Malomed, M. Trippenbach, *Phys. Rev. A*, **65** (2002) 033607 .

[51] V.A. Kashurnikov, N.V. Prokofev, B.V. Svistunov, *Phys. Rev. A*, **66** (2002) 031601 .

[52] C. Kollath, U. Schollwöck, J. von Deft, W. Zwerger, *Phys. Rev. A*, **69** (2004) 031601 .

[53] L. Pollet, S. Rombouts, K. Heyde, J. Dukelsky, *Phys. Rev. A*, **69** (2004) 043601 .

[54] M. Rigol, A. Muramatsu, *Phys. Rev. A*, **70** (2004) 031603 .

[55] S. Wessel, F. Alet, M. Troyer, G.G. Batrouni, *Phys. Rev. A*, **70** (2004) 053615 .

[56] B. De Marco, C. Lannert, S. Vishveshwara, T.-C. Wei, *Phys. Rev. A*, **71** (2005) 063601 .

[57] M. Rigol, A. Muramatsu, *Phys. Rev. A*, **72** (2005) 013604 .

[58] O. Gygi, H.G. Katzgraber, M. Troyer, S. Wessel, G.G. Batrouni, *Phys. Rev. A*, **73** (2006) 063606.

[59] M. Rigol, G.G. Batrouni, V.G. Rousseau, R.T. Scalettar, *Phys. Rev. A*, **79** (2009) 053605 .

[60] M. Campostrini, E. Vicari, *Phys. Rev. A*, **81** (2010) 023606 .

[61] M. Campostrini, E. Vicari, *Phys. Rev. A*, **81** (2010) 063614 .

[62] M. Campostrini, E. Vicari, *Phys. Rev. A*, **82** (2010) 063636 .

[63] I. Hen, M. Rigol, *Phys. Rev. A*, **82** (2010) 043634 .

[64] F. Crecchi, E. Vicari, *Phys. Rev. A*, **83** (2011) 035602 .

[65] S. Fang, C.-M. Chung, P.-N. Ma, P. Chen, D.-W. Wang, *Phys. Rev. A*, **83** (2011) R031605 .

[66] G. Ceccarelli, C. Torrero, E. Vicari, *Phys. Rev. A*, **85** (2012) 023616.

[67] G. Ceccarelli, C. Torrero, *Phys. Rev. A*, **85** (2012) 053637 .

[68] J. Carrasquilla, M. Rigol, *Phys. Rev. A*, **86** (2012) 043629 .

[69] E.L. Pollock, D.M. Ceperley, *Phys. Rev. B*, **36** (1987) 8343 .

[70] M.P.A. Fisher, P.B. Weichman, G. Grinstein, D.S. Fisher, *Phys. Rev. B*, **40** (1989) 546 .

[71] A.W. Sandvik, J. Kurkijärvi, *Phys. Rev. B*, **43** (1991) 5950 .

[72] D.S. Rokhsar, B.G. Kotliar, *Phys. Rev. B*, **44** (1991) 10328 .

[73] A.W. Sandvik, *Phys. Rev. B*, **56** (1997) 11678 .

[74] A.W. Sandvik, *Phys. Rev. B*, **59** (1999) R14157 .

[75] K. Bernardet, G.G. Batrouni, J-L. Meunier, G. Schmid, M. Troyer, A. Dorneich, *Phys. Rev. B*, **65** (2002) 104519 .

[76] J.A. Lipa, J.A. Nissen, D.A. Stricker, D.R. Swanson, T.C.P. Chui, *Phys. Rev. B*, **68** (2003) 174518 .

[77] E. Burovski, J. Machta, N. Prokof'ev, B. Svistunov, *Phys. Rev. B*, **74** (2006) 132502 .

[78] M. Campostrini, M. Hasenbusch, A. Pelissetto, E. Vicari, *Phys. Rev. B*, **74** (2006) 144506 .

[79] B. Capogrosso-Sansone, N.V. Prokof'ev, B.V. Svistunov, *Phys. Rev. B*, **75** (2007) 134302 .

[80] K.W. Mahmud, E.N. Duchon, Y. Kato, N. Kawashima, R.T. Scalettar, N. Trivedi, *Phys. Rev. B*, **84** (2011) 054302 .

[81] G. Ceccarelli, C. Torrero, E. Vicari, *Phys. Rev. B*, **87** (2013) 024513 .

[82] G. Ceccarelli, J. Nespolo, A. Pelissetto, E. Vicari, *Phys. Rev. B*, **88** (2013) 024517 .

[83] A. Dorneich, M. Troyer, *Phys. Rev. E*, **64** (2001) 066701 .

[84] O.F. Syljuasen, A.W. Sandvik, *Phys. Rev. E*, **66** (2002) 046701 .

[85] O.F. Syljuasen, *Phys. Rev. E*, **67** (2003) 046701 .

[86] F. Alet, S. Wessel, M. Troyer, *Phys. Rev. E*, **71** (2005) 036706 .

[87] S.L.A. de Queiroz, R.R. dos Santos, R.B. Stinchcombe, *Phys. Rev. E*, **81** (2010) 051122 .

[88] C.C. Bradley, C.A. Sackett, J.J. Tollett, R.G.Hulet, *Phys. Rev. Lett.*, **75** (1995) 1687 .

[89] K.B. Davis, M.-O. Mewes, M.R. Andrews, N.J. van Druten, D.S. Durfee, D.M. Kurn, W. Ketterle, *Phys. Rev. Lett.*, **75** (1995) 3969 .

[90] J.A. Lipa, D.R. Swanson, J.A. Nissen, T.C.P. Chui, U.E. Israelsson, *Phys. Rev. Lett.*, **76** (1996) 944 .

[91] M.B. Dahan, E. Peik, J. Reichel, Y. Castin, C. Salomon, *Phys. Rev. Lett.*, **76** (1996) 4508 .

[92] D. Jaksch, C. Bruder, J.I. Cirac, C.W. Gardiner, P. Zoller, *Phys. Rev. Lett.*, **81** (1998) 3108 .

[93] G.G. Batrouni, V. Rousseau, R.T. Scalettar, M. Rigol, A. Muramatsu, P.J.H. Denteneer, M. Troyer, *Phys. Rev. Lett.*, **89** (2002) 117203 .

[94] T. Stöferle, H. Moritz, C. Schori, M. Köhl, T. Esslinger, *Phys. Rev. Lett.*, **92** (2004) 130403 .

[95] T. Kinoshita, T. Wenger, D.S. Weiss, *Phys. Rev. Lett.*, **95** (2005) 190406 .

[96] S. Fölling, A. Widera, T. Müller, F. Gerbier, I. Bloch, *Phys. Rev. Lett.*, **97** (2006) 060403 .

[97] I.B. Spielman, W.D. Phillips, J.V. Porto, *Phys. Rev. Lett.*, **98** (2007) 080404 .

[98] R.B. Diener, Q. Zhou, H. Zhai, T.L. Ho, *Phys. Rev. Lett.*, **98** (2007) 180404 .

[99] I.B. Spielman, W.D. Phillips, J.V. Porto, *Phys. Rev. Lett.*, **100** (2008) 120402.

[100] D. Clément, N. Fabbri, L. Fallani, C. Fort, M. Inguscio, *Phys. Rev. Lett.*, **102** (2009) 155301 .

[101] M. Campostrini, E. Vicari, *Phys. Rev. Lett.*, **102** (2009) 240601; (E) **103** (2009) 269901 .

[102] Q. Zhou, Y. Kato, K. Kawashima, N. Trivedi, *Phys. Rev. Lett.*, **103** (2009) 085701 .

[103] L. Pollet, N.V. Prokof'ev, B.V. Svistunov, *Phys. Rev. Lett.*, **104** (2010) 245705 .

[104] L. Pollet, N.V. Prokof'ev, B.V. Svistunov, *Phys. Rev. Lett.*, **105** (2010) 199601 .

[105] Q. Zhou, T-L Ho, *Phys. Rev. Lett.*, **105** (2010) 245702 .

[106] T. Yefsah, R. Desbuquois, L. Chomaz, K.J. Günter, J. Dalibard, *Phys. Rev. Lett.*, **107** (2011) 130401 .

[107] S.M. Stishov, *Phys. Usp.*, **47** (2004) 789 .

[108] M. Vojta, *Rep. Prog. Phys.*, **66** (2003) 2069 .

[109] D.C. Mc Kay, B. De Marco, *Rep. Prog. Phys.*, **74** (2011) 054401 .

[110] L. Pollet, *Rep. Prog. Phys.*, **75** (2012) 094501 .

[111] S.L. Sondhi, S.M. Girvin, J.P. Carini, D. Shahar, *Rev. Mod. Phys.*, **69** (1997) 315

[112] S. Chu, *Rev. Mod. Phys.*, **70** (1998) 685 .

[113] C. Cohen-Tannoudji, *Rev. Mod. Phys.*, **70** (1998) 707 .

[114] W.D. Phillips, *Rev. Mod. Phys.*, **70** (1998) 721 .

[115] F. Dalfovo, S. Giorgini, L.P. Pitaevski, S. Stringari, *Rev. Mod. Phys.*, **71** (1999) 463 .

[116] E.A. Cornell, C.E. Wieman, *Rev. Mod. Phys.*, **74** (2002) 875 .

[117] N. Ketterle, *Rev. Mod. Phys.*, **74** (2002) 1131 .

[118] O. Morsch, M. Oberthaler, *Rev. Mod. Phys.*, **78** (2006) 179 .

[119] I. Bloch, J. Dalibard, W. Zwerger, *Rev. Mod. Phys.*, **80** (2008) 885 .

[120] F.M. Gasparini, M.O. Kimball, K.P. Mooney, M. Diaz-Avilla, *Rev. Mod. Phys.*, **80** (2008) 1009.

[121] M.H. Anderson, J.R. Ensher, M.R. Matthews, C.E. Wieman, E.A. Cornell, *Science*, **269** (1995) 198 .

[122] T. Kinoshita, T. Wenger, D.S. Weiss, *Science*, **305** (2004) 1125 .

[123] G.K. Campbell, J. Mun, M. Boyd, P. Medley, A.E. Leanhardt, L.G. Marcassa, D.E. Pritchard, W. Ketterle, *Science*, **313** (2006) 649 .

[124] T. Donner, S. Ritter, T. Bourdel, A. Öttl, M. Köhl, T. Esslinger, *Science*, **315** (2007) 1556 .

[125] V.S. Berezinskii, *Sov. Phys. JETP*, **34**(3) (1972) 610 .

# Ringraziamenti

Ringrazio Ettore Vicari, relatore di questa tesi, per aver costantemente seguito lo sviluppo del lavoro e per essere sempre stato pronto a discutere.

Ringrazio Christian Torrero, con il quale è stato un piacere lavorare alla stesura del codice usato nelle simulazioni.

Ringrazio i membri del INFN GRID DATA center di Pisa per aver condiviso e risolto innumerevoli traversie.

Infine, ringrazio tutti gli amici con i quali ho avuto la fortuna di trascorrere questi anni di dottorato e l'occasione di discutere sui più svariati argomenti di fisica, e non solo: a tutti loro vanno il mio affetto e la mia gratitudine.